TÉCNICO LISBOA

DEVELOPMENT OF NOVEL MEMBRANES WITH COMPETITIVE BINDING PROPERTIES FOR THE ARTIFICIAL KIDNEY

Maria Inês Martins dos Santos

Thesis to obtain the Master of Science Degree in

Msc. in Bioengineering and Nanosystems

Supervisors: Dr. Mónica Cristina Faria Besteiro
Prof. Maria Clara Henriques Baptista Gonçalves

Examination Committee

Chairperson: Prof. Jorge Manuel Ferreira Morgado
Supervisor: Dr. Mónica Cristina Faria Besteiro
Member of the Committee: Prof. Frederico Castelo Alves Ferreira

October 2022

Preface

The work presented in this thesis was performed at the Center of Physics and Engineering of Advanced Materials of Instituto Superior Técnico (Lisbon, Portugal), during the period March-October 2022, under the supervision of Mónica Cristina Faria Besteiro and Maria Clara Henriques Baptista Gonçalves.

I declare that this document is an original work of my own authorship and that it fulfills all the requirements of the Code of Conduct and Good Practices of the Universidade de Lisboa.

Acknowledgments

Foremost, I would like to express my sincere gratitude to my advisors Dra. Mónica Faria and Prof. Maria Clara Gonçalves for their unconditional support, guidance and suggestions for improvement throughout my MSc studies and for the opportunity collaborate on this project.

I would also like to acknowledge my colleagues from the Laboratory of Membrane Processes for all their help and collaboration. A special thanks to Dra. Rita Pires for her patient, utmost support, and encouragement and to Prof. Vítor Geraldes for the deepest insights.

To my parents for their unconditional love and emotional support.

Abstract

A competitive binding strategy was used to functionalize monophasic hybrid cellulose acetate/silica (CA/SiO_2) membranes with ibuprofen (IBF) to enhance protein-bound uremic toxins (PBUTs) removal. Three monophasic hybrid membranes were synthesized by combining phase inversion and sol-gel techniques: CA22-APT, CA22-APT-IBF(15%), and CA30-TEOS-APT-IBF(3%). Furthermore, it was developed four pure cellulose acetate membranes, CA22, CA30, CA33, and CA35, to evaluate the formamide influence through permeation studies.

All the membranes were characterized in the Artificial Kidney (AK) in terms of hydraulic permeability (Lp), permeation to PBUTs as well as Human Serum Albumin (HSA) filtration. The molecular weight cut-off (MWCO) was accessed through the CELFA P-28 ultrafiltration installation. The morphological characterization was performed by Scanning Electron Microscopy (SEM), and the chemical composition was analyzed by Fourier Transform Infrared Spectroscopy in Attenuated Total Reflection mode (ATR-FTIR). Results for the CA30-TEOS-APT-IBF(3%) and CA30 membranes showed a Lp of 97.6 and 68.6 $Kg \cdot h^{-1} \cdot m^{-2} \cdot bar^{-1}$, respectively. The MWCO for CA30-TEOS-APT-IBF(3%) showed a decrease in average pore sizes in comparison with the pure CA30 membrane. CA30-TEOS-APT-IBF(3%) and CA30 membranes both permeated Indoxyl Sulfate (IS) and rejected 100% of HSA.

Overall, the new membranes' performance is promising, and research should be continued to prove, for the first time, the permeation of Protein-Bound Uremic Toxin (PBUT)s through competitive binding membranes.

Keywords

monophasic hybrid membranes; sol-gel; phase inversion; artificial kidney; competitive binding; blood purification

Resumo

Foi utilizada uma estratégia de ligação competitiva para desenvolver membranas híbridas monofásicas à base de acetato de celulose, funcionalizadas com ibuprofeno para melhorar a remoção de toxinas uremicas ligadas a proteínas. Assim, três membranas híbridas monofásicas foram sintetizadas combinando técnicas de inversão de fases e sol-gel: CA22-APT, CA22-APT-IBF(15%), e CA30-TEOS-APT-IBF(3%). Para além disso, foram desenvolvidas quatro membranas de acetato de celulose puras, CA22, CA30, CA33 e CA35, de forma a avaliar a influência da formamida em diversos estudos de permeação.

Todas as membranas foram caracterizadas no rim artificial em termos de permeabilidade hidráulica (Lp), permeação a toxinas, bem como rejeição à albumina. O *Molecular Weight cut-off (MWCO)* foi obtido através da instalação de ultrafiltração CELFA P-28. A caracterização morfológica foi realizada por Scanning Electron Microscopy (SEM), e a composição química foi analisada por Fourier Transform Infrared Spectroscopy em modo de Reflexão Total Atenuada (ATR-FTIR). Em termos de resultados, as membranas CA30-TEOS-APT-IBF (3%) e CA30 apresentaram um Lp de 97,6 e 68,6 $Kg \cdot h^{-1} \cdot m^{-2} \cdot bar^{-1}$, respectivamente. O MWCO para a membrana CA30-TEOS-APT-IBF(3%) demonstrou uma diminuição do tamanho médio dos poros em comparação com a membrana CA30. Ainda assim, ambas as membranas, permearam a toxina IS e rejeitaram 100% da albumina presente.

No geral, o desempenho das novas membranas é promissor, e os estudos devem ser continuados de forma a provar, pela primeira vez, a permeação de toxinas uremicas ligadas a proteínas, através de membranas de ligação competitiva.

Palavras Chave

membranas híbridas monofásicas; sol-gel; inversão de fases; rim artificial; ligação competitiva; purificação do sangue

Contents

List of Figures

List of Tables

Acronyms

AC	Activated Carbon
APTES	(3-AminoPropyl)TriEthoxySilane
AK	Artificial Kidney
ATR-FTIR	Attenuated Total Reflection - Fourier Transform Infrared Spectroscopy
BSA	Bovin Serum Albumin
CA	Cellulose Acetate
CKD	Chronic Kidney Disease
CMPF	Carboxy-4-Methyl-5-Propyl-2-Furan-Propanoic acid
DHA	DocosaHexaenoic Acid
DLS	Dinamic Light Scattering
ESRD	End Stage Renal Disease
FUR	Furosemide
HA	Hippuric Acid
HD	Hemodialysis
HF	High Flux
HPLC	High-Performance Liquid Chromatography
HSA	Human Serum Albumin
IAA	Indole-3 Acetic Acid
IBF	Ibuprofen
IS	Indoxyl Sulfate
LF	Low Flux
MMM	Mixed Matrix Membrane
MMMs	Mixed Matrix Membranes

MOFs	Metal-Organic Frameworks
MW	Molecular Weight
MWCO	Molecular Weight Cut Off
NCDs	Non-Communicable Diseases
PAA	PhenylAcetic Acid
PAH	Para-Aminohippuric Acid
PBS	Phosphate-Buffered Saline
PBUT	Protein-Bound Uremic Toxin
pCS	p-Cresyl Sulfate
PEG	PolyEthylene Glycol
PES	PolyEtherSulfone
PLA	PolyLactid Acid
PVDF	Poly(vinylidenefluoride)
PVP	PolyVinylPyrrolidone
RR	Retention Rate
RRT	Renal Replacement Therapy
RRTs	Renal Replacement Therapies
SEM	Scanning Electron Microscopy
SHDMM	Single Hemodialysis Membrane Module
SF	Super Flux
SWSC	Small Water-Soluble Compounds
TEOS	TetraEthyl OrthoSilicate
TMP	Transmembrane Pressure
TOC	Total Organic Carbon
TRP	Tryptophan
UT	Uremic Toxins

1

Introduction

Chronic Kidney Disease (CKD) remains a predominant health problem and it is estimated to affect between 11% and 13% of the entire worldwide population. The global increase of this disease is mainly associated with the increase in the prevalence of other health problems such as diabetes, hypertension, obesity, and primary renal disorders. CKD deteriorates the quality of life of the patients and often leads to End Stage Renal Disease (ESRD). Furthermore, CKD has been associated with cardiovascular diseases and premature mortality of the patients. Currently, approximately 3 million ESRD patients depend on Renal Replacement Therapies (RRTs), such as Hemodialysis (HD), to survive. Even though this technology has been around for 75 years, current HD membranes only partially restore kidney function as they are very effective in removing small water-soluble metabolites and some middle molecular weight toxins through diffusion and convection but fail to remove significant amounts of larger molecules and Protein-Bound Uremic Toxin (PBUT)s. PBUTs circulate in the blood strongly bound to Human Serum Albumin (HSA) (a protein vital to the body which cannot be removed from circulation) forming large structures which cannot be filtered through current HD membranes. Therefore, there is great need for research on novel HD membranes which target the removal of PBUTs for more efficient RRTs. Infusion of HSA binding competitors into the bloodstream is one innovative strategy for removing PBUTs from

patients. In 2015, Tao et al. [7] were the first to placed the binding competition concept to the test for improving PBUTs dialysis removal, as detailed afterward in this thesis.

1.1 Chronic Kidney Disease (CKD) and End Stage Renal Disease (ESRD)

The human kidney, among other things, is responsible for removing water, toxins, drugs, and waste products from the blood. CKD is defined as abnormalities of kidney structure or inefficient removal of uremic toxins. It is characterized by an irreversible loss of renal function which can lead to ESRD. Presently, there are only two options for the ESRD treatment: Renal Replacement Therapy (RRT) or transplantation. However, there are some issues for both methods: transplantation is the most effective treatment but the scarcity of organ donors, the surgical risk of kidney transplantation, and the need for life-long immunosuppressive therapy greatly limit this option [8]. On the other hand, RRTs greatly limit the quality of life of ESRD patients as they require the visit to specialized clinics for more than four hours, three times a week – a routine procedure which must be maintained until transplantation or death. In addition, this type of therapy for ESRD only partially restores kidney function, as they are mainly effective in removing the Small Water-Soluble Compounds (SWSC) which circulate without significant protein binding [8].

1.2 Renal Replacement Therapies (RRTs)

The most widely used RRT is HD - an extracorporeal blood cleansing procedure used to eliminate metabolic waste products from patients with ESRD. The principle of HD involves the clearance of several solutes across a semipermeable membrane by diffusion and ultrafiltration processes, including the permeation of water excesses and several Uremic Toxins (UT) across the membrane, and retention of vital blood components such as albumin and blood cells. This type of RRT may be influenced by a variety of dialysis-related factors, including dialysis dose, use of convection and/or diffusion methods, use of adsorptive particles and use of different dialysis membranes [9, 10].

Figure 1.1 represents the extracorporeal blood circuit characteristic of hemodialysis. Here, blood is drawn from the body through a vein and routed through an Artificial Kidney (Dialyzer), which is a bundle of hollow fibers made of a partially permeable membranes. The dialyzer contains a dialysing fluid solution with similar concentrations of substances to blood and allows only wastes to pass through and retain cells or proteins. The permeated wastes are diffused into the solution which is constantly replaced. Heparin, an anti-clotting agent, is also added to prevent clotting and after that, the purified blood is returned to the body [11, 12].

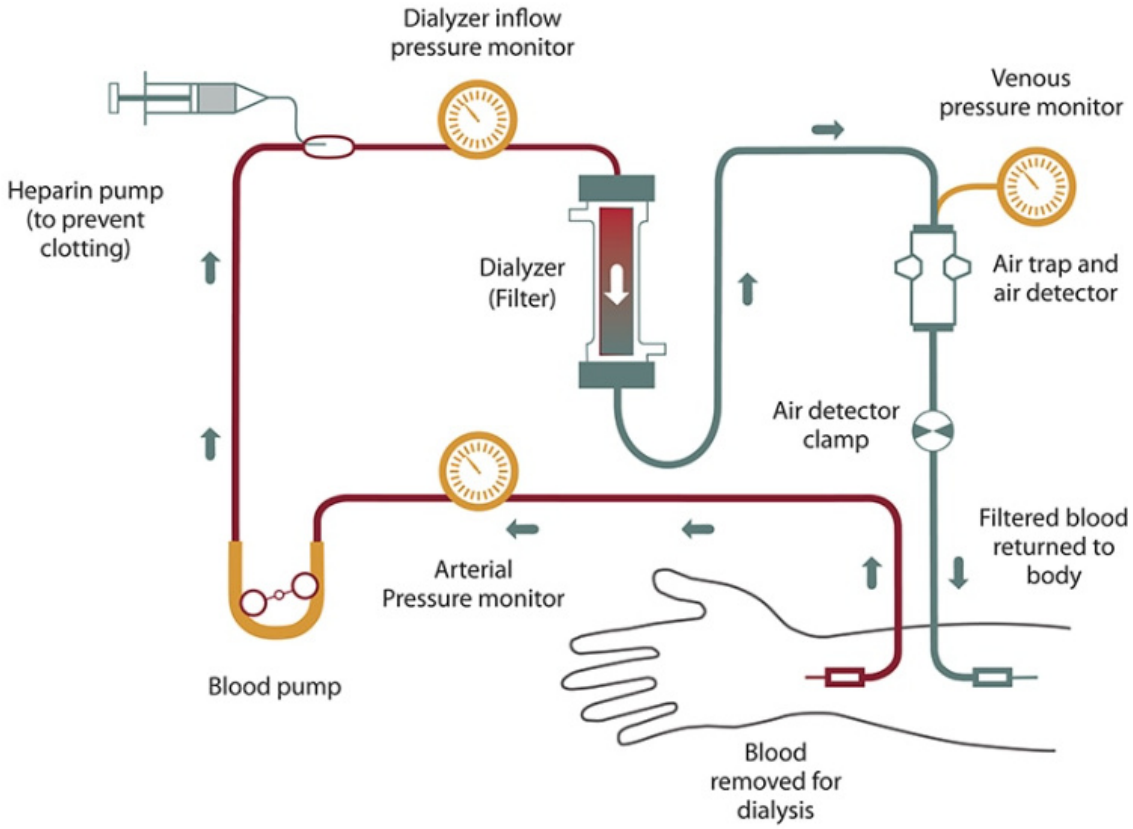

Figure 1.1: Schematic of extracorporeal blood circuit characteristic of hemodialysis. Adapted from [1]

Different mass separation mechanisms are used to remove solutes and water through semipermeable membranes (diffusion, convection, and adsorption). Traditionally, dialysis membranes were classed commonly based on their composition (cellulosic or non-cellulosic) and water permeability (low or high flux). The advancement of biomaterials and improved fiber production (spinning) technology have resulted in novel membranes with distinct characteristics and refined properties, requiring a reconsideration of conventional membrane classification methods. The incorporation of novel producing processes, such as polymer blending and surface functionalization, has resulted in the consideration of several additional parameters for membrane categorization, such as new permeability indices, hydrophilic versus hydrophobic balance, adsorption capacity, and electrical potential [9]. Therefore, the HD membranes can be classified according to several parameters such as thickness, biocompatibility, diffusive mass transfer coefficient, hydraulic permeability, structure, composition, and Molecular Weight Cut Off (MWCO). The MWCO is defined as the lowest molecular weight solute (in Da) in which 90% of a specific solute is retained by the membrane. [9].

In terms of structure, there are two main types of HD membranes: pure polymer membranes and Mixed Matrix Membranes (MMMs). Pure polymer membranes are generally composed of a single polymer such as polysulfone and cellulose triacetate membranes while MMMs result from the incorporation

of a solid phase in a continuous polymer matrix such as polysulfone/activated carbon membranes. Different HD efficiencies are achieved according to the type of membrane used during the experiments since they exhibit different dialysis-related characteristics. Nevertheless, in recent years, another option for HD therapies has emerged: integral asymmetric monophasic hybrid membranes which will be discussed further in this study.

Current MWCO membranes, even those classified as highly permeable, only enable limited clearance of UTs larger than 10 kDa [9]. Low Flux (LF) membrane dialyzers feature ultrafiltration rates lower than $15\,\mathrm{mL}\cdot\mathrm{mmHg}^{-1}\cdot\mathrm{h}^{-1}$ and elimination of small toxins with Molecular Weight (MW) of up to 5 kDa. Due to this limitation, High Flux (HF) membrane dialyzers have ultrafiltration rates higher than $15\,\mathrm{mL}\cdot\mathrm{mmHg}^{-1}\cdot\mathrm{h}^{-1}$ and pore structures that allow for the passage of so-called middle molecules with MWs up to 20 kDa.

1.3 Protein-Bound Uremic Toxins (PBUTs) and Human Serum Albumin (HSA)

Uremic toxins UTs can be classified in three main groups: i) Small Water Soluble Compounds (SWSC) (MW lower than 500 Da) such as urea, creatinine and uric acid; ii) middle molecules such as β_2-microglobulin (MW between 500 and 60000 Da); and iii) Protein-bound uremic toxins (PBUTs) (MW lower than 500 Da when free) as in case of Indoxyl Sulfate (IS) and p-Cresyl Sulfate (pCS) [6, 8]. Current HD membranes efficiently remove most SWSC, however only some HF hemodialyzers composed of membranes with larger pore size can efficiently clear all types of middle molecules due to their higher MWs.

Table 1.1 depicts the main uremic toxins studied in this work as well as their molecular weights (in Da).

Group	MW range (Da)	Uremic Toxin	MW (Da)
Small Water-Soluble Compounds	$<$500	Urea Creatinine Uric Acid	60 113 168
Middle Molecules	500 - 60 000	β_2 - Microglobulin	11 818
Protein-Bound Uremic Toxins	$<$500	p-Cresyl Sulfate Indoxyl Sulfate	31 212

Table 1.1: Classification of uremic toxins. [5, 6]

The third group of toxins, PBUTs, are characterized as the main bottleneck to the efficient removal of all UTs. IS and pCS have been the focus of most PBUT related studies and are, therefore, considered to be prototype molecules with a well-documented toxicity. These toxins are associated with several

CKD complications such as clinical symptoms of uremia, cardiorenal syndrome, chronic ischemic heart disease, cardiovascular diseases and have been linked to higher mortality rates in ESRD patients [13]. Other PBUTs include Indole-3 Acetic Acid (IAA), PhenylAcetic Acid (PAA), Carboxy-4-Methyl-5-Propyl-2-Furan-Propanoic acid (CMPF), and Hippuric Acid (HA).

The difficulty to remove PBUTs remains in the fact that these toxins exhibit high affinity to HSA (MW 66.4 kDa), a very large vital protein which cannot be removed in HD therapy. Approximately 90% of IS and pCS circulate in the blood bound to HSA while only 10% of these PBUTs circulate in their free form or unbound to HSA and only this small free fraction is dialyzable [14]. Due to the large size of the protein-toxin complex (MW higher than 66.4 kDa), PBUTs concentrations in the blood of ESRD patients who undergo HD remain essentially untouched. Since the two molecules, HSA and PBUTs, are linked by noncovalent bonds (mainly driven by electrostatic and/or van der Waals forces), the binding is reversible [15, 16] and follows the law of mass action, where the degree of binding is determined by the association and dissociation rate constants, among other things [17]. When an exogenous compound is introduced (Equation 1.1) that binds to the same HSA binding site as the one where the PBUT binds to, it results in lower free protein concentration, leading to a shift in dynamic equilibrium (Equation 1.2) to provide more free protein, as per Le Chatelier's law of chemical equilibria. Equations 1.1, 1.2, and 1.3 are shown below [18].

$$[Protein - Toxin] + [Drug] \longleftrightarrow [Protein - Drug] + [Toxin] \tag{1.1}$$

$$[Protein - Toxin] \longleftrightarrow [Protein] + [Toxin] \tag{1.2}$$

$$[Protein - Drug] \longleftrightarrow [Protein] + [Drug] \tag{1.3}$$

Albumin is one of the most essential and abundant proteins in the blood, with a concentration of 35-50 mg/mL in human serum [19]. despite the strong affinity to PBUTs, HSA is responsible for transporting a variety of substances throughout the body, including enzymes, hormones, toxins, and pharmaceutical drugs. Therefore, it is essential that albumin does not pass through the HD membranes from the blood to the ultrafiltrate due to their significance in human systems. In addition, it is important to know how long HD membranes can endure without suffering extensive protein deposition and adhesion which might result in membrane fouling [13]. The literature shows that most compounds bind to 1 of 2 primary binding sites commonly referred to as Sudlow's binding sites I and II and IS, pCS, and IAA, bind to Sudlow's site II while CMPF is described to bind to Sudlow's site I. HA is known to bind to both site I and site II, however, relatively more strongly to the latter [8]. The IS binds to the Sudlow's site II in subdomain IIIA with an association constant $K_A = 9.1 \cdot 10^5$ to $16.1 \cdot 10^5\ M^{-1}$ (corresponding to a dissociation constant

K_D = 0.6 to 1.1 μm) [20, 21].

In terms of binding between pharmaceutical drugs and HSA, warfarin is the prototypical ligand of Sudlow's site I, which is also known for binding other drugs like Furosemide (FUR), aspirin and benzylpenicillin. Sudlow's site II is known to be the binding site of diazepine, Tryptophan (TRP) and Ibuprofen (IBF) [8]. Ibuprofen shows a very high affinity for albumin, with measured association constants up to $2 \cdot 10^6\ M^{-1}$ [22–24], higher than the association constants of HSA-IS mentioned previously.

Several strategies to decrease the accumulation of PBUTs in the blood have been proposed by clinical researchers and scientists: i) maintenance of residual kidney function, ii) limitation of PBUTs generated in the colon, iii) administration of oral adsorbents, iv) use of adsorbent technology in current RRTs, v) membrane-based technology targeting the removal of PBUTs, and vi) infusion of HSA binding competitors [8]. The main focus of this work combines strategies v) and vi) and therefore will be discussed in detail.

1.4 Motivation and Aim

One of the targets of Goal 3 of the 2030 Agenda is to reduce premature mortality from Non-Communicable Diseases (NCDs), the leading causes of premature death and morbidity, by one-third, with significant implications for healthcare costs, productivity, and growth. As it is associated with an 8 to 10-fold increase in cardiovascular mortality and is a risk multiplier in patients with diabetes and hypertension, CKD is a key determinant of poor health outcomes for major NCDs such as cardiovascular disease and diabetes. Innovative treatments for CKD, such as the development of novel membranes with competitive binding properties for the artificial kidney, will improve diabetes and cardiovascular disease outcomes, increase patient well-being, and significantly reduce morbidity and mortality from NCDs.

Thus, introducing competitive binding as a strategy to remove PBUTs using pharmaceutical drugs as displacers is an essential approach that must be studied further to overcome these issues.

The aim of this study is to develop novel HD membranes which target the removal of PBUTs by competitive binding. The proposal is to use pharmaceutical drugs as HSA displacers which will disrupt the PBUT-HSA structures to form new displacer-HSA complexes increasing the concentration of the free form of PBUTs. Higher concentrations of the free form of PBUTs are then removed by the novel HD membranes. Our approach is to functionalize monophasic hybrid cellulose acetate/silica (CA/SiO_2) membranes with IBF which will compete with PBUTs for the HSA binding site at the blood/membrane interface.

2

State of the Art

2.1 Membrane-based technology targeting the PBUTs removal

As mentioned before, hemodialyzers are typically classified as either LF membrane dialyzers or HF membrane dialyzers [25]. The very first HD membranes were composed of natural cellulose, which had very small pores and thus, low MWCO values. The overall mass transfer mechanism in LF dialyzers is diffusion, therefore, the SWSC are effectively removed by LF membranes, however, they are demonstrated to be inefficient in middle-molecule clearance, which are considered more toxic and difficult to remove through diffusion and are efficiently removed by healthy kidneys. Current dialyser membranes are produced either from chemically modified cellulose materials, such as cellulose acetate and cellulose triacetate or by synthetic polymers, such as polysulfone. In general, synthetic membranes have larger pore sizes than cellulosic membranes and are therefore used in HF dialyzers. HF dialysers commonly allow the transfer of middle-sized molecules while simultaneously preventing proteins such as HSA from being removed from the blood [26]. HSA is the most important plasma protein that must be retained in chronic dialysis patients. Thus, HF membranes have higher solute permeability for middle-sized solutes and higher hydraulic permeability than LF membrane dialyzers. [25, 27]. Because the mass transfer of

LF membranes is mainly diffusive and is not suitable for use in therapies that require high convective transport, such as hemofiltration (HF) and hemodiafiltration (HDF), membranes with higher permeability like HF were required [27].

As an alternative to these two main types of HD membranes, a new generation of membranes known as MMMs were developed. MMMs combine diffusion, convection, and adsorption mechanisms in a single step. and are fabricated by introducing solid microparticles which have a propensity to adsorb UTs, such as Activated Carbon (AC) in a continuous polymer matrix. In general, the MMMs are composed of two layers: a thicker macro-porous layer in which adsorptive particles are inserted and a thinner particle-free layer and a particle-free layer which is the blood-contacting surface of the membrane to increase hemocompatibility and avoid particle release into the blood circulation.

Since most RRTs do not remove PBUTs, known to have deleterious effects on the health of ESRD patients, there has been a substantial surge in the scientific community's interest in the field of membranes which target the clearance of these toxins. As mentioned before, different types of approaches have emerged in order to improve the PBUTs removal in blood plasma of the patients. Currently there is a wide range of HD membranes on the market and the efficiency of dialysis therapy is ultimately determined, at least in part, by the properties of these membranes as well as the HD modality (high flux, low flux, adsorption etc.) employed. In this section, membrane-based therapies and developments of HD membranes will be highlighted by first addressing different HD modalities which use pure polymer and MMMs followed by clinical studies which involve the infusion of HSA binding competitors into the blood stream of ESRD patients.

2.1.1 Pure Polymer Membranes

Gerrit Lesaffer et al. [28] compared the removal of two SWSC, urea and creatinine, and four PBUTs, IS, HA, pCS and CMPF, using two different HD modalities: i) low flux hemodialysis (LFHD) where the HD membranes have low MWCO (i.e., small pore sizes), and ii) high flux hemodialysis (HFHD) where the HD membranes have high MWCO (i.e., larger pore sizes). Two high-flux hemodialyzers composed of HF polysulfone (HFPS) and HF cellulose triacetate (HFCTA) membranes, respectively, and a LF hemodialyzer composed of polysulfone (LFPS) membranes were used in a clinical trial involving 10 stable HD patients. Firstly, the patients were dialysed with the LF membrane (by which the patients were treated routinely) and after with the HF membranes in a crossover design. At the end of the HD session samples from the blood and the dialysate were collected and analysed. Results showed that the concentration of all the compounds decreased except for CMPF and TRP. Furthermore, no direct correlation was obtained between the decrease in concentration of urea and creatinine and that of the PBUTs. Finally, it was concluded that, in terms of the removal of IS, HA, pCS and CMPF, there are no significant differences between the HF and the LF hemodialyzers and that the three types of membranes

are inefficient in the clearance of PBUTs. It is also important to reinforce that only minor quantities of protein crossed the HF membranes into the dialysate and that even though protein permeation was higher for the HFCTA hemodialyzer compared to the HFPS hemodialyzer, it did not present a different solute removal.

Rita De Smet et al. [29] reported on the removal of UTs by large pore Super Flux (SF) cellulose triacetate membranes (CTA). The aim of this study was to propose novel large pore size membranes that can be a potential alternative to already available low flux cellulose triacetate (LF-CTA) membranes, which have been proved to be successful in the removal of SWSC in previous investigations, and perhaps present better PBUTs clearance. The PBUTs studied were IS, HA, IAA, pentosidine (PENT) and CMPF. The clearance of SWSCs such as urea, creatinine, and uric acid as well as middle molecules (low molecular weight advanced glycation end products) was also investigated. The study was carried out in 12 homogeneous HD patients and the HD sessions started with the LF-CTA followed by the SF-CTA hemodialyzer, each for 3 weeks. Different important parameters such as Retention Rate (RR) (%) of each compound (pre-HD and post-HD), dialytic clearance (mL/min), the amount of UTs in the dialysate and the protein binding were determined. Results showed the presence of some albumin in the spent dialysate for the SF membrane while no albumin was detected in the dialysate of the LF membrane. The pre-HD and post-HD concentrations decreased for all compounds, except IAA. Another relevant result was the RRs of LF and HF membranes for PBUTs: the RR ranged between -17.7% and 69.0% for LF membrane and between -10.2% and 69.7% for the SF membrane. These values were significantly lower than the ones obtained for the SWSCs. The SF-CTA membrane reported a better RR for IS than the LF-CTA membranes. The dialytic clearance with SF vs LF results showed that: for IS (20 ± 5 vs $24 \pm 6 mL/min$, $P < 0.05$), for HA (91 ± 11 vs $100 \pm 19 mL/min$, $P < 0.05$), for IAA (52 ± 39 vs $65 \pm 48 mL/min$, $P < 0.05$) and no dialytic clearance was calculated for CMPF and PENT since none of them were detectable in dialysate. Moreover, the lowest KoA (mass transfer area coefficient) was observed for IS and was 216 and 267 mL/min for LF and SF membranes. Therefore, analysing the main results it was concluded that 1) SF membranes removed PBUTs, however IS removal was much more efficient than for LF membranes; 2) an improvement of dialytic clearance and KoA for most solutes was observed for the SF membranes; 3) RR of PBUTs were lower for both LF and SF membranes; 4) the concentration of all solutes decreased during the HD sessions with both membranes. The removal of PBUTs by the SF-CTA hemodialyzer may be due to the albumin loss through the membranes with larger pore sizes representing a bottleneck of this study as it is known that albumin loss during HD sessions is cause of major concern regarding ESRD patients' health. The correlation between the urea RR and the RRs of HA, IS and IAA using the SF hemodialyzer was analysed in order to evaluate a potential relationship between the SWSC and the PBUTs. Results show that, in contrast to LF, in the SF-setting several correlations of the RR of urea with HA, IS and IAA, indicating that the PBUTs behave more like

non-protein-bound solutes with the SF-CTA membranes when compared to the LF-CTA membranes. In summary, SF-CTA membranes show significant improvements compared to LF-CTA membranes, however issues pertaining to albumin loss must be addressed.

Detlef H. Krieter et al. [30] emerged with a new approach for the removal of PBUTs by two types of HF PolyEtherSulfone (PES) membranes (PU - and PU + where the PU + is the most permeable membrane) where the main difference between both membranes is the albumin permeability. The removal of PBUTs, IS and pCS, by the PU- and PU+ membranes was studied under conventional HD sessions as well as online high-efficiency post-dilution hemodiafiltration. The studies were carried out with 8 patients that were submitted to one week of regular treatments (three times weekly) and after this period, a session of online post-dilution hemodiafiltration was performed with each of the membranes. However, it will highlight the results only associated with hemodialysis experiments. In order to determine the efficacy of the HD treatments, the plasma clearances as well as the dialytic clearances and the reduction rates. As a result, the data demonstrated a relevant reduction of the plasma concentrations of free and total IS and total pCS with both membranes for the HD experiments, except for the free fraction of pCS. It was not noted considerable differences in the clearance of the total form in both membranes: for pCS, the RR was between 45.6$\pm$2.0% in PU - HD and 47.3$\pm$14.8% in PU + HD and in IS was between 50.4$\pm$2.6% in PU - HD and 52.2$\pm$12.2% in PU + HD. As expected, for both membranes, the dialytic removal of the free portion of IS and pCS were significantly higher than the total fraction: for example, the dialytic clearance of pCS free fraction for the PU + membranes was in the range of 40.0 $\pm$ 24.4% while for the total portion was between 24.5 $\pm$ 14.7% and the same characteristics were observed for the PU - membrane. The same behaviour of clearance rate was verified for the IS (in the PU + membrane between 42.5 $\pm$ 21.5% for the free fraction and 25.5 $\pm$ 12.7% in the total amount and between and 51.7 $\pm$ 18.1% for the free fraction 31.7$\pm$12.6% for the total portion in the PU - membrane). Another crucial aspect was studied the albumin permeability for both types of membranes where it was observed remarkable differences in the albumin loss into dialysate during hemodialysis: in the hemodialysis with PU - membrane the albumin loss was always less than 200 mg (detection limit) whereas with PU + membrane it averaged at 482 $\pm$ 154 mg per treatment. For reminder, the total form of PBUTs is characterized by the amount that is not bound to albumin (free form) but also by the bound fraction. Since the bound fraction of the total form of PBUTs cannot pass through these HD membranes, the dialysate contained the same amount of free fraction and total fraction in both membranes: for example, the mass (mg) of the total fraction of pCS in PU- membrane dialysate was in the range of 88 $\pm$ 84 mg, and the mass of the free portion was the same value. The same conclusions were reached when it came to the IS toxin. Regarding the main results obtained during the experiments, the authors had achieved some conclusions. Firstly, relative to the removal of protein-bound toxins, there were not observed significant differences in the performance of both membranes. Nevertheless, the main difference was achieved in the albumin loss:

the most permeable PU + membrane obtained higher values, as expected. Secondly, the two types of toxins analysed, IS and pCS demonstrated to be similarly removed by the membranes. Thirdly, the RR were attributed as inadequate for both membranes since they were in the range of 50% and therefore, did not successfully remove the PBUTs. Finally, since both membranes only remove the free portion in whole form, their inefficiency in removing protein-bound substances can be noticed.

2.1.2 Mixed Matrix Membranes

Tijink et al. [31] developed a new concept that combines two commonly used methodologies in HD membranes: diffusion and adsorption. On the one hand, they developed MMMs with a thin dense polymeric layer that directly contacts blood. This particle-free membrane layer was designed to be the blood-contacting surface in order to increase membrane hemocompatibility and prevent particle release into the circulation. Below this thin layer lies a much thicker macroporous layer containing particles which are known to increase PBUT clearance. The macro-porous membrane matrix was created using a polymer combination of PES and PolyVinylPyrrolidone (PVP) and activated carbon was chosen as the adsorptive particles since it had previously been used as adsorbents for uremic toxins [32]. Two markers, creatinine as a model for small water-soluble solutes and Para-Aminohippuric Acid (PAH), which is typically used as a marker for organic anion transport and a model protein-bound solute. The MMMs were fabricated with an initial mixture of 14 wt.% PES and 1.4 wt.% PVP, followed by the addition of different amounts of dry activated carbon particles: 50, 60 and 70 wt.% in relation to the PES quantity in the MMMs. The very thin particle-free membrane layer was prepared using 15 wt.% PES and 7 wt.%PVP. Scanning Electron Microscopy (SEM) was used to characterize the membranes, pure water fluxes and the BSA sieving coefficients of the single and dual-layer membranes were evaluated at room temperature. In order to be used as a model, the creatinine adsorption capacity was also measured. The adsorption of creatinine achieved by activated carbon alone, by the particle-free membrane and by the dual-layer MMMs was studied using the plasma of 6 different ESRD patients. The adsorption capacity was represented as mg of adsorbed creatinine per gram of adsorptive particles. Results revealed that all the fabricated membranes had a porous structure and that there was no substantial particle shedding and consequent particle loss. As expected, membranes loaded with 70 wt.% of activated carbon particles contained more adsorptive sites per gram of membrane than lower loadings. Results also showed that the creatinine adsorption of single and dual-layer MMMs was 29 mg of creatine per gram of activated carbon for a plasma concentration of 0.05 mg/mL. This value is substantially higher than values previously obtained in other works. Besides this, it was also observed that both single and dual-layer membranes removed more than 80% of total creatinine and PAH concentrations. Moreover, it was found that the activated carbon particles have no significant effect on the plasma characteristics, which is an additional benefit. To summarise, the Mixed Matrix Membrane (MMM) layer containing activated carbon and the particle-free

membrane layer could prove to be a long-term improvement toward the removal of PBUTs since they have been shown to significantly reduce PAH and creatinine, and thus might be successful in the elimination of other PBUTs. Nonetheless, because this approach combines two methods (adsorption and membrane-based removal) in a single step, the authors propose that the device could be miniaturized and the MMM placed in a separate circuit for dialysate regeneration, potentially preventing endotoxins from the dialysate from entering the patient's circulation.

Following this discovery, the same research group refocused their efforts on the same membrane concept and goal, but with some improvements: previously [31], they demonstrated the concept of a membrane with embedded adsorptive particles, a so-called porous MMM. These flat sheet MMMs are composed of a porous particle free layer attached to the MMM layer with embedded particles. Here [33], it was developed a dual layer hollow fiber MMM to remove protein bound uremic toxins. Thus, the authors created a two-layer PES/PVP hollow fiber MMM with a porous macro-void free inner membrane layer that is well attached to the MMM outer layer containing active carbon particles for the removal of PBUTs. This type of membrane may sustain a concentration difference and hence a diffusion driving force along its whole length, and as previously proven, combine diffusion and adsorption in one step. The MMMs were fabricated using a novel triple layer spinneret for spinning a polymeric inner layer and a thicker outer MMM layer. Creatinine was used as a model for small water-soluble compounds whereas HA, IS and pCS as representatives for PBUTs. The MMM were characterized in terms of clean water permeance, adsorption and removal of creatinine, IS, pCS and HA, and the rejection coefficient to albumin. Results showed that the most permeable membrane had a water permeance of 58.4 ± 9.3 $l/m^2/h/bar$ and showed higher adsorption rates of creatinine, IS, and HA than the previous dual layer MMMs mentioned before [31]. For example, the flat sheet dual layer MMM, mentioned in the study before, adsorbed approximately 29 mg creatinine per gram of AC, whereas the MMMs in this study adsorbed approximately 100 mg per gram of AC. In terms of adsorption from human blood plasma, the MMMs were able to remove up to $83 \pm 4\%$ of creatinine. Furthermore, the MMMs were able to efficiently remove pCS, IS, and HA even at low solute concentrations, whereas the PES/PVP did not successfully adsorb these solutes. Results also showed that after 4h, which is a common duration of a HD treatment, both diffusion and adsorption contributed equally to total creatinine removal in the MMM. Nonetheless, in terms of PBUTs, it was observed that their removal was mostly due to the adsorption on the MMM. Moreover, in the diffusion experiment, these membranes removed on average 2.27 mg pCS/g membrane and 3.58 mg IS/g membrane after 4h, while in the convection experiments, these membranes removed 2.68 mg pCS/g membrane and 12.85 mg IS/g membrane, and thus it was concluded that the amount adsorbed in the convection experiments was higher than in the diffusion set up. Another significant difference that was found between the diffusion and convection experiments is that in diffusion tests, the membrane retains albumin, whereas in convection experiments, there is partial

permeation of albumin – a highly undesired phenomenon in HD. Despite certain adjustments that need to be made to optimise these membranes, mainly in terms of albumin leakage, this work presented a unique and very efficient method for eliminating PBUTs via novel dual layer hollow fiber membranes, and it proved to be a promising alternative to traditional HD membranes.

Kim et al. [34] developed new membranes to address several concerns. Previously [33], it was demonstrated that combining filtration and adsorption on a single hollow fiber membrane, MMM, can remove a wide range of toxins, including PBUTs. However, these MMMs either had LF and thus were unsuitable for convective therapies, or had HF but also albumin leakage, which is undesirable for HD therapies. Here, it was pretended to develop a new generation of MMM that combines high water flux with high albumin retention and very low total protein adsorption and protein leakage. As a result, a new generation of PES/PVP-AC MMMs was designed that combines high water flux with high albumin retention and very low total protein adsorption and protein leakage. It has already been demonstrated that fibres with small internal diameters remove PBUTs more efficiently and this was taken into consideration in this study. In order to provide a comparison between novel/commercially available membranes, three control commercial membranes labelled as COM1, COM2, and COM3 were used as well as several dual layer hollow fiber MMM identified as MMM1, MMM2 and MMM3 that differ in spinning conditions used throughout their formation. The membrane water permeance and membrane pore range were investigated in order to characterize the membranes. The experiments were carried out by injecting IS (40 mg/l) and HA (110 mg/l) into human plasma, and 1 mL samples of human plasma and dialysate were taken every hour, which were then diluted and deproteinized, to observe the changes in toxin elimination. Finally, the concentrations of IS and HA were determined using High-Performance Liquid Chromatography (HPLC), and the total protein loss/leakage in dialysate and human plasma was evaluated using UV-spectroscopy. Through SEM visualizations, it was observed that the surface of the MMM3 presented to be smoother with pores in the order of a few nanometers whereas commercial membranes showed a rougher surface with larger pores than MMM3. In addition, MMM3 revealed the highest water performance and albumin retention of all membranes, resulting in decreased rates of protein leakage. To support the MMM3's superior performance, it was estimated that the total IS and HA clearance of this membrane was roughly 3-fold higher than that of COM1. Toxin removal is mainly due to diffusion generated by the toxin concentration gradient between blood plasma and dialysate in commercial HD membranes. On the other hand, since the adsorptive layer for the MMMs raises the concentration gradient across the membranes, resulting in greater toxin elimination, the MMM3's clearance of both toxins IS and HA was mostly due to adsorption. Nonetheless, the IS and HA removal processes in the COM1, COM2, and COM3 membranes differed, which can be explained by the protein/membrane interaction. Considering their bound fraction to albumin is substantially lower, HA achieved higher clearance rates than IS. It should be noted that these results were obtained from human plasma, and the outcome may

differ when extrapolated to blood due to multiple components that may interfere with the process. To sum up, MMM3 was revealed to be very desirable for conventional HD therapy and artificial devices due to its high toxin elimination and very low albumin leakage and therefore, the study's purpose was accomplished. It is necessary for future research to apply this experimental approach from whole blood.

Limin Lu et al. [35] reported on the fabrication of a new type of PES-zeolite membranes to enhance the PBUTs removal by adsorption. Zeolites are 3D aluminosilicates with a microporous and crystalline structure. The main concept was to incorporate adsorbents into polymer HD membranes in order to allow the adsorption of PBUTs on porous particles and facilitate their removal. The experiments started by the preparation of the PES-zeolite (P87 powders) composite membranes through a spin-coating process and a subsequent liquid-liquid phase separation in water. SEM and Dinamic Light Scattering (DLS) were used to analyse the membrane morphology and size distribution of zeolites powders. The depletion of IS from the feed solution was quantified by fluorescence. Through this analysis, it was verified that 46.5% of P87 were incorporated into the membranes, which is very close to the theoretical value of 50%. Moreover, the quantity of composite in the precursor solution and in the resulting membrane was found to be negligible, indicating that spin-coating is a viable approach for producing composite membranes with a high percentage of particles. Furthermore, an interesting fact was that the P87 powders by themselves presented a higher IS adsorption level than its membranes which can indicate that the PES membranes hide some parts of the P87 surface leading to a decrease in the adsorption rate. The zeolite powders prove to be effective after 1h of adsorption. SEM and DLS results showed three main differences between the PES-zeolite composite membranes and the pristine PES membranes: 1) PES-zeolite membranes presented roughness and pores in their surface while the pristine membrane showed a smooth surface; 2) the channels of pristine membranes were clear without particles whereas the composite membranes exhibited channels with particle-like surfaces; 3) the pristine membranes presented a smaller thickness than the PES-zeolites membranes. The water flux for the PES composite membranes was 112 $g/m^2/h/mmHg$ and was 0.52 $g/m^2/h/mmHg$ for the pristine PES membranes. These results showed that PES-zeolite membranes have higher water permeation flux due to the existence of nanopores on the surface that connect with the inner channels and form a flow route. The effect of pH and salts on the IS adsorption and desorption levels was another relevant test that was considered: the research revealed that in the presence of salt and pH-adjusted PBS, the P87 zeolite no longer adsorbs IS. However, in deionized water the composites adsorbed approximately 42% of IS. It was also observed that the membranes adsorbed $500\mu g$ IS per g of membrane in deionized water. The authors pointed out other parameters that can influence the IS adsorption such as Van der Waals forces, hydrophobic and hydrophilic interaction, attraction generated by electrical double layer and H-bond interaction. Despite all these interactions, adsorption forces between the electrical double layer and IS were suggested as the main cause for the adsorption of this toxin. In summary, this type of polymer-zeolite

membrane could be a possible hypothesis for dialysis applications due to the ability of zeolites to adsorb certain PBUTs such as IS. Nevertheless, in order to demonstrate the successful permeabilization of PBUTs through PES-zeolite composite membranes, the adsorption rates must be improved.

Zeng et al. [36] developed a novel type of membrane capable of efficiently permeating PBUTs in order to compete with the already established membranes. The aim of the study was to incorporate Zr Metal-Organic Frameworks (MOFs) into a PolyLactid Acid (PLA) matrix to fabricate MOFs-based MMMs. UiO-66 is a Zr-MOFs composed of octahedral [$Zr_6O_4(OH)_4$] clusters which are coupled to twelve 1,4-benzene dicarboxylic acid molecules. Due to their excellent properties such as chemical stability, non-toxicity, and hydrophilicity, the UIO-66 family has been widely studied. The Zr-MOFs were incorporated into the MMMs which were prepared using PLA. The MMMs were synthesised through pre-dispersion and phase-inversion methods, and the MOFs particles were dispersed in acetone. Human embryonic hepatocytes were used to test the biocompatibility of membranes (LO-2). In addition, it used three different types of Zr-MOFs: $UiO-66-SO_3H$, $UiO-66-(COOH)_2$ and UiO-66 to evaluate the differences. The results demonstrated that MMMs with 20% MOFs loading maintain good mechanical properties, while MMM with 25% and 30% MOFs loading exhibit reduced characteristics. Therefore, MMM containing 20% MOFs were used in the experiments, which were performed in Phosphate-Buffered Saline (PBS) (a model medium of mimic blood). From the performed analysis the following was concluded: The saturated adsorption capacities of the Zr-MOFs for IS and HA were significantly higher than those of other porous materials such as zeolite/PES membranes and carbon-based sorbents; Zr-MOFs had a chemical affinity for the two uremic toxins, which results in the positive adsorption capacities observed; the three Zr-MOFs predominantly combined with the two uremic toxins through van der Waals interactions between the Zr-MOFs ligands and the benzene rings of the IS and HA molecules; superior adsorption of toxin molecules onto $UiO-66-(COOH)_2$ and $UiO-66-SO_3H$ than onto UiO-66 which can be attributed to higher binding energies; IS presented higher binding energies than HA with the Zr-MOFs which might indicates a better adsorption; MMMs possessed good retention efficiency for large molecules as albumin; when compared to the pure PLA membrane, the MMMs removed significantly more HA and IS, with relative concentrations dropping to around 0.25 and 0.22 after 4 hours, respectively; the incorporation of MOFs into MMMs might increase water flux and MMM adsorption capability toward PBUTs; MMMs based on sulfonated MOFs demonstrated anticoagulant efficacy, as well as good biocompatibility and hemocompatibility. Thus, this further suggests that MOFs present a high potential to be used in the fabrication of novel HD membranes with high flux and high absorbability for enhancing PBUTs removal efficiency.

2.2 Infusion of HSA binding competitors into bloodstream of ESRD patients

Binding competition is a well-known and often-used process in pharmacology as most pharmaceutical drugs are transported in the blood connected to several proteins including HSA. Much of occupancy-driven drug pharmacology assumes a binding to a receptor/protein of interest. A given pharmacological molecule can act as a receptor agonist, antagonist, or inhibitor, whereas an endogenous ligand molecule may compete for the same binding site on the receptor. Binding competition studies are also important for understanding potential drug–drug interactions, particularly in patients who have a complicated medication regimen due to several co-occurring conditions [18]. Since most PBUTs are relatively small in their free form, their removal from the blood that flows through the hemodialyzer during traditional RRTs is effective and rapid. The restoration of equilibrium, however, is not immediate, resulting in an increase in the proportion of protein binding during HD sessions. PBUTs are reversibly attached to HSA by weak Van der Waals forces and are in constant dynamic equilibrium with the carrier protein. When an exogenous molecule binds to the HSA - PBUT binding site, the free protein concentration decreases, causing a shift in dynamic equilibrium to provide more free protein. As a result, more toxins become liberated and thus dialyzable [8, 18]. Thus, a potential method for improving the removal of PBUTs is the use of binding competitors to displace the UTs from the protein either directly through competition for binding sites or indirectly through allosteric interference with protein binding [8].

In the past ten years, many studies have focused on molecules, specifically hydrophobic pharmaceutical drugs, which compete with the PBUTs for the same binding site located on the different subdomains of HSA. If the affinity of the competitor with HSA is higher than that of the PBUT, it is suggested that the competitor will displace the UT from the HSA, increasing the free form of the PBUT. This sequence of events is envisioned as a plausible strategy to remove PBUTs from the blood circulation of ESRD patients. As a result, a larger fraction of the PBUTs becomes unbound, which increases the diffusion gradient and may improve dialytic removal [8] [18]. Binding competitors between different albumin ligands have been reported and recent clinical studies have proposed competitive binding as a strategy to remove PBUTs using pharmaceutical drugs as displacers [7, 18, 37].

Tao et al. [7] were the first to test the binding competition concept for improving PBUTs dialysis removal in 2015. They tested the idea by measuring IS concentration in the dialysate output stream using TRP and DocosaHexaenoic Acid (DHA) as IS competitors. A 4 HSA solution spiked with IS was cycled through the dialyzer in their in vitro system. Binding competitors (TRP and DHA), which were infused on the blood side of the circuit upstream of the dialyzer, competed for the IS binding site on HSA, resulting in a rise in IS concentration in the dialysate output stream. The fractional removal of IS was calculated by dividing the quantity per unit of time exiting the dialysate output by the amount per

unit of time entering at the blood input. IS removal is 10.2% when infusing a PBS without any added binding competition but enhanced to 18.5% with TRP and 27.7% with DHA added to the infusion. Since DHA has a substantially higher binding affinity to albumin than TRP does [38], is the stronger binding competitor of the two, resulting in a greater improvement in IS elimination during dialysis.

In 2016, *Tao et al.* [37] validated the binding competition approach ex vivo, dialyzing human whole blood spiked with IS, IAA, and HA with either an IBF + FUR infusion or a TRP infusion only. Toxin removal in the dialysate output stream was compared to phosphate-buffered saline infusion without binding competitors. The combination of IBF + FUR boosted IS fractional removal from 6.4 to 18.3% and IAA fractional removal from 16.8 to 34.5%. TRP infusion increased IS and IAA fractional removal to 10.5 and 27.1%, respectively. In all infusion settings, HA moderate effects. This study confirmed important aspects of toxin binding affinity as well as had binding competitors. Binding competitors provided only moderate improvements in toxin removal for PBUTs with low albumin binding affinity. Competitors with higher binding affinity, on the other hand, provided greater improvement in PBUTs removal. In this case, the IBF binding affinity was much higher than the TRP binding affinity.

Li et al. [39] used chronic kidney disease rat models as well as salvianolic acid infusion during microdialysis. Salvianolic acids are phytochemicals that have a remarkable affinity for albumin. They are thought to have antioxidant properties. The authors took a dialysate sample every 30 minutes for 4 hours in 5/6 nephrectomized Sprague-Dawley rats on microdialysis. The first 2 hours of the experiment were used as a control, whereas Danhong injection (DHI, a combination of salvianolic acids) was administered intravenously during the final 2 hours of microdialysis. When the infusion period was compared to the control phase, the IS and pCS elimination improved by 135.6% and 272%, respectively. The authors also used only lithospermic acid (one of the salvianolic acids), which increased IS and pCS clearance by 119.5% and 127.5%, respectively, when compared to the control. The higher removal by Danhong injection compared to lithospermic acid could be attributed to a cumulative effect of the amount of salvianolic acid contained in DHI. This approach highlights an important point about using a binding competitor cocktail that targets multiple binding sites on albumin, resulting in higher PBUTs clearance rates during dialysis.

Madero et al. [40] were the first to investigate the effect of binding competition in a clinical proof-of-concept trial with 18 patients. From minutes 21 to 40 of a 240-minute standard HD, it was administered 800 mg IBF into the arterial line of the extracorporeal circuit, upstream of the dialyzer. They measured the clearances of IS and pCS and non-protein bound solutes in dialysate. Moreover, improved IS and pCS clearance was reported in all the patients. IBF only competes with one of HSA's binding sites. This could be overcome by using more than one drug during diffusion which was investigated by *Li et al.* [39]

However, all these binding competitors as a strategy to improve PBUTs removal are administered in the patients' bloodstream. Nonetheless, the binding competition approach, while effective and attractive,

presents important side effects of long-term administration of high quantities of pharmaceutical drugs such as IBF, FUR and TRP into the bloodstream of ESRD patients. Moreover, the accumulation of binding competitors in long-term patients may accelerate the loss of residual renal function [18].

Thus, our research team is focusing on the development of novel HD membranes with the incorporation of HSA binding competitors to improve PBUT removal without the administration of drugs into the blood circulation. The strategy is based on the direct incorporation of IBF into HD membranes, taking advantage of its high binding affinity to HSA. The functionalization of HD membranes with IBF as a competitive binding technique is another interesting approach to enhance PBUTs removal.

3

Development of Novel Integral Asymmetric Monophasic Hybrid Membranes

Cellulose Acetate (CA), a thermoplastic polymer derived from cheap and renewable resources, is notable for its high flexibility, low protein adsorption, excellent water affinity, enhanced film-forming properties, low footprint, and low cost, as well as a wide range of production processes [41]. Regardless, no matter how much the synthesis protocols are modified or improved, CA membranes exhibit poor mechanical strength, low chemical resistance, low thermal stability, sensitivity to cleaning agents, and vulnerability to fouling resistance, failing to achieve the desired separation/purification in some cases. The incorporation of different materials into the polymeric CA matrix, resulting in MMMs and hybrid membranes, may overcome some of the limitations of CA membranes. The formation of hybrid membranes involves the implementation of a novel monophasic material. One strategy is to select a coupling agent capable of promoting and maintaining an interconnected network.

Zoppi et al. [42] were the first to create hybrid CA/SiO_2 membranes. The aim of the work was to prepare and characterize CA/TetraEthyl OrthoSilicate (TEOS) hybrids. The hybrid organic–inorganic films were prepared using the sol–gel process. It was prepared several CA/TEOS ratios which were scattered on a Poly(vinylidenefluoride) (PVDF) porous support. It was studied different important parameters such as permeation and retention properties, morphology, thermal and mechanical characteristics. Solutes with a molar mass of 9000 g/mol were retained by hybrid membranes (98% retention). It was also discovered that the membranes became more rigid with the addition of SiO_2 and that the hybrids' thermal stability was comparable to pure CA films. The water permeability of the CA homopolymer and CA/TEOS (with 40% of SiO_2) hybrid composite membranes was 1.82 ± 0.06 and 0.3 ± 0.1 $L/h/m^2/bar$, respectively. It was explained that the incorporation of an inorganic phase into the polymeric matrix resulted in more rigid materials with a denser morphology. Thus, the decrease in water permeability is consistent with the fact that hybrid composite membranes have a more rigid and dense filter layer. Furthermore, the alkoxy groups in the resultant materials may not be entirely removed. Because of their hydrophobic nature, organic groups linked to Si atoms can also alter the penetration property of water molecules. These properties also influenced the retention of different molar masses of solutes. Biodegradation studies were also performed on hybrid films in the presence of *T. Harzianum fungus* and it was verified that the presence of the inorganic phase had no effect on fungal development. Several monophasic hybrid CA/SiO_2 membranes (with inorganic phase dispersed at the nanoscale scale and linked to the organic matrix through covalent bonds) have been developed since their pioneer work by the sol-gel co-condensation of SiO_2 alkoxisilane precursors and polymer molecules [43–45].

Mendes et. al [46] created hybrid asymmetric CA/SiO_2 membranes containing up to 40% SiO_2. One pot reactive casting solutions was prepared for each membrane by allowing SiO_2 sol-gel hydrolysis and condensation to occur inside the polymeric solution.To assess the effect of incorporating SiO_2 into CA membranes, all results are compared and correlated with those obtained for a non-hybrid, pristine CA membrane (CA0).TEOS was used as a silica precursor and the content of silica varied between 5% and 40%.The asymmetric structure of the membranes was confirmed by SEM, and the presence of a monophasic inorganic-organic network composed of cellulose acetate and silica connected by Si-O-C bonds was confirmed by Attenuated Total Reflection - Fourier Transform Infrared Spectroscopy (ATR-FTIR). Hydraulic permeability for pure water increased from 32 $Kg/h/m^2/bar$ for the pure CA membrane to 82 and 81 $Kg/h/m^2/bar$ for the membranes with 5 and 10% silica addition, respectively.However, for silica contents higher than 10%, a decrease in the hydraulic permeability value was observed, as previously observed [42]. It was also observed a reduction in the MWCO as the silica content increases and this behavior was attributed to the increasing contribution of strongly bonded water molecules to the Si-OH groups, as well as the reduction of pore sizes and water permeation flows. It was also observed that Even though the results show that it is possible to incorporate 40 mol% silica

into CA/SiO_2 hybrid membranes with successful Si-O-C bond formation, the presence of free, uncondensed, and highly reactive Si-OH species in membranes containing more than 20 mol% silica should be considered. This work showed an interesting way to produce a monophasic hybrid membrane at room temperature, with minimal thermal degradation and low energy processing costs, high chemical homogeneity obtained in solution on a molecular scale.

Janeca et al. [47] produced a monophasic hybrid membrane for application in blood purification devices such as HD. For this, a monophasic hybrid $CA - SiO_2 - (CH_2)_3NH_2$ membrane containing 95 wt% CA and 5 wt% SiO_2 + $SiO_2 - (CH_2)_3NH_2$ was synthesised and characterised under dynamic conditions in an in-house-built Single Hemodialysis Membrane Module (SHDMM). In this case, it was used (3-AminoPropyl)TriEthoxySilane (APTES) as a silica percursor. A pure CA membrane was also synthesised and characterised for comparison. Both membranes were prepared by coupling the phase inversion method with the sol-gel technique. The presence of a thin dense active layer and a much thicker, porous layer was confirmed by SEM analysis of the $CA - SiO_2 - (CH_2)_3NH_2$ membrane cross-sections. This result confirms the asymmetric structure of the membrane. The total thickness of the hybrid membrane (103 µm) was approximately two times higher than the thickness of the CA membrane (54 µm). Permeation studies revealed that the monophasic hybrid membrane had improved mass transfer properties when compared to the pure CA membrane, as evidenced by an increase in hydraulic permeability from 37.09 $kg/h/m^2/bar$ for the CA membrane to 66.61 $kg/h/m^2/bar$ for the $CA - SiO_2 - (CH_2)_3NH_2$ membrane. Moreover, The MWCO increased as well, from 18.1 kDa for the CA membrane to 24.5 kDa for the $CA - SiO_2 - (CH_2)_3NH_2$ membrane. Both membranes ensured that water-soluble toxins like urea, creatinine, and uric acid could pass through. Long-term continuous Bovin Serum Albumin (BSA) filtration studies revealed that both membranes reject albumin completely and that there is no evidence of irreversible fouling or albumin leakage in the SHDMM. Current hemodialysis equipment should provide ultrafiltration rates ranging from 10-13 $mL/(h \cdot kg)$ [48], with an operating Transmembrane Pressure (TMP) of 0.133 to 0.200 bar (100 to 150 mmHg). As a result, in a clinical scenario, the expected ultrafiltration rate for a 70 kg adult should not be less than 700 mL/h. In this study, with an estimated hydraulic permeability of 89.40 $mL/h/m^2/mmHg$ for the $CA - SiO_2 - (CH_2)_3NH_2$ membrane and an average TMP of 0.167 bar (125 mmHg) to achieve the 700 mL/h threshold, a total membrane surface area of 0.06 m^2 would suffice. Here, a novel cellulose acetate-based monophasic hybrid skinned amine-functionalized $CASiO_2 - (CH_2)_3NH_2$ membrane was successfully synthesized and proved to be effective in HD therapies, permeating several toxins while completely retaining albumin.

In this study, the membranes were developed using the phase inversion method, producing integral asymmetric membranes with a very thin dense active layer and a much thicker, porous substructure. Porous asymmetric membranes are made by the phase inversion method [49] and are applied in several approach's such as dialysis, ultrafiltration and microfiltration. As exemplified in Figure A.1 a), asymmetric

membranes are the most fouling resistant because the majority of the rejected materials are retained at their surface. These materials can be removed by the shear forces exerted by the feed solution as it moves tangentially to the membrane surface [2]. On the other hand, symmetric structures act as depth filters and retain the majority of particles within their structure as shown in Figure A.1 b). As a result of the particles trapped inside the structure plugging the membrane, a flux decrease is observed with use [2].

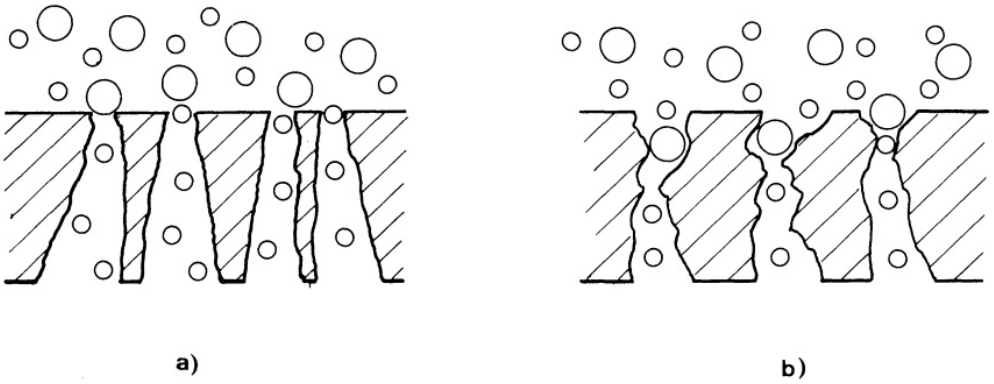

Figure 3.1: Schematic diagram depicting the filtration behaviour of an a) asymmetric and b) symmetric membrane. Adapted from [2]

By combining sol-gel and phase inversion technologies, monophasic hybrid membranes were fabricated.

A casting solution, containing cellulose acetate, acetone, and formamide, is required for the phase inversion method. Phase inversion is characterized as the controlled polymer transformation from a solution to a solid state and is considered as the most versatile technique for polymeric membrane preparation. It is characterized by the precipitation of a polymer-rich phase from an initially homogeneous casting solution. This precipitation can be promoted using different techniques such as precipitation bath or can also be induced by the suppression of water vapour in a humid environment. The polymer is dissolved in a mixture of a volatile good solvent as well as a non-volatile poor solvent.

In the case of cellulose acetate membranes, it is used acetone as the good/strong solvent and formamide as the bad/poorer solvent. The role of formamide is essentially of pore promoter since it is not a true solvent for cellulose acetate [50]. In fact, formamide can be classified as a swelling agent [51, 52], which means that when cellulose acetate is exposed to it, the polymer swells as the total volume of the polymer-liquid system increases. It also increases the solvent power of acetone [51]. Given this, when the cast film is exposed to air, the more volatile solvent - acetone - evaporates and the solution is brought to the point of polymer precipitation.

It is critical to ensure the complete homogenization of all solvents - a solubilization time of about

24 hours is sufficient for the polymer and other reagents form a homogeneous mixture. To form a thin polymer film, the resulting homogenised casting solution is dispersed over a suitable surface, such as a glass plate, while controlling the solvent evaporation time. Following that, the film is precipitated in a coagulation bath. The acetone (stronger solvent) evaporates from the film surface that is in contact with air during the solvent evaporation time. Evaporation increases the polymer concentration at the air-contacting surface, and the residual solvent that remains in the film is insufficient to keep the polymer in solution. Therefore, an active layer is formed at that point. When the film formed on top of the glass plate is immersed in the coagulation bath, the solvents and water diffuse in opposite directions at the same time, resulting in the formation of a porous structure. As a result, an asymmetric membrane is formed, with a denser active layer at the surface exposed to air and a porous support sublayer on the surface in direct contact with the glass plate. The proper time interval between casting and immersion is determined by the rate of evaporation of the most volatile solvent from the membrane and thus, by the temperature at which the membrane is cast and allowed to remain prior to immersion. This refers to the evaporation period of the solvent, which has been shown to increase average pore size at longer evaporation periods [49]. Consequently, the evaporation period is a particularly important variable in the ultrafiltration membrane development.

Furthermore, it is important to ensure the correct and complete exchange of solvents and there are several factors that can influence the formed membrane such as casting solution composition, solubilization time, casting and atmosphere temperature, solvent evaporation, and immersion precipitation. By adjusting the preparation settings, membranes with a wide range of characteristics and structures are obtained [53]. The composition of the casting solution has a significant influence on the final asymmetric membrane structure, such as pore size, pore distribution, and selective permeation performance. By varying the conditions and reagent proportions, different structures can be obtained. For example, the solvent-polymer ratio ensures that the casting solution has the proper viscosity to form a membrane film. An acetone/CA ratio of 3 is found to be effective for the pure CA membrane [54].

The addition of silica and the subsequent formation of complex C-O-Si 3D networks is expected to improve membrane selectivity and permeation properties, as well as antifouling and mechanical stability, overcoming the limitations associated with pristine CA membranes. In hybrid monophasic SiO_2 membranes, the inorganic phase is dispersed and covalently bonded to the organic matrix. This type of membrane is synthesized in the casting solution homogenization phase by the co-condensation of SiO_2 alkoxysilane precursors during the sol-gel process [46, 55]. Thus, different silica precursors, such as TEOS and APTES and their derivatives, can be used to integrate SiO_2 into the polymer matrix by two processes: hydrolysis and condensation. Nitric acid is used to provide the acidic environment required to accelerate sol-gel hydrolysis and hetero-condensation processes. When this occurs at pH 3, above SiO_2's isoelectric point, the condensation rate is proportional to the concentration of hydroxide groups,

and the following processes - hydrolysis (3.1) and condensation (3.2) - occur:

$$\equiv \mathrm{Si{-}OH} + \mathrm{OH^-} \xrightarrow{\text{Fast}} \equiv \mathrm{Si} - \mathrm{O^-} + \mathrm{H_2O} \tag{3.1}$$

$$\equiv \mathrm{Si{-}O^-} + \mathrm{OH{-}Si} \xrightarrow{\text{Slow}} \equiv \mathrm{Si{-}O{-}Si} \equiv + \mathrm{OH^-} \tag{3.2}$$

The ethoxy group is rapidly protonated during the hydrolysis process, decreasing electron density from silicon and making it more electrophilic and sensitive to water attack. The water molecule gains access to the SiO_2 precursor's back, acquiring a positive charge and weakening the protonated ethoxy group. As the positively charged ethoxy group is displaced from the SiO_2 precursor, it becomes a better leaving group. The condensation reaction occurs between silanol groups from silica precursors or with hydroxyl groups from the polymer, producing Si-O-Si or Si-O-C bonds, as shown in Figure 3.2. The sort of structure formed is heavily influenced by the balance of hydrolysis and condensation reactions, both of which are greatly influenced by the pH of the solution [46]. Since hydrolysis occurs significantly faster than condensation under acid circumstances ($pH < 5$), monomers are swiftly hydrolysed and most functional groups $-OH$ are available for condensation, resulting in considerable branching and a more open, less dense 3D network. On the other hand, under basic conditions ($pH > 10$) the hydrolysis and condensation rates are similar, resulting in fewer functional groups -OH that are available for condensation, leading to linear, less branched, but more dense structures [46, 55, 56].

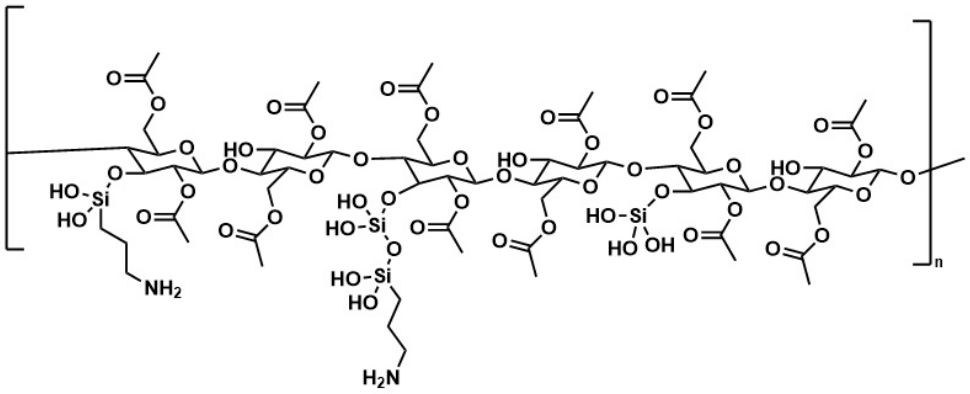

Figure 3.2: Incorporation of silica into CA matrix.

The new hybrid casting solution is then cast through the phase inversion method described before in order to form a monophasic hybrid membrane based on carbon, silica, and amine chemical species, resulting in complex carbon-silica networks.

4

Materials and Experimental Methods

4.1 Materials

CA ($C_6H_7O_2(OH)_3$, ∼30 000 g/mol, reagent grade ≥ 97%, esterification degree 40%), BSA (MW 66.5 g/mol), IS (212 Da), APTES ($C_9H_{23}NO_3Si$, 221.37 g/mol, reagent grade ≥ 98%), creatinine (MW 113.12 g/mol) and PolyEthylene Glycol (PEG) 20000 (MW 20000 g/mol), triethylamine $(C_2H_5)_3N$, 101,19 g/mol, reagent grade ≥ 99.5%), and 1-hydroxypyrrolidine-2,5-dione ($C_4H_5NO_3$, 115.09 g/mol) were purchased from Sigma-Aldrich.

Acetone (C_3H_6O, 58.08 g/mol, ≥ 99.6%) and nitric acid (HNO_3, 63.01 g/mol, 1.39 g/mL at 20℃, 65% v/v) were purchased from LabSolve. Formamide (CH_3NO, 45.02 g/mol, ≥ 99.5%) and n-hexane (≥ 95%) were purchased from Carlo Erba.

TEOS ($Si(OC_2H_5)_4$, 208.33 g/mol, reagent grade 98%) and uric acid (MW 168.11 g/mol) were purchased from Alfa Aesar.

IBF ($C_{13}H_{18}O_2$, 206.29 g/mol, racemic, reagent grade ≥ 98.0%) was purchased from TCI.

Isopropanol (≥ 99.8%) and phosphoric acid (H_3PO_4, 98.00 g/mol, 1.71 g/mL at 20℃, reagent grade 85%) purchased from Honeywell.

Dicyclohexylcarbodiimide $C_{13}H_{22}N_2$, 206.3 g/mol, reagent grade 99%) was purchased from Thermo Fisher Scientific.

Human plasma was obtained from healthy donors (IPO, Lisboa). PEG 3000 (MW 3000 g/mol), PEG 6000 (MW 6000 g/mol), PEG 10 000 (MW 10000 g/mol), PEG 35 000 (MW 35 000 g/mol), urea (MW 60.06 g/mol), sodium chloride (NaCl, 58.44 g/mol, $\geq$ 99.5%), potassium dihydrogen phosphate (KH_2PO_4, 136.09 g/mol, $\geq$ 99.5%), disodium hydrogen phosphate dihydrate ($Na_2HPO_4 \cdot 2\,H_2O$, 177.99 g/mol, $\geq$ 99.5%) purchased from Merck.

Potassium chloride (KCl, 74.56 g/mol, $\geq$ 99.5%) and Coomassie Brilliant Blue G-250 ($C_{47}H_{48}N_3NaO_7S_2$, 854.04 g/mol) were purchased from Panreac, ethanol (C_2H_6O, 46.07 g/mol, 96%v/v) was purchased from Manuel Vieira and dextran T40 (40 000 g/mol) was purchased from Amersham Pharmacia Biotech AB.

4.2 Synthesis of SiO_2 precursors

The aim of this work is the incorporation of IBF into the active layer of the membranes with possible applications in HD. For this purpose, the approach intended the conjugation of IBF into the membrane matrix through a covalent linkage to silica. The membrane synthesis precursors proved to be integrated in the polymer matrix [46]. The precursor IBF-APTES was linked to the CA matrix through the sol-gel reactions mentioned in Chapter 3.

4.2.1 Conjugation of ibuprofen (IBF) with (3-aminopropyl)triethoxysilane (APTES) (IBF-APTES)

In 5 mL of acetonitrile, APTES (53,6 mg, 0.242 mmol) was mixed with IBF (50,0 mg, 0.242 mmol). The mixture was treated with 99% dicyclohexylcarbodiimide (74,9 mg, 0,363 mmol), 1-hydroxypyrrolidine-2,5-dione (41,8 mg, 0,363 mmol), and triethylamine (36,7 mg, 0,363 mmol) for 8 hours. After several washes with acetonitrile, the solvent was evaporated to dryness in a rotavapor, yielding a colourless oil. Figure 4.1 represents the mechanism for the IBF-APTES synthesis which was detailed in previous studies [13].

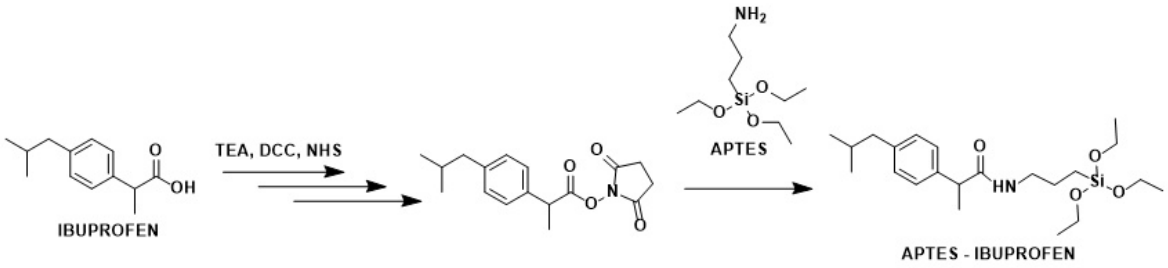

Figure 4.1: Mechanism for synthesis of IBF-APTES.

4.3 Membrane Preparation

4.3.1 Pure Cellulose Acetate Membranes

CA membranes, CA22, CA30, CA33, CA35, were prepared from four casting solutions containing cellulose acetate, acetone and formamide with different formamide:acetone ratios. Table 4.1 shows the composition of the casting solutions. The CA was mixed with the acetone and formamide thoroughly by mechanical agitation using the Shaker S50 (CAT, M. Zipperer GmbH,Ballrechten-Dottingen, Alemanha) for 24h. The membranes were then cast onto a glass plate (16 cm X 28 cm) at room temperature using a film casting knife with a thickness of 250 µm and after a solvent evaporation time of 30 seconds the glass plate was quenched into a gelation bath (ice-cold deionized water). After a residence time of approximately 24 h the membranes were detached from the glass plate, washed with deionized water (to remove any traces of solvent) and stored in deionized water at $4 \pm 1\,^{\circ}$C.

Membrane	CA22	CA30	CA33	CA35
Cellulose Acetate (wt.%)	17	17	17	17
Formamide (wt.%)	22	30	33	35
Acetone (wt.%)	61	53	50	48

Table 4.1: Casting solution composition (wt.%) of the pure cellulose acetate (CA) membranes.

4.3.2 Monophasic Hybrid Membranes

The integral asymmetric monophasic hybrid CA/SiO_2 membranes, CA22-APT, CA22-APT-IBF(15%), CA30-TEOS-APT-IBF(3%), were formed adding to homogeneous casting solution composed by a solvent system (formamide and acetone) and CA, different TEOS or APTES ratios, depending on the membrane, and nitric acid to promote the acidic hydrolysis. This solution will be stirred for 24 hours and then cast onto a glass plate (16 cm X 28 cm) at room temperature using a film casting knife with a thickness of 250 µm and after a solvent evaporation time of 30 seconds the glass plate was quenched into a gelation bath (ice-cold deionized water). After a residence time of approximately 24 h the membranes

were detached from the glass plate, washed with deionized water (to remove any traces of solvent) and stored in deionized water at $4 \pm 1\,^{\circ}$C.

Monophasic hybrid SiO_2/CA membranes incorporating competitive binders were produced using the silica derivatives prepared and detailed in Section 4.2.1. Since the competitive binder (ibuprofen) was conjugated with the silica precursor APTES, when all of the other reagents (CA, acetone, and formamide) have been thoroughly mixed, the compound IBF-APTES is added to the casting solution and is incorporated through the sol-gel process. Following that, the phase inversion method is carried out as previously described.

Figure 4.2 represents the incorporation of the compound IBF-APTES into the CA matrix for the CA22-APT-IBF(3%) membrane synthesis.

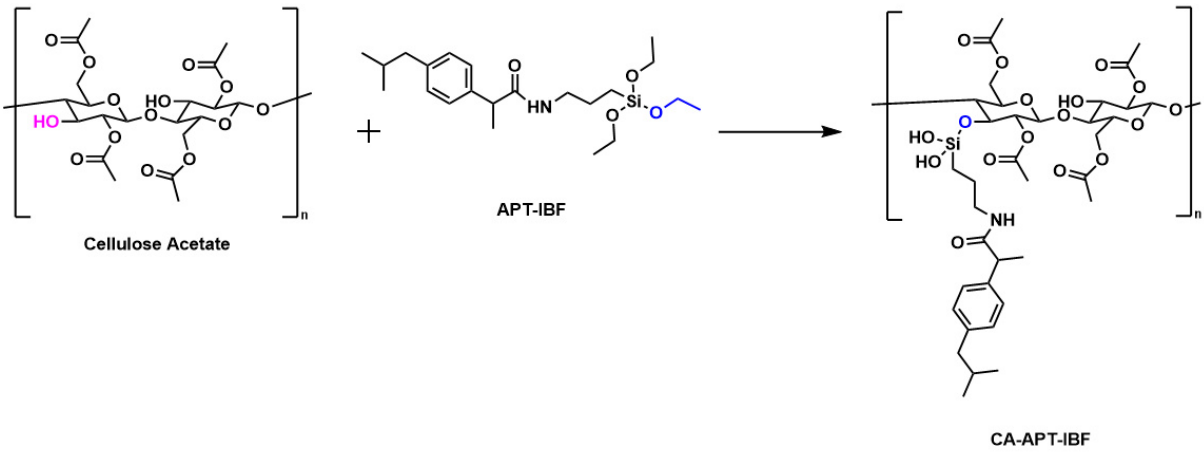

Figure 4.2: Incorporation of the compound APTES-IBF into the CA matrix for the synthesis of the CA22-APT-IBF(15%) membrane.

Figure 4.3 represents the schematic representation of the incorporation of the silica precursor APTES into the CA matrix for the synthesis of the CA22-APT membrane.

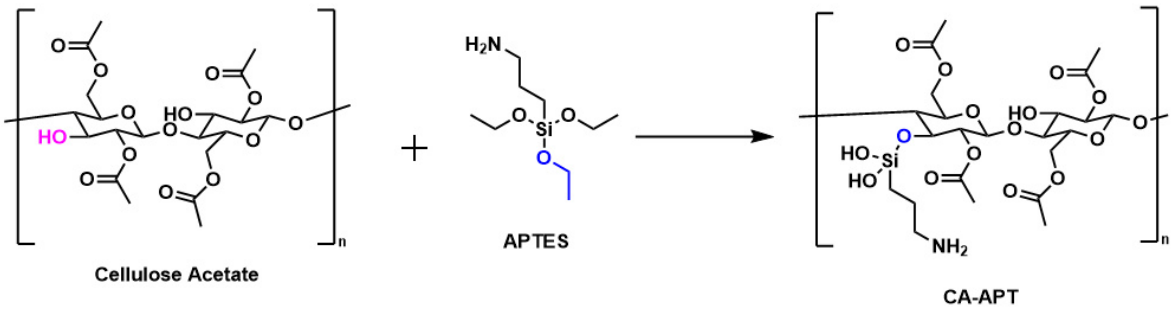

Figure 4.3: Incorporation of APTES into the CA matrix for the synthesis of the CA22-APT membrane.

Figure 4.4 represents the schematic representation of the incorporation of TEOS and the compound

IBF-APTES into the CA matrix for the synthesis of the CA30-TEOS-APT-IBF(3%) membrane.

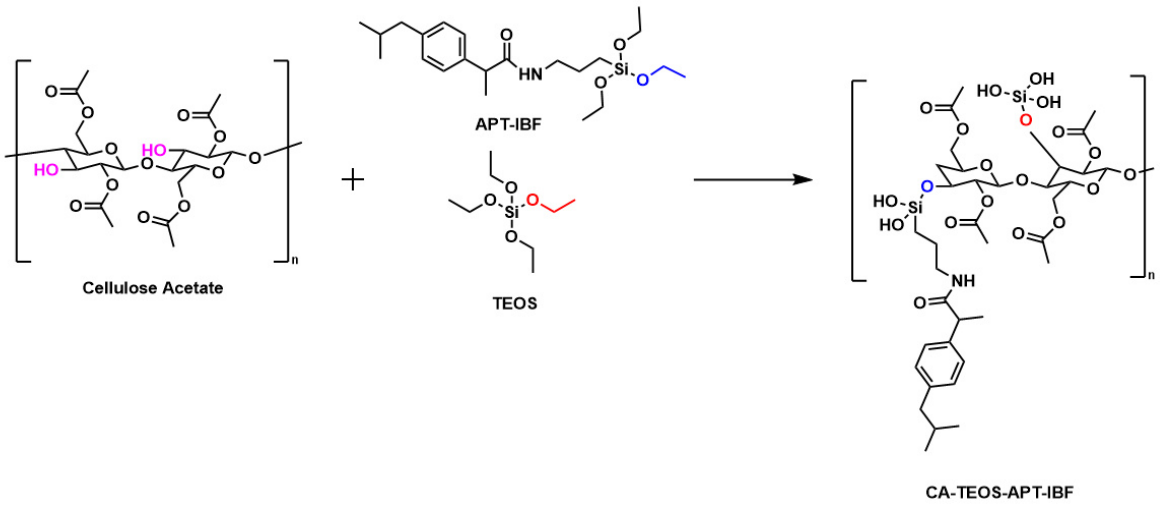

Figure 4.4: Incorporation of the compound TEOS-APTES-IBF into the CA matrix for the synthesis of the CA30-TEOS-APT-IBF(3%) membrane.

Table 4.2 represents the composition of monophasic hybrid CA/SiO_2 membranes casting solutions. The percentage of IBF present in the name of the CA22-APT-IBF(15%) membrane (15%) is only relative to the CA and APTES-IBF mass (do not include the formamide and acetone quantities). The same rationale was applied to the CA30-TEOS-APT-IBF(3%) membrane: 3% is relative to the quantity of CA, TEOS, and APTES-IBF.

Membrane	CA22-APT	CA22-APT-IBF(15%)	CA30-TEOS-APT-IBF(3%)
Cellulose Acetate (wt.%)	16.43	15.87	15.96
Formamide (wt.%)	21.26	20.54	28.20
Acetone (wt.%)	58.52	56.85	49.70
TEOS (wt.%)	-	-	4.85
APTES (wt.%)	3.78	-	-
HNO_3	3 drops*	3 drops*	3 drops*
APTES-IBF (wt.%)	-	6.74	1.29

*were not consider for the total mass

Table 4.2: Casting solution composition of the monophasic hybrid CA/SiO_2 membranes.

4.4 Membrane Drying

Typically, CA based membranes are stored in water at 4 ℃ and are used in the wet state when characterizing them in terms of permeation performance do determine the hydraulic permeability (Lp), MWCO, permeation of uremic toxins, etc. However, when the membranes need to be imaged by SEM, in order to analyse the membrane structure, the membranes must be dried by a method which ensures the

preservation of the original membrane properties, such as pore size, pore structure, etc. Letting the membranes to dry naturally when exposed to atmospheric conditions, or, direct water evaporation leads to the deterioration of the microporous membrane structure and generation of a membrane structure which is not the same as the membrane when wet [57]. In turn, this leads to permeation performance loss. Several drying processes, such as vacuum drying, freeze drying, and solvent exchange, have been proposed to maintain the original structure of the membrane [58]. The solvent exchange method involves the replacement of the water in the membrane pores by a water-miscible solvent that is a non-solvent for the membrane material in the multi-stage solvent exchange process. This solvent is then replaced by another, more volatile solvent which is then evaporated to produce the dry membrane with a structure similar or equal to the wet membrane. [59]. Replacing high surface tension water with a lower surface tension solvent reduces capillary pressures acting during drying, preventing pore collapse. The solvent is selected based on the membrane material since it must be a non-solvent for the membrane material [60].

In this work, the drying method used was adapted from Lui et al. [61] and briefly, this method involves soaking the membranes in different solutions for 24 hours at room temperature: deionized water, isopropanol as the first solvent, and n-hexane as the second solvent. The process begins with a 100% water solution and progresses to higher isopropanol solutions (25, 50, 75, and 100% V/V). The process is then repeated with isopropanol and n-hexane, increasing the n-hexane content each 24 hours. After being immersed in a 100% n-hexane solution, the membranes are allowed to dry at room temperature before being stored in a desiccator to ensure that they remain dry.

4.5 Membrane Characterization

4.5.1 Membrane structure by Scanning Electron Microscopy

Samples of the dry membranes were broken in liquid nitrogen, mounted on a stub, and gold-sputtered prior to being analysed by SEM (Thermo Scientific Phenom ProX). The top dense surface of the membranes was analysed and images were taken at a magnification of 1000x, cross-sections were imaged at a magnification of 700x, 1800x, and 4200x and the porous bottom layer was analysed and imaged at a magnification of 4000x. The software ImageJ (version 1.53t, from National Institutes of Health) was used to calculate the total and active layer thickness of the membranes on five different areas of each image of the cross-section of the membrane samples of each membrane, and the mean thickness and standard deviation were computed. The images were binarized using a threshold adjustment and then analysed using the Measure tool to calculate the average pore size of the porous bottom layer.

4.5.2 Membrane chemical composition by ATR-FTIR Spectroscopy

The chemical composition of the active layer surfaces of dried membrane samples was analysed by ATR-FTIR. The samples' infrared spectra were collected using a PerkinElmer Frontier FT-IR spectrometer (940 Winter Street, Waltham, MA 02451, USA), a Pike Miracle Single Reflection ATR sampling accessory from Pike Technologies, and a Ge crystal (Graseby Specac, Smyrna; sampling depth: 0.2-1.1 m at 4000-600 cm^{-1}). Averaging 256 images with a resolution of 4 cm^{-1} yielded each spectrum. The received infrared spectra were reported as percentage transmittance values as a function of wave number.

4.6 Membrane permeation performance

4.6.1 Artificial Kidney Experimental Setup

The permeation performance of the pure CA and monophasic hybrid membranes was determined in an experimental setup which simulates the pressure and flow conditions of a hemodialysis machine which is referred to in this thesis by the Artificial Kidney (AK) setup. Parameters, such as the hydraulic permeability (Lp), MWCO, permeation to SWSC and PBUTs, and long-term albumin filtration, were studied in a Single Hemodialys Membrane Module (SHDMM) to determine the mass transfer properties related with the metabolic functions of the kidney. Figure 4.5 shows the schematic representation of the AK experimental setup. The feed solution, stored in the feed reservoir, is circulated throughout the system by a peristaltic pump (ISM1079B, Pennsylvania, USA). A damper positioned before the first pressure sensor (P1) dampens the flow pulsations imposed by the peristaltic pump before entering the SHDMM. The feed solution is then returned to the feed reservoir with a second pressure sensor (P2) registers the pressure at the outlet of the SHDMM. The permeate (which crosses the membrane) is collected in a permeate reservoir after passing a third pressure sensor (P3). The medical grade pressure sensors (DPT-100, Westmeath, Ireland), capable of registering fluctuations as low as 1 mmHg, are connected to a computer, where the Labview software registers the pressures every 2 seconds. The tubing where feed and permeate solutions are circulated is made of medical grade tygon (ND 100-65, Ohio, USA).

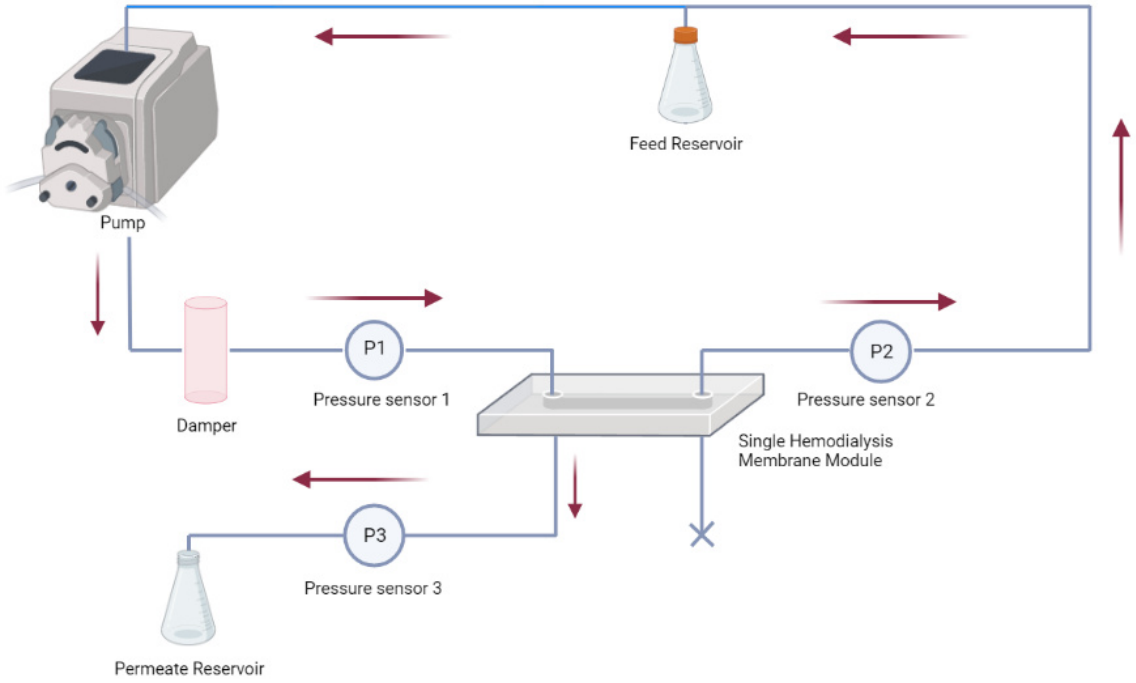

Figure 4.5: Experimental Setup for permeation studies.

Figure 4.6 shows the schematic representation of the SHDMM which was designed by the Onshape software and printed on a 3D printer (Ultimaker 2^+, Gelderland, Netherlands). The top piece seals the feed flow chamber and the bottom piece seals the permeate collecting chamber; between them is the membrane sheet with its active layer facing upwards on top piece. The membrane must be held in place by a spacer with a slit´geometry presenting an effective area of 4.76 cm^2 (middle piece). Due to the transmembrane pressure imposed in the AK setup, the filtration of fluids and solutes through the membrane occur exclusively by convection processes. The height of the feed flow channel is an important parameter when assessing fouling events. The channel height (2B) may vary during permeation studies due to the deposition of molecules on top of the membrane. The dimensions of the feed and permeate microchannels are 2B = 0.3 cm, width (W) = 1.5 cm, and length (L) = 5 cm. Moreover, the total membrane surface area assumes the value of 7.5 cm^2.

Prior to each permeation study, the system is primed with water and the membrane is compacted. Membrane compaction enables the membrane to adapt and accommodate to the module compartment without causing structural damage. This procedure is carried out at a pressure which is 20% higher than the maximum working TMP. Compaction was carried out by circulating milli-Q water through the installation, at a feed flow rate of approximately 135 mL/min and a TMP in the range of 200-250 mmHg for 2 hours.

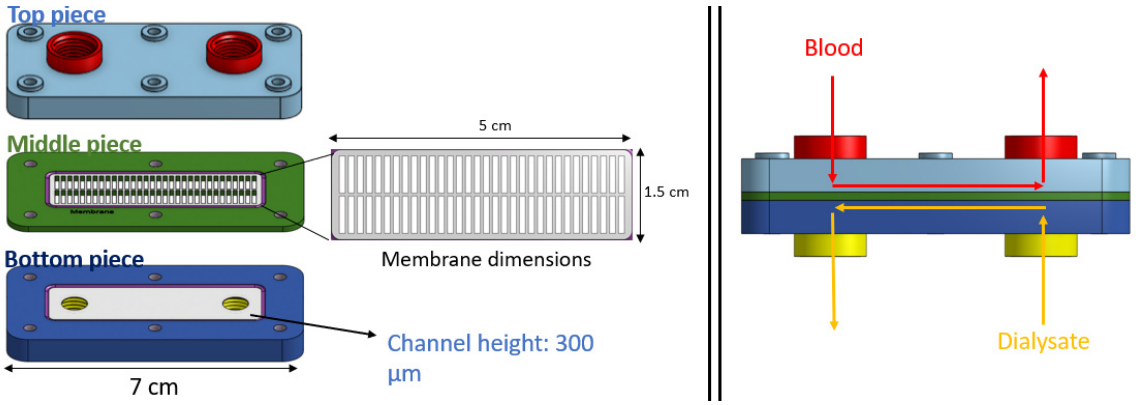

Figure 4.6: Schematic representation of Single Hemodialysis Membrane Module (SHDMM). Unit I seals the feed flow chamber. Unit II seals the permeate collecting chamber. Spacer is the supporting surface for the membrane. Adapted from [3].

TMP is determined as the average pressure in the blood compartment minus the average pressure in the dialysate compartment. It is defined as the hydrostatic pressure gradient that enables for ultrafiltration or convection through a dialyzer membrane, i.e. the force required to circulate water through the membrane [47]. In this case, TMP is given by Equation 4.1:

$$TMP = \frac{P1 + P2}{2} - P3 \tag{4.1}$$

Where P1, P2, and P3 are the pressure values of the different sensors.

The pressure drop (ΔP) given by Equation 4.2 is the difference in pressures between the input and output of the blood compartment from the membrane module. This parameter aids in monitoring membrane performance because, assuming flow rate and temperature are constant, pressure drop should remain constant until there is fouling or a physical barrier.

$$\Delta P = P1 - P2 \tag{4.2}$$

The microchannel's half-height (B) is obtained by adjusting Equation 4.3, which is comparable to the Hagen-Poiseuille law for circular tubes and describes the fully-developed laminar flow of a Newtonian fluid in a narrow slit [62]:

$$B = \sqrt[3]{\frac{2}{3}\frac{\mu L}{W}\frac{Q_F}{\Delta P}} \tag{4.3}$$

Where Q_F is the volumetric feed flow rate collected by pump calibration curve present in Appendix A.1, W and L is width and length of the spacer, μ is the viscosity of the fluid and Δ P is the pressure drop.

Shear stress (τ) is a fluid dynamics parameter that is essential for avoiding blood damage such

as platelet activation and hemolysis. It is crucial to operate the artificial devices in a safe mode to guarantee that the maximum shear stress is less than the hemolysis threshold stress. A healthy human vessel exhibits a shear stress of roughly 0.1 to 20 Pa: 0.1 to 1 Pa for veins and 1 to 20 Pa for arteries [63]. Platelet activation increases dramatically when exposed to shear stress higher than 20 Pa and mechanical cell damage, hemolysis, at 30 Pa, according to previous studies [63, 64].

The shear stress at the flow boundaries, or microchannel walls, can be determined by balancing the shear force at the wall against the pressure gradient in a slit channel [62], as shown in Equation 4.4.

$$\tau = \frac{3\mu Q_F}{2B^2 W} \tag{4.4}$$

Shear rates, γ, at the wall are determined by dividing shear stress by viscosity, as shown in Equation 4.5.

$$\gamma = \frac{\tau}{\mu} = \frac{3Q_F}{2B^2 W} \tag{4.5}$$

Figure 4.7 depicts the filtration process that occurs in the AK setup. The ultrafiltration membrane permeates both uremic toxins and water, and it is expected to retain vital blood components such as serum albumin. Thus, it is important that the pores of the membrane have a certain MW that allow toxins to pass through while also retaining proteins.

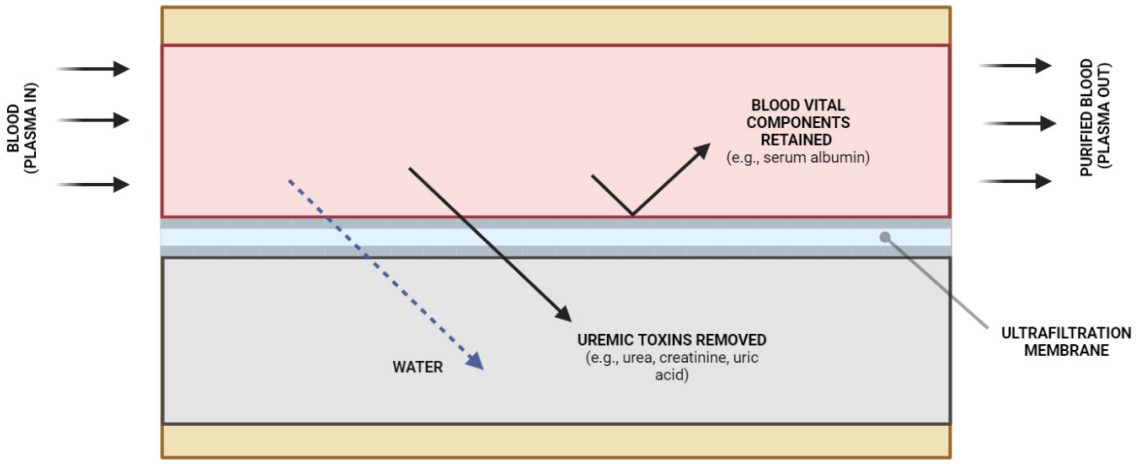

Figure 4.7: Representation of the filtration process of blood (plasma).

4.6.2 Ultrafiltration Experimental Setup: CELFA P-28

The permeation performance of the membranes in terms of hydraulic permeability (Lp) and MWCO was also evaluated in a lab-scale crossflow ultrafiltration installation, Celfa P-28 represented in Figure 4.8.

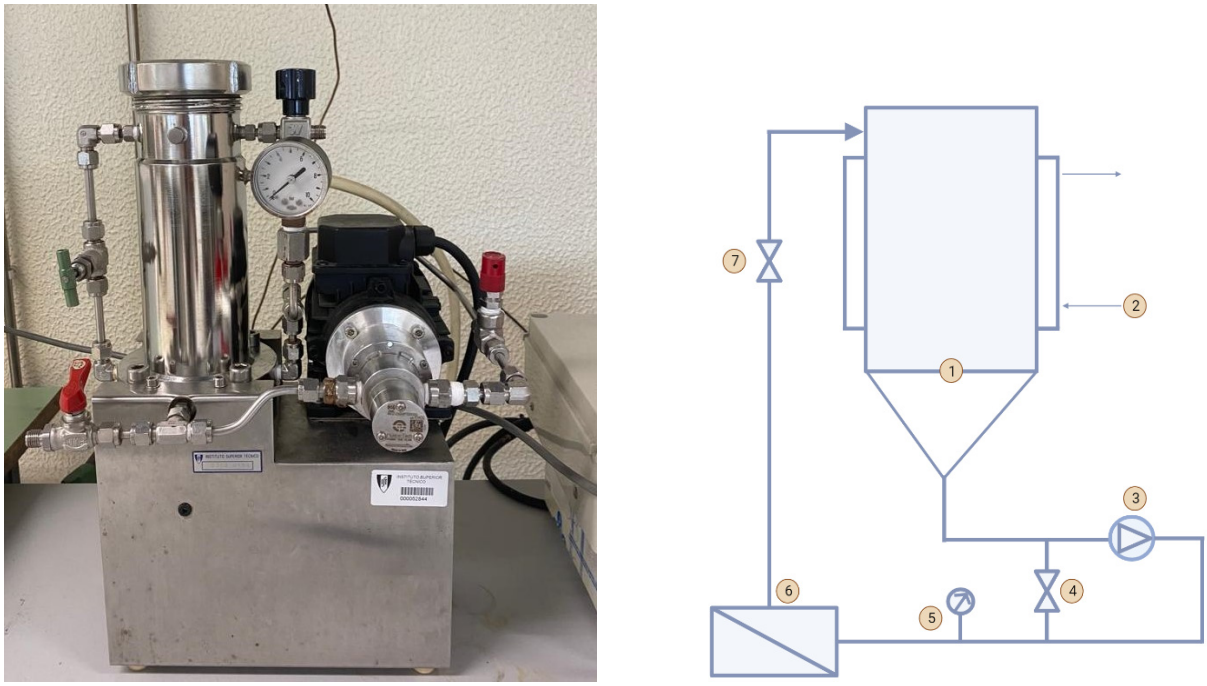

(a) CELFA P-28 ultrafiltration installation.

(b) Schematic representation.

Figure 4.8: CELFA P-28 ultrafiltration experimental setup. Adapted from [4]

A feed tank, a heat/cooling jacket, a pump and potentiometer, a manometer, a pressure retention valve, a permeate and a concentrate collector are all part of the installation. The feed tank (1) has a capacity of 500 mL and is covered by a heat/cooling jacket (2), which allows the temperature of the feed solution to be controlled. The pump (3) contains a potentiometer that, in combination with the pressure retention valve (7), controls the flow rate of the feed solution recirculation. The selected pressure can be read from the manometer (5). If the concentrate collector (4) is open, the feed solution permeated by the membrane is collected. If the concentrate collector's valve is closed, the solution is recirculated back into the feed tank. The calibration curve of the volumetric flow rate Vs pump potency is present in Appendix A.2. The membrane in study is placed on top of a filter paper with an area of 25 cm^2. The membranes were compacted before the beginning of all permeation experiments. This experimental setup can operate at transmembrane pressures ranging between 0 and 7 bar.

4.7 Permeation Studies

4.7.1 Hydraulic Permeability, Lp

The hydraulic permeability (Lp) describes the diffusive or convective transport through a membrane under the influence of a hydrostatic pressure driving force. It indicates the water flux per unit area

per unit time per unit of applied pressure. [13]. It is most directly influenced by the membrane mean pore size [65]. Equation 4.6 describes the permeate water flux (J_w) which is defined as the amount of permeate produced per unit area of membrane surface per unit of time:

$$J_w = \frac{V}{A_{eff} \cdot t} = \frac{Q_{UF}}{A_{eff}} \tag{4.6}$$

where V is the volume of permeate, t is the measuring time, A_{eff} is the effective membrane filtration area, and Q_{UF} is the ultrafiltration flowrate measured.

When J_w is expressed as a function of TMP, a linear correlation is obtained and the Lp is determined from the slope of the straight line:

$$Lp = \frac{J_W}{TMP} \tag{4.7}$$

All experiments were made with deionized water at room temperature. Permeate is collected, weighed, and transformed in volume by water density and corrected for a temperature of 25ºC. Full Lp data is described in Appendix B.

4.7.2 Molecular Weight Cut-Off (MWCO)

A membrane's MWCO is frequently used to characterize a membrane in terms of pore size distribution and retention. It is defined as the lowest molecular weight (in Da) at which the membrane retains more than, 90% of a solute with a known molecular weight [66]. Linear and neutral polymers such as PEG or dextran are used to determine the MWCO. A retention curve is constructed by measuring the rejection coefficient, R, to several PEGs with increasing molecular weights of 1000 Da, 3000 Da, 6000 Da, 10 000 Da, 20 000 Da and 35 000 Da, respectively. The increasing MW sequence is selected on purpose because 90% of rejection may be attained with a lower MW than the highest established.

The rejection factor, f, defined by Equation 4.8, is characterized as the percentage of how much solute, initially in the feed solution, passes through the membrane to the permeate after a given time. This parameter tends to be zero for molecules that are able to cross the membrane pores and close to 100% for molecules retained by the membrane.

$$f = \frac{C_f - C_p}{C_f} \tag{4.8}$$

Where C_p corresponds to the solute concentration that was permeated by the membrane after a certain time and C_f corresponds to the initial feed solution concentration.

The initial concentration of the feed solutions of each PEG was 500 ppm and the permeation studies were performed in the Celfa-p28 under total recirculation mode with a feed flowrate of 11.85 cm^3/s and

at a TMP of 1 bar.

Solute concentrations in the permeate and feed solutions were determined in triplicate using a Total Organic Carbon (TOC) analyzer (TOC-VCPH/CPN, Shimadzu, Japan). The total organic carbon of each sample was estimated using the calibration curves for different PEGs which are present in Appendix A.3

Thus, the MWCO is determined from the intersection of the linearized curve of $log(\frac{f}{1-f})$ as a function of MW and the MWCO value is provided by the intersection of the 90% rejection factor and the line connecting all rejection factors.

4.7.3 Permeation to uremic toxins

4.7.3.A Small Water-Soluble Compounds (SWSC)

SWSC have molecular weights lower than 500 Da and are easily removed by current HD membrane. Thus, the novel membranes must be efficient in their removal, i.e., must possess low rejection factors. SWSC such as creatinine, urea, and uric acid can be used to assess membrane performance in their removal. A healthy person with normal renal function has lower blood concentrations of these UTs, while CKD patients have significantly higher concentrations.

The rejection coefficients, R, to urea, creatinine, and uric acid of CA30-TEOS-APT-IBF(3%) were evaluated according to Equation 4.8. The initial feed solutions for urea and creatinine were 4.6 g/L, and 240 mg/L, respectively. These concentrations were used according to the highest reported concentrations of urea [6] and creatinine [6] in patients with ESRD. The concentration of uric acid in patients with ESRD can be as high as 83 mg/L [5] but due to its very low solubility, a concentration of 60 mg/L was used. Urea and creatinine were dissolved directly in healthy patients' plasma, whereas uric acid was first dissolved in 25 mL of PBS before being dissolved in plasma.

The permeation studies were performed with plasma from healthy patients spiked with the toxins mentioned before (one at a time) for 4 hours at a feed flow rate of 100 mL/min and a TMP of 200 mmHg. Solute concentrations in the permeate and the feed solution were determined by UV-VIS spectroscopy (spectrophotometer UV-1700 PharmaSpec, Shimadzu, Japan). Absorption is highest at wavelengths of 200, 230, and 293 nm for urea [67], creatinine [68], and uric acid [47], respectively.

However, it was observed that for all the three toxins, the concentrations obtained in the permeate samples were much higher than the initial feed solution. These results were not considered since the toxin quantification was not correctly performed. After some research, it was concluded that there are some plasma components, such as immunoglobulin, that can be permeated by the membrane (MW = 150 Da) and absorb in the wavelengths used for the protein quantification [69]. As a result, these plasma components can interfere with toxin quantification by UV-VIS spectroscopy and explain the results obtained. Some studies [33, 47] reported several experiments aimed at the SWSCs quantification where it

was used PBS instead of plasma as a feed solution.

4.7.3.B Protein-Bound Uremic Toxins (PBUTs)

Permeation of IS, a surrogate marker for PBUTs, was evaluated in the AK experimental setup using plasma from healthy patients spiked with Indoxyl Sulphate (IS). 200 mL of plasma spiked with 40 mg/L of IS (simulating mean uremic concentrations in dialysis patients [6]) was recirculated through the SHDMM containing the CA30 and CA30-TEOS-APT-IBF(3%) membranes in the AK setup for 8 hours at a feed rate of 100 mL/min and a TMP of 200 mmHg. The plasma spiked with IS was previously incubated overnight at 37℃ (human body temperature) to ensure enough time for the binding between IS and HSA to occur. Previous studies suggest that 98% of the total concentration of IS binds to HSA during this time [14].

Concentrations of IS were determined in samples taken from the permeate and feed solutions at different times of the experiment by fluorescence spectroscopy (fluorometer - FluoroJasco FP8500, Pfungstadt, Alemanha). The samples were excited at 275 nm and the emission spectra was collected from 300-500 nm at a scan speed of 200 nm/min using Xe as a light source. The calibration curve (emission vs concentration) can be found in Appendix A.4.

To quantify the free amount of IS, three samples (30 mL) are collected from the feed reservoir at the beginning, middle, and end of the assay. 10 mL of each sample is centrifuged (Sorvall RC 6 equipment, 10800 rpm; 30 min; 20℃; acceleration 7; deceleration 3) with a CA membrane (MWCO 20 kDa) in order to separate the free portion of IS from the bound part. (the MW of HSA is 66.5 kDa which is much higher than the MWCO of the CA membrane). The concentration of the IS free portion, which is in the permeate of the centrifuge tubes, is then determined by fluorescence spectroscopy.

The initial total form of IS is the total amount spiked in plasma (40 mg/L), which is quantified by fluorescence spectroscopy at the beginning of the experiment. The final total form of IS in the feed solution, on the other hand, is calculated by subtracting from the initial total form the IS free form (collected from the feed reservoir as explained above) and the IS quantified in the permeate. Furthermore, the bound form is calculated by subtracting the free form from the total form obtained.

The HSA concentration in the permeation solutions is also measured using spectroscopy to confirm that the membrane does not allow protein passage.

4.7.4 Long-term HSA filtration

Permeation of HSA experiments were carried out using plasma collected from healthy patients in the AK experimental setup. 150-200 mL of plasma were circulated between 4 and 8 hours through the SHDMM containing the membranes CA30, CA30-TEOS-APT-IBF(3%), and CA35 at a feed rate of 100 mL/min and a TMP of 200 mmHg. Samples from the feed reservoir and permeate were collected every 60

minutes and HSA was quantified by the Bradford and modified Bradford methods, respectively. The Blue Coomassie reagent, also called Bradford reagent, is commonly used for the protein detection, and was prepared as described [70]. UV spectrophotometry is used for detection. The standard Bradford method is used to quantify high protein concentrations between 100 and 1000 g/L and concentrations in this range exhibit linear behaviour at 595 nm with a sample:Bradford reagent ratio of 1:50. On the other hand, for lower concentrations ($<$ 100 mg/L), linearization is made with different peaks and proportions [71] and it is used the modified method (0-100 mg/L). A calibration curve is described by the ratio of two peaks, 450 and 590 nm, as well as a ratio of 1:4 sample/Bradford. Moreover, since it is expected that membranes do not permeate proteins, significant amounts of protein are expected in feed solutions and are measured using the standard Bradford method, whereas low HSA concentrations are expected in permeate stream samples and are measured using the modified method. Absorbance values are converted to albumin concentrations by the calibration curves shown in Appendix A.5.

5

Results and Discussion

5.1 Membrane Characterization

5.1.1 Membrane structure by Scanning Electron Microscopy

Figure 5.1 shows the SEM micrographs obtained for the active layer surface of the dried 5.1a CA22-APT and 5.1b CA35 membranes. The active layer of the membranes is responsible for the membrane selectivity, and both exhibit completely dense active layers with no visible pores at a magnification of 1000x. The CA22, CA22-APT-IBF(15%) and CA33 membranes also showed a complete dense active layer with no significant differences. On the other hand, Figure 5.2 depicts the active layer surface of the dried 5.2a CA30 and 5.2b CA30-TEOS-APT-IBF(3%) membranes. Observation of the CA30 membrane reveals several parallel marks at the active layer surface, which were previously reported for a monophasic hybrid membrane with also 30% formamide [72]. Moreover, the CA30-TEOS-APT-IBF (3%) exhibits a similar pattern, but with larger and more irregular marks. These patterns discovered for both membranes must be investigated further to determine whether the parallel features are caused by the drying process rather than the actual membrane synthesis process.

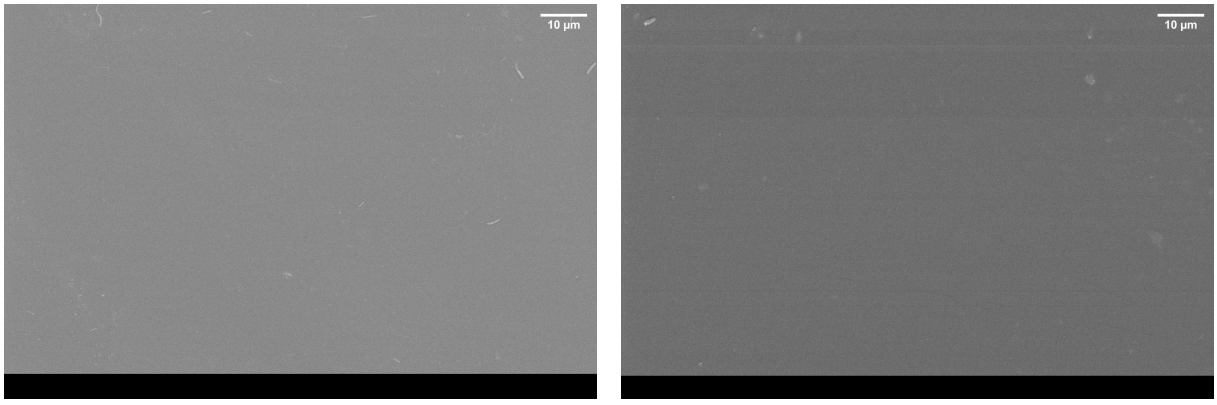

(a) **(b)**

Figure 5.1: SEM images: top dense surface imaged at a magnification of 1000x and 4000x for (a) CA22-APT and (b) CA35 membranes.

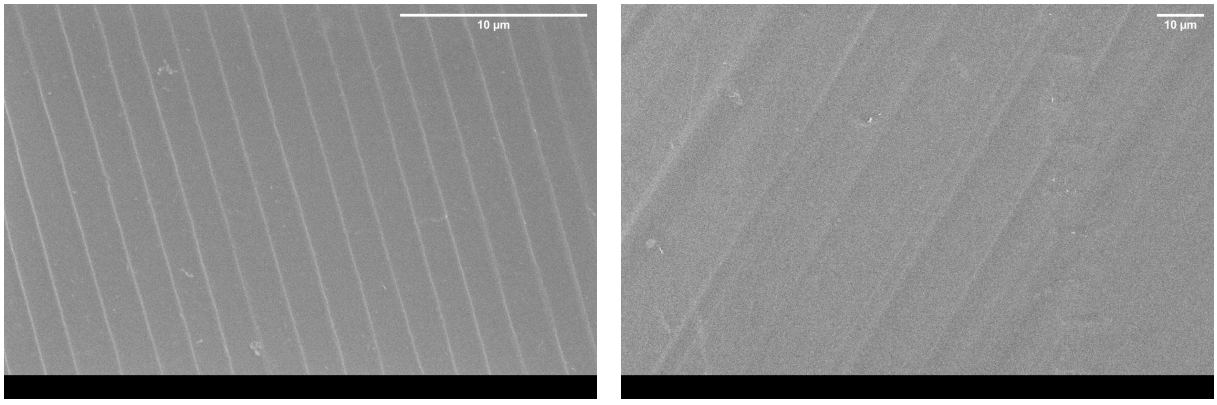

(a) **(b)**

Figure 5.2: SEM images: top dense surface imaged at a magnification of 1000x for (a) CA30 and (b) CA30-TEOS-APT-IBF(3%) membranes.

Figure 5.3 represents the cross section of the 5.3a CA22 and 5.3b CA22-APT-IBF(15%) membranes. From these images it is possible to confirm the integral asymmetric structure with a very thin dense active layer and a much thicker, porous substructure.

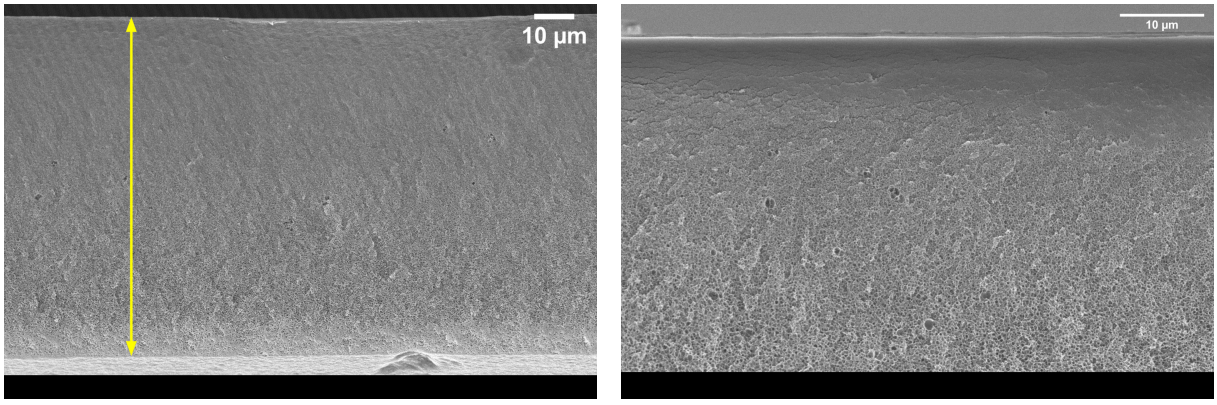

(a) **(b)**

Figure 5.3: SEM images: cross section imaged at a magnification of 860x and 1800x for (a) CA22 and (b) CA22-APT-IBF(15%) membranes.

Figure 5.1 depicts a more detailed analysis of the structure of the CA22-APT (Figure 5.1a and Figure 5.1b) and CA22-APT-IBF(15%) (Figure 5.1c, Figure 5.1d, Figure 5.1e and Figure 5.1f) membranes. Figure 5.1a shows several macroporous structures present in CA22-APT membrane. Inside these macroporous (Figure 5.1b) it is possible to observe the existence of several clusters. Previous works [73] also detected the existence of these clusters. Further investigation (chemical qualitative and quantitative analysis) is required to determine whether the clusters were formed by polymer, silica, or amine groups. It is also possible to observe the existence of macroporous throughout the entire CA22-APT-IBF(15%) membrane (Figure 5.1c and Figure 5.1e). Figure 5.1d depicts a higher magnification image of these macropouros, and it would seem that these structures do not enable water or other fluids to pass through and be permeated. As a result, the membrane structure can clarify the very low hydraulic permeability of these two membranes, as discussed further in this study. All of the other membranes (CA22, CA30, CA30-TEOS-APT-IBF(3%), CA33, and CA35) lack these macroporous structures. As a result, the hypothesis that these structures were formed by the silica precursor APTES alone (without TEOS) can be reinforced.

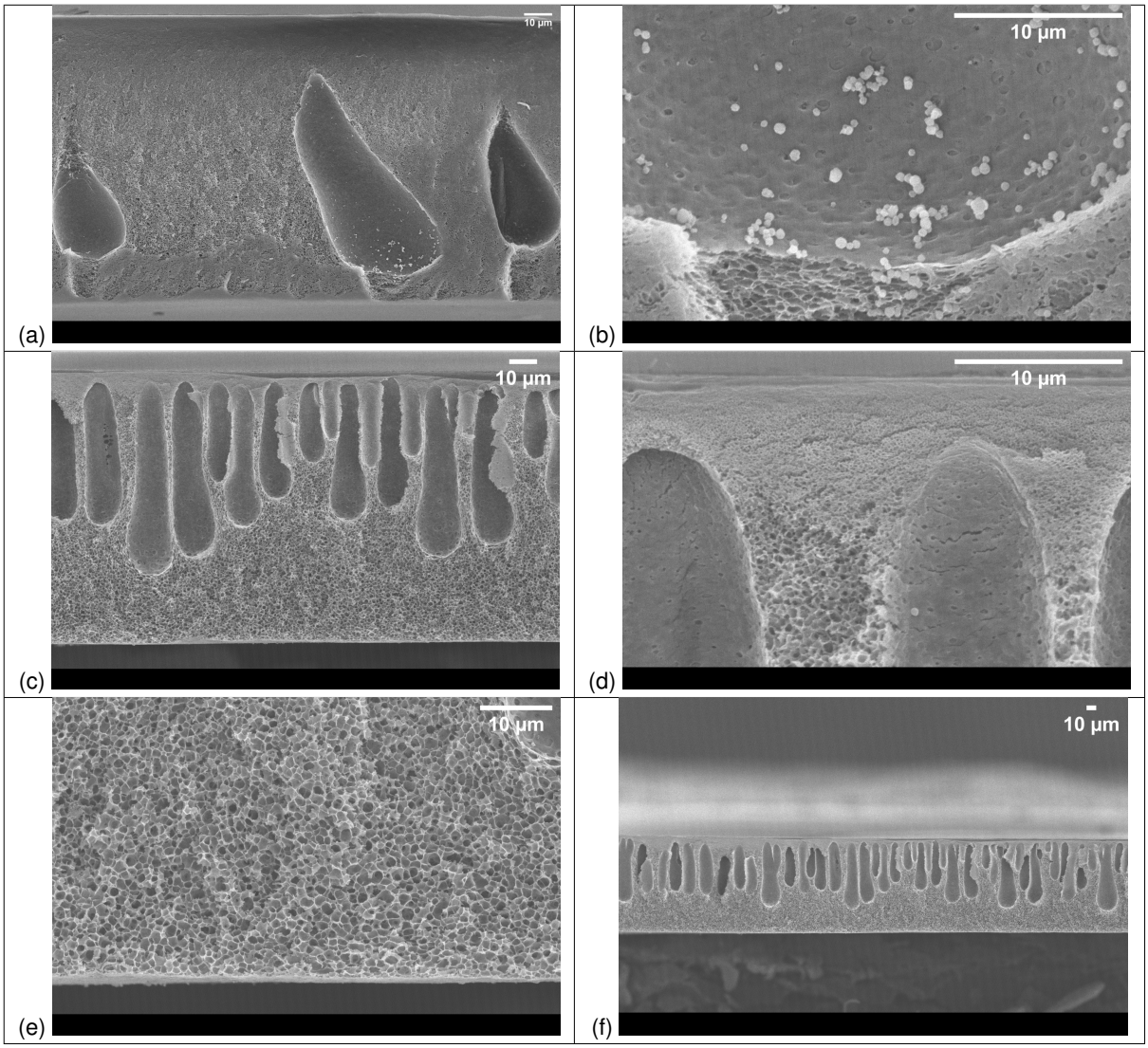

Table 5.1: SEM images: cross section imaged at a magnification of 700x, 1800x, 4200x for the CA22-APT (Figure 5.1a and Figure 5.1b) and CA22-APT-IBF(15%) (Figure 5.1c, Figure 5.1d, Figure 5.1e and Figure 5.1f) membranes.

Table 5.2 represents the overall membrane thickness of the membranes which was obtained from the cross-section images. For the CA22, CA22-APT, CA22-APT-IBF(15%), CA30, CA30-TEOS-APT-IBF(3%), CA33, and CA35 membranes were obtained a thickness of 83.8 ± 0.39, 101.3 ± 0.74, 95.3 ± 1.56, 77.3 ± 0.53, 83.4 ± 1.13, 96.2 ± 0.19, 88.6 ± 0.65 µm, respectively. Formamide is considered a swelling agent, and it is expected that an increase in its content percentage, in the casting solution, translates into an increase in the total thickness of the membrane [51]. Analyzing the thickness of the pure cellulose acetate membranes (CA22, CA30, CA33, and CA35), it is possible to conclude that the CA33 membrane has the highest membrane thickness (96.2 ± 0.19 µm)), while the CA30 has the lowest (77.3 ± 0.53 µm)). However, due to the formamide content, CA35 membrane was expected to

be the thickest, while CA22 membrane would be the thinnest. Furthermore, when comparing the CA22, CA22-APT, and CA22-APT-IBF(15%) membranes, it can be observed that the CA22-APT and CA22-APT-IBF(15%) are thicker (101.3 ± 0.74 and 95.3 ± 1.56 µm, respectively) than the CA22 (83.8 ± 0.39 µm), indicating that the APTES and IBF can both have an effect on the final thickness of the membrane. The same results were obtained for the membranes with 30% of formamide: the CA30-TEOS-APT-IBF(3%) membrane is thicker (83.4 ± 1.13 µm) than the CA30 membrane (77.3 ± 0.53 µm). However, the difference is only 6 µm, indicating that the silica precursor had no significant influence on the membrane thickness in this case.

Membrane	Thickness (µm)
CA22	83.8 ± 0.39
CA22-APT	101.3 ± 0.74
CA22-APT-IBF(15%)	95.3 ± 1.56
CA30	77.3 ± 0.53
CA30-TEOS-APT-IBF(3%)	83.4 ± 1.13
CA33	96.2 ± 0.19
CA35	88.6 ± 0.65

Table 5.2: Mean membrane thickness and standard deviation for the cross-section images calculated by the ImageJ image analysis programme.

5.1.2 Membrane chemical composition by ATR-FTIR Spectroscopy

The ATR-FTIR spectra of the CA22, CA30, CA33, and CA35 membranes are compared in Figure 5.4. The broad band centred at approximately 3478 cm^{-1} is assigned to the OH stretching mode, ν(OH), and contains contributions from non-esterified cellulose hydroxyl groups as well as silanol groups.

Identically to previous work [50], the strong carbonyl stretching mode, ν(C=O), appears at 1742 cm^{-1}, while the antisymmetric, ν_{as}(C-O-C), and symmetric, ν_s(C-O-C) stretching modes of the ester appear as strong bands at 1228 cm^{-1} and 1040 cm^{-1}, respectively. Moreover, the band centered at 1370 cm^{-1} is assigned to δCH_3 [56]. The weak band centered at 904 cm^{-1} confirms the presence of acetate methyl groups [56].

All the pure cellulose acetate membranes studied, CA22, CA30, CA33, and CA35 present the same ATR-FTIR spectra, as expected.

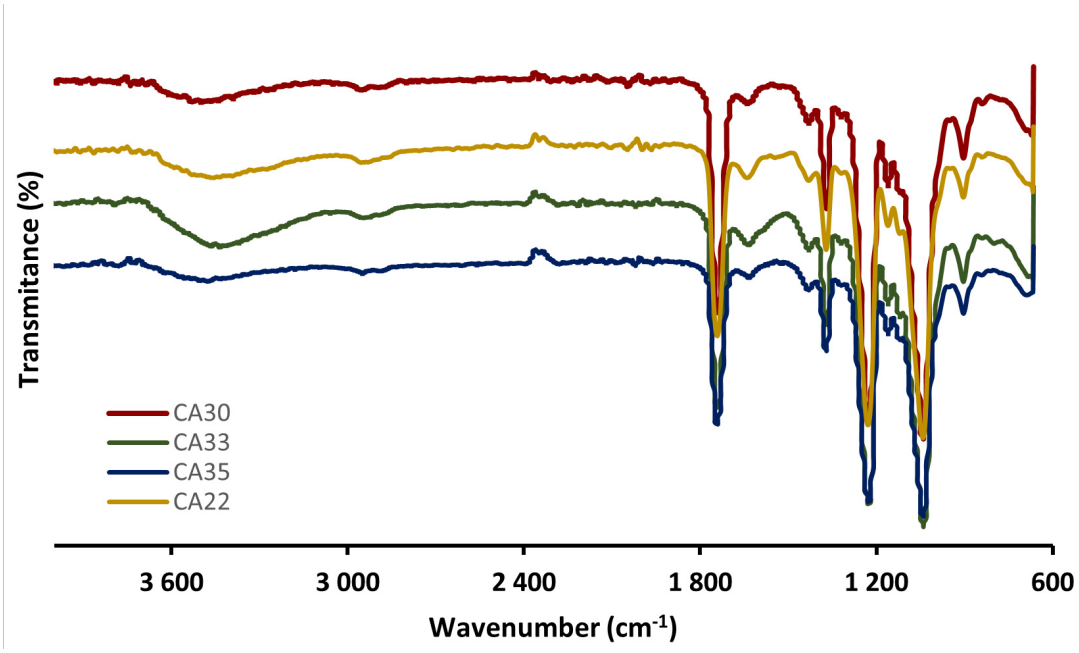

Figure 5.4: Wide-range ATR-FTIR spectra (4000-600 cm^{-1}) of the CA22, CA30, CA33, and CA35 membranes.

In order to analyse the ATR-FTIR spectra of the monophasic hybrid membranes (CA22-APT, CA22-APT-IBF(15%), and CA30-TEOS-APT-IBF(3%)), the ATR-FTIR spectra of the silica precursors TEOS and APTES, as well as the ATR-FTIR spectra of the binding competitor IBF, were accomplished.

Figure 5.5a depicts the comparison between the ATR-FTIR spectra of APTES with the CA22 and CA22-APT membranes. It is possible to observe that the CA22-APT membrane presents the same bands than the CA22 membrane which were detailed previously. Throughout the data interpretation, it is possible to observe some bands of the APTES and CA22-APT spectrums overlapped, mainly between 1040 and 1200 cm^{-1}. *Mendes et al.* [46] reported the existence of important bands of monophasic hybrid membranes such as ν(Si–O–Si) and ν(Si–O–C) which occur in the regions 1055 to 1165 cm^{-1} and 1115 to 1175 cm^{-1}, respectively. Therefore, since in this range there are some conflicts between bands from the cellulose acetate and SiO_2 groups, it is possible that there are some overlapping peaks from the SiO_2 groups which are not identified in the spectrum of the membrane or due to the low percentage of APTES in the membrane, the bands were not identified.

On the other hand, Figure 5.5b represents the comparison between the ATR-FTIR spectra of the CA22, CA22-APT-IBF(15%) membranes with the ATR-FTIR spectra of IBF. The literature [74] shows that for a characteristic vibration frequency of 3095 cm^{-1} and between 1579 and 1408 cm^{-1}, there are located the aromatic C-H and C=C stretching, respectively. From the data observation, it is possible to observe these peaks in the ATR-FTIR spectra of IBF, however for the CA22-APT-IBF(15%) membrane, these bands are not visible. This observation can be attributed to a variety of factors: the superposition of the characteristic peaks or the very low amount of IBF in the membrane composition.

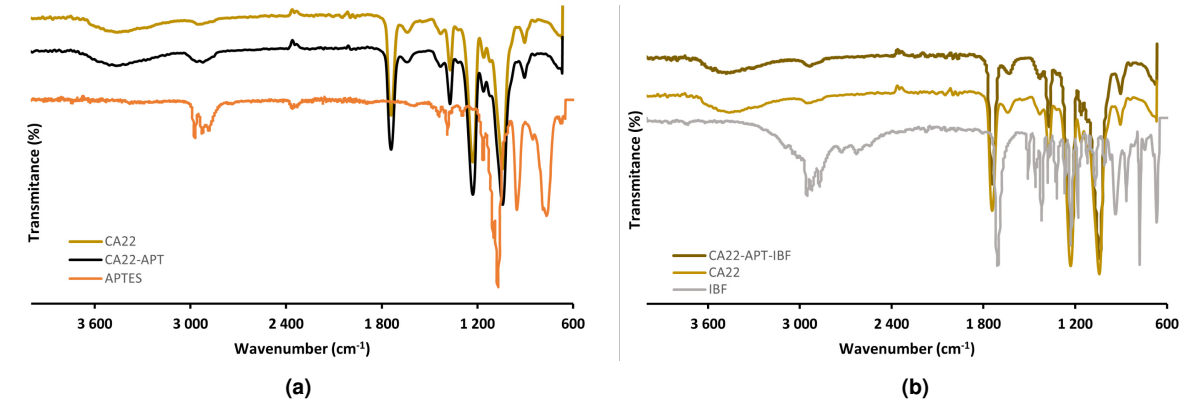

Figure 5.5: Wide-range ATR-FTIR spectra (4000-600 cm^{-1}) of the (a) APTES, CA22 and CA22-APT membranes and (b) IBF, CA22 and CA22-APT-IBF(15%) membranes.

Figure 5.6a represents the comparison between the ATR-FTIR spectrum of the CA30, CA30-TEOS-APT-IBF(3%) membranes and SiO_2 precursors, TEOS and APTES. Some overlapping bands can be detected in the 1055 to 1175 cm^{-1} range. Similarly to the previously described, there are some SiO_2 groups in this region that are not identified in the CA30-TEOS-APT-IBF(3%) spectra, possibly due to the intersection of peaks from the cellulose acetate and SiO_2 groups. *Al-Oweini et al.* [75] reported the existence of the ν_s(Si-O-Si) vibration band at 794 cm^{-1}. This peak can be detected in the TEOS and APTES ATR-FTIR spectrum, however it is not visible in the CA30-TEOS-APT-IBF(3%) membrane spectra.

Figure 5.6b depicts the ATR-FTIR spectrum of the CA30 and CA30-TEOS-APT-IBF(3%) membranes, as well as the binding competitor IBF. Once again, several vibration bands of the IBF spectra do not appear in the ATR-FTIR spectrum of the CA30-TEOS-APT-IBF(3%) membrane. These results can be attributed to the membrane's lower IBF content.

For future analysis, the ATR-FTIR spectra of the precursor APTES-IBF should also be included.

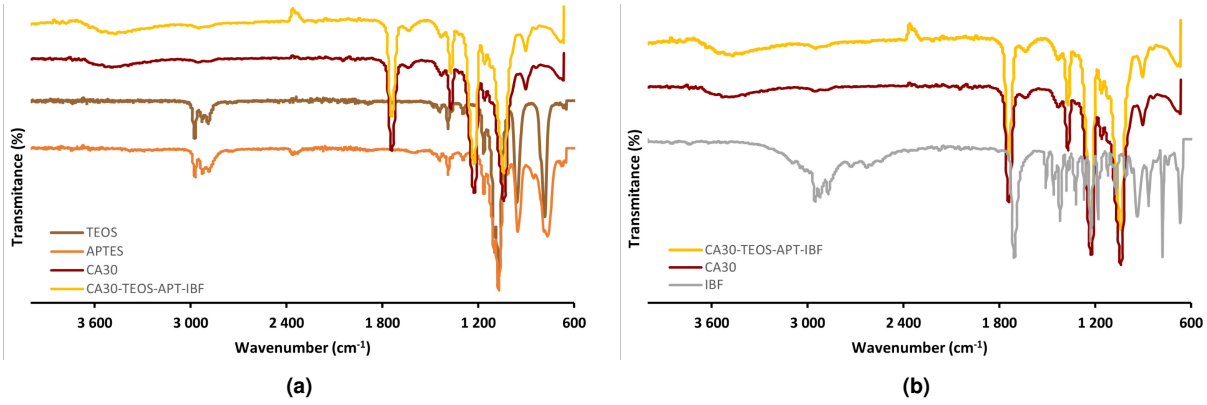

Figure 5.6: Wide-range ATR-FTIR spectra (4000-600 cm^{-1}) of the (a) APTES, TEOS, CA30 and CA30-TEOS-APT-IBF(3%) membranes and (b) IBF, CA30 and CA30-TEOS-APT-IBF(3%) membranes.

Table 5.3 access the information about the assignment of the ATR-FTIR spectra bands of the hybrid and pure CA membranes.

Wavenumber (cm^{-1})	Type of vibration
3478	ν(OH) [46, 56]
1742	ν(C=O) [46, 50]
1370	δCH_3 [46, 56]
1228	ν_{as}(C-O-C) [46, 56]
1040	ν_s(C-O-C) [46, 56]

Table 5.3: Assignment of the ATR-FTIR spectra bands of the hybrid and pure CA membranes.

5.2 Pressure drop, microchannel height, shear rate and shear stress at the wall

Table 5.4 contains the microchannel height (2B) results obtained for the SHDMM when containing the CA30, CA30-TEOS-APT-IBF(3%), CA33, and CA35 membranes. The height of the channel when no membrane is present is 300 µm but when a membrane is placed inside the SHDMM this value will change. According to the data, for the CA30, and CA30-TEOS-APT-IBF(3%) membranes the value of 2B is identical (260 and 258 µm, respectively). On the other hand, the CA33, and CA35 membranes also present a very similar 2B, being 229 µm for the CA33 and 226 µm for the CA35 membrane. In addition, the differences observed can be related to the composition of the membranes: the CA33 and CA35 membranes contain a higher percentage of formamide than the CA30 and CA30-TEOS-APT-IBF(3%) membranes, and thus are thicker, as confirmed by SEM, resulting in a decrease in 2B for these membranes. Both the CA30 and CA30-TEOS-APT-IBF(3%) membranes contain 30% formamide, so the 2B is nearly the same, since have similar thickness values, as proved previously by SEM.

	CA30	CA30-TEOS-APT-IBF(3%)	CA33	CA35
2B (µm)	260	258	229	225

Table 5.4: Microchannel´s height (µm) for the CA22, CA30, CA30-TEOS-APT-IBF(3%), CA33, and CA35 membranes at Q_F = 100 mL/min. Experiments were carried out with ultra-pure water.

The data reported in Table 5.5 contains the shear stress (τ), shear rate (γ), and ΔP obtained for the CA30, CA30-TEOS-APT-IBF(3%), CA33, and CA35 membranes. The experiments were performed with ultra-pure water at $25^{\circ}C$ in the AK setup at a feed flow rate (Q_F) of 100 mL/min and for TMPs ranging from 125 – 135 mmHg. Furthermore, the shear stress assumed very similar values for all of the membranes studied, ranging from 9.9 to 12.0 Pa, with the CA30 exhibiting the lowest value. The shear rate is also very similar for all the membranes ranging from $1.11 \cdot 10^4$ to $1.36 \cdot 10^4$ s^{-1} as well as the ΔP which vary from 26.0 to 39.7 mmHg. These results are consistent with expectations; it is implied that

these parameters do not vary depending on the membrane used since they are mainly determined by the feed flow rate, fluid viscosity, and SHDMM dimensions. However, it is important to confirm that these values are within the normal range for each membrane and assay.

	CA30	CA30-TEOS-APT-IBF(3%)	CA33	CA35
τ (Pa)	9.90	12.0	11.6	11.9
γ (s^{-1})	$1.11 \cdot 10^4$	$1.35 \cdot 10^4$	$1.30 \cdot 10^4$	$1.36 \cdot 10^4$
ΔP (mmHg)	26.0	34.9	38.1	39.7

Table 5.5: Shear stress (Pa), shear rate (s^{-1}), and ΔP (mmHg) obtained at 25°C for the CA22, CA30, CA30-TEOS-APT-IBF(3%), CA33, and CA35 membranes at Q_F = 100 mL/min. Experiments were carried out with ultra-pure water.

It is important to compare the shear stress, shear rate, and pressure drop in experiments performed with different types of fluids. Table 5.6 contains the results obtained for experiments carried out with plasma at a 25°C and a Q_F of 100 mL/min for the CA30, CA30-TEOS-APT-IBF(3%), and CA35 membranes. Comparing the data from the experiments performed with water (Table 5.5) and plasma (Table 5.6), carried out at the same temperature and Q_F, it is possible to conclude that the shear stress achieved the highest results for the testes with plasma for all membranes except for the CA30-TEOS-APT-IBF(3%) membrane. These values are still within the range of shear stress that can be used to safely operate artificial devices while avoiding hemolysis mentioned before. However, *Holme et al.* [76] noticed platelet activation and aggregation at shear rates of 10500 s^{-1} and above in an in vitro study. Thus, these considerations should be considered in future experiments performed with blood and if necessary, decrease the Q_F of the experimental setup. For the same Q_F, plasma achieved higher ΔP than water for all the membranes studied. These results might be attributed to the plasma's higher viscosity: the viscosity of water at 25°C is $9.0 \cdot 10^{-4}$ $Pa \cdot s^{-1}$ whereas the plasma viscosity at 25°C is $1.2 \cdot 10^{-3}$ $Pa \cdot s^{-1}$ [77].

	CA30	CA30-TEOS-APT-IBF(3%)	CA35
τ (Pa)	14.50	11.3	15.46
γ (s^{-1})	$1.21 \cdot 10^4$	$9.39 \cdot 10^3$	$1.30 \cdot 10^4$
ΔP (mmHg)	41.1	32.7	50.4

Table 5.6: Shear stress (Pa), shear rate (s^{-1}), and ΔP (mmHg) obtained at 25°C for the CA30, CA30-TEOS-APT-IBF(3%), and CA35 membranes at Q_F = 100 mL/min. Experiments were carried out with plasma.

5.3 Permeation Studies

5.3.1 Hydraulic Permeability, Lp

The hydraulic permeability (Lp) of all the fabricated membranes was evaluated in the AK setup as well as in the Celfa P-28 ultrafiltration setup. This was performed so that two ranges of TMP could be tested: from approximately 0.1 to 0.3 bar in the AK setup and from 0.5 to 4 bar in the Celfa P-28. Since Lp is

an intrinsic property of each membrane it is expected that Lp will be similar for the same membrane, no matter which setup was used to measure it. As explain previously, the Lp is represented as the slope of the ultrafiltration flux, J, as a function of the transmembrane pressure, TMP, applied.

In the AK setup, the ultrafiltration fluxes obtained for the CA22, CA30, CA33, and CA35 membranes were measured at a flow rate of 100 mL/min and a TMP ranging from 100 mmHg to 250 mmHg. Figure 5.7 shows the J versus TMP, measured at 25 °C for the four different membranes. Lp assumed the value of 20.4, 54.6, 64.5, and 68.6 $Kg \cdot h^{-1} \cdot m^{-2} \cdot bar^{-1}$, for the CA22, CA33, CA35 and CA30 membranes, respectively. These membranes are all pure cellulose acetate membranes; the only difference is the amount of acetone and formamide present. A higher concentration of formamide, the pore-forming solvent, is expected to increase membrane porosity, resulting in higher permeate water fluxes. However, this was not observed in the results obtained. It was expected that the CA35 membrane would have the highest $Lp^{25^\circ C}$ since it contains the highest formamide percentage - 35 wt.%. However, according to the results, the $Lp^{25^\circ C}$ of the CA30 membrane (with 30 wt.% formamide) is higher (68.6 $Kg \cdot h^{-1} \cdot m^{-2} \cdot bar^{-1}$) than the CA33 and CA35 membranes (54.6 and 64.5 $Kg \cdot h^{-1} \cdot m^{-2} \cdot bar^{-1}$, respectively). As expected, the CA22 had the lowest $Lp^{25^\circ C}$ with a value of 20.41 $Kg \cdot h^{-1} \cdot m^{-2} \cdot bar^{-1}$.

Moreover, *Janeca et al.* [47] reported a different value of $Lp^{25^\circ C}$ for the CA30 membrane corresponding to 28.27 $Kg \cdot h^{-1} \cdot m^{-2} \cdot bar^{-1}$ in the TMP range from 45 to 100 mmHg and a flow rate of 49 to 148 mL/min. Both membranes were prepared from casting solutions with the same compositions. However, there are some factors that can influence the water permeability such as the casting conditions and the experimental setup used. It is also important to highlight that all of the Lp results are in the order of magnitude of what was reported.

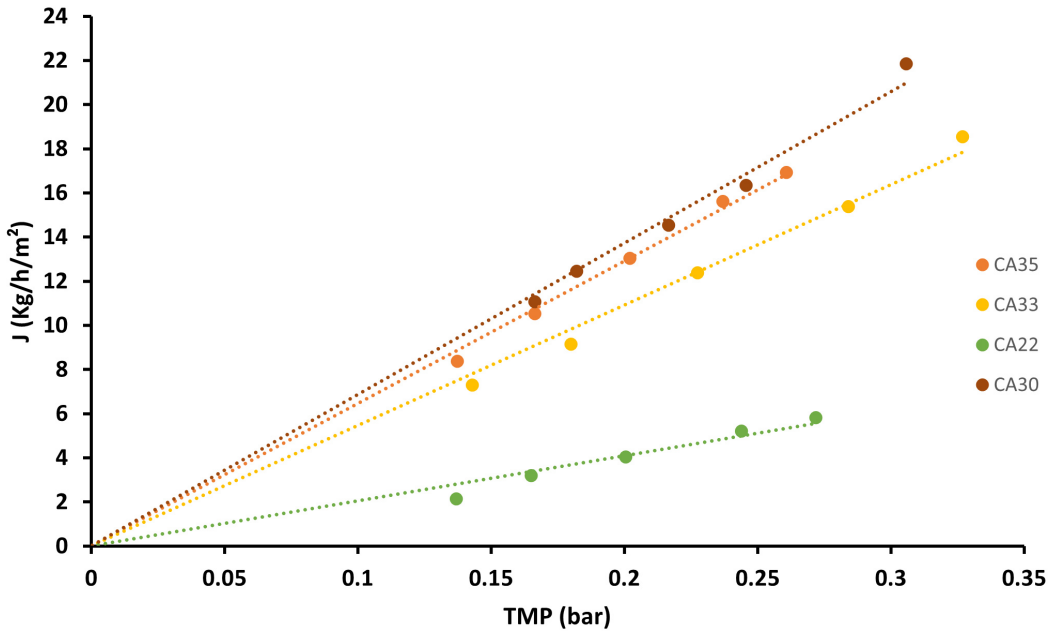

Figure 5.7: Ultrafiltration flux at 25°C, $J^{25^\circ C}$, in $Kg/h/m^2$, as a function of the applied transmembrane pressure (TMP), in bar, for the CA22, CA30, CA33, and CA35 membranes measured in the AK setup. The ultrafiltration fluxes were measured at a volumetric feed flow rate of 100 mL/min and with an effective area of 4.76 cm^2.

Figure 5.8 shows the ultrafiltration flux versus TMP of CA22, CA30, and CA35 membranes which was also evaluated in CELFA P-28 at a flow rate of 9.80 $cm^3 \cdot s^{-1}$ and in the TMP range from 0.5 to 2.5 bar. It was obtained a $Lp^{25^\circ C}$ of 24.0, 50.7, and 73.9 $Kg \cdot h^{-1} \cdot m^{-2} \cdot bar^{-1}$ for the CA22, CA30, and CA35 membranes, respectively. It can be seen that the CA35 exhibit the highest $Lp^{25^\circ C}$ value of 73.9 $Kg \cdot h^{-1} \cdot m^{-2} \cdot bar^{-1}$. Furthermore, these results are concordant with the expected behavior as explained before.

Comparing the results from the AK setup and CELFA P-28 it can be observed that for all the membranes tested in both experimental setups (CA22, CA30, and CA35), the $Lp^{25^\circ C}$ value is slightly different being higher in the CELFA P-28 than in the AK setup for CA22, and CA35 membranes while for the CA30 membrane is lower in the CELFA P-28. All of the Lp measured in both installations are of the same order of magnitude and within the expected ultrafiltration range.

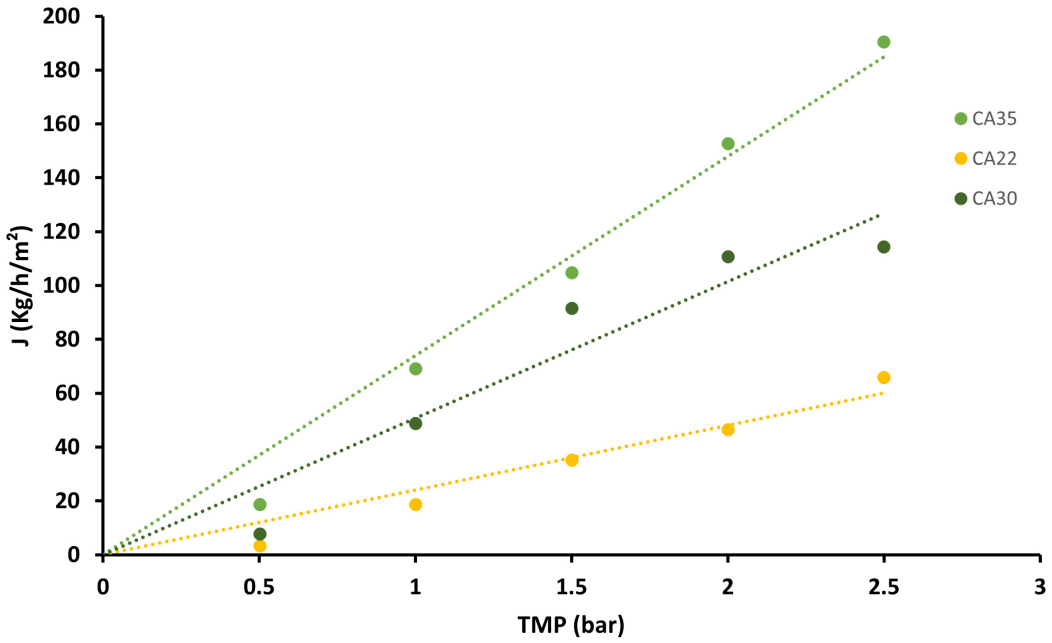

Figure 5.8: Ultrafiltration flux at $25^{\circ}C$, $J^{25^{\circ}C}$, in $Kg/h/m^2$, as a function of the applied transmembrane pressure (TMP), in bar, for the CA22, CA30, and CA35 membranes measured in CELFA P-28. The ultrafiltration fluxes were measured at a volumetric feed flow rate of 9.80 $cm^3 \cdot s^{-1}$ and with an effective area of 15 cm^2.

It is also important to compare the Lp of pure cellulose acetate and hybrid monophasic membranes. Therefore, Figure 5.9 represents the $Lp^{25^{\circ}C}$ for the CA22, CA22-APT and CA22-APT-IBF(3%) performed in CELFA P-28 at a flow rate of 11.80 and 22.52 $cm^3 \cdot s^{-1}$ and in the TMP range from 0.5 to 4 bar. It was obtained a $Lp^{25^{\circ}C}$ of 24.0, 8.7, and 1.0 $Kg \cdot h^{-1} \cdot m^{-2} \cdot bar^{-1}$ for the CA22, CA22-APT, and CA22-APT-IBF(15%) membranes, respectively. All of these membranes contain the same formamide content; CA22-APT and CA22-APT-IBF(15%) have APTES in their composition as a silica precursor and CA22-APT-IBF(15%) present the binding competitor linked to APTES. It can be seen that the lowest $Lp^{25^{\circ}C}$ was achieved for the CA22-APT-IBF membrane corresponding to 1.0 $Kg \cdot h^{-1} \cdot m^{-2} \cdot bar^{-1}$ while for the CA22 and CA22-APT, the $Lp^{25^{\circ}C}$ present the value of 24.0 and 8.7 $Kg \cdot h^{-1} \cdot m^{-2} \cdot bar^{-1}$, respectively. Through these results, it is possible to observe that the pure cellulose acetate membrane (CA22) showed a higher Lp than the monophasic hybrid membranes (CA22-APT and CA22-APT-IBF(15%)). The very low Lp values for the CA22-APT and CA22-APT-IBF (15%) can be attributed to the presence of several macroporous structures in both membranes, visualized by SEM, that difficult the passage of water and thus, result in very low ultrafiltration fluxes.

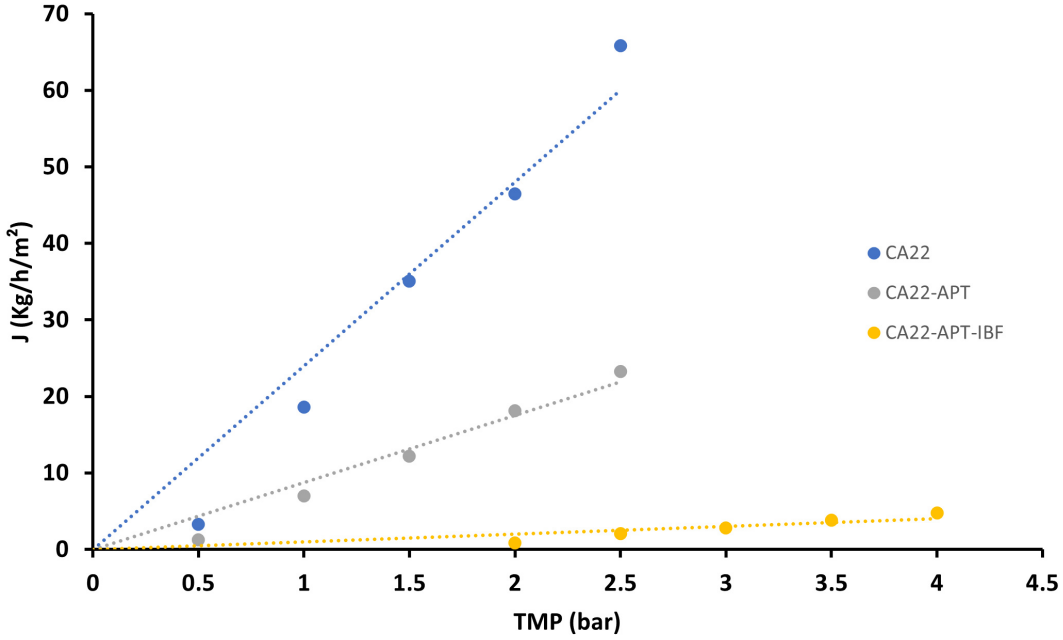

Figure 5.9: Ultrafiltration flux at $25^{\circ}C$, $J^{25^{\circ}C}$, in $Kg/h/m^2$, as a function of the applied transmembrane pressure (TMP), in bar, for the CA22, CA22-APT, and CA22-APT8IBF) membranes measured in CELFA P-28. The ultrafiltration fluxes were measured at a volumetric feed flow rate of 9.80 $cm^3 \cdot s^{-1}$ and with an effective area of 15 cm^2.

Figure 5.10 depicts the $Lp^{25^{\circ}C}$ of CA30 and CA30-TEOS-APT(3%) membranes measured in the AK setup at a flow rate of 100 mL/min and a TMP ranging from 100 mmHg to 250 mmHg. The $Lp^{25^{\circ}C}$ is 68.6 $Kg \cdot h^{-1} \cdot m^{-2} \cdot bar^{-1}$ for the CA30 membrane while for the CA30-TEOS-APT(3%) membranes is 97.6 $Kg \cdot h^{-1} \cdot m^{-2} \cdot bar^{-1}$. Both membranes have the same amount of formamide; CA30-TEOS-APT(3%) is a hybrid monophasic membrane that has TEOS and APTES as silica precursors and IBF linked to APTES. From the graphic observation, it can be seen that the $Lp^{25^{\circ}C}$ of CA30-TEOS-APT(3%) membrane is higher than the $Lp^{25^{\circ}C}$ of the CA30 membrane. In contrast to the previous membranes with 22% formamide, the monophasic hybrid membrane here has a higher Lp than the pure cellulose acetate membrane. Previously, it was reported [13] a different behavior for these two membranes where their $Lp^{25^{\circ}C}$ value is very similar (37.50 $Kg \cdot h^{-1} \cdot m^{-2} \cdot bar^{-1}$ for CA30 and 35.90 $Kg \cdot h^{-1} \cdot m^{-2} \cdot bar^{-1}$ for CA30-TEOS-APT-IBF(3%)).

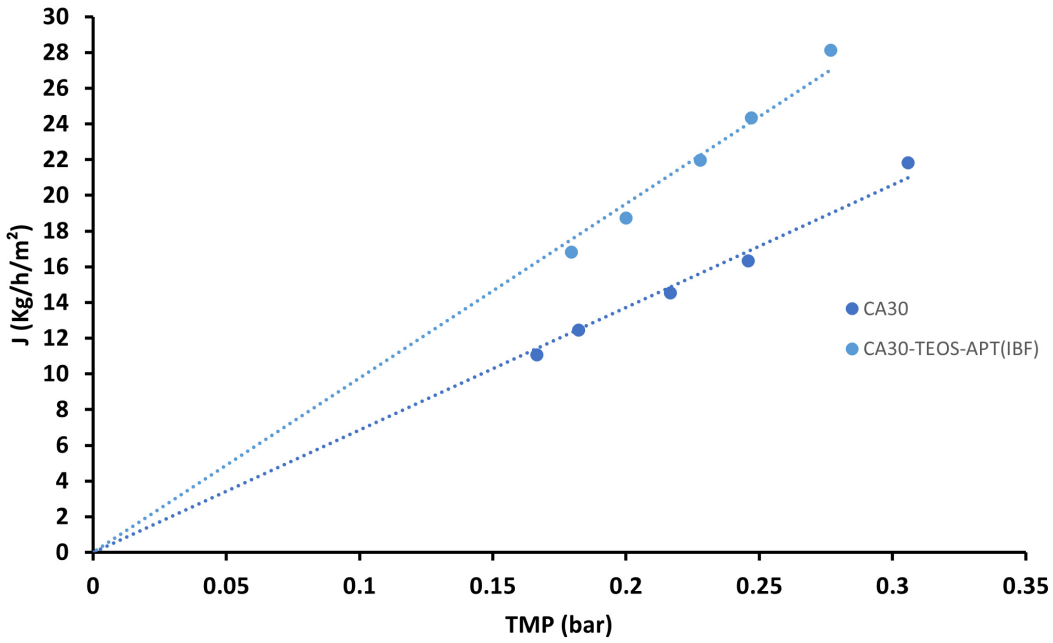

Figure 5.10: Ultrafiltration flux at $25^{\circ}C$, $J^{25^{\circ}C}$, in $Kg/h/m^2$, as a function of the applied transmembrane pressure (TMP), in bar, for the CA30, and CA30-TEOS-APT(IBF) membranes measured in the AK setup. The ultrafiltration fluxes were measured at a volumetric feed flow rate of 100 mL/min and with an effective area of 4.76 cm^2.

Throughout the analysis of the results, it can be seen that the presence of silica precursors functionalized with IBF affects the hydraulic permeability of the membranes. However, it can be obtained different conclusions according to different membranes: for the membranes with 22% of formamide (CA22, CA22-APT, and CA22-APT-IBF(15%)) the introduction of silica followed by functionalization with amine groups and IBF decreased the hydraulic permeability of the hybrid membrane. On the other hand, membranes with 30% of formamide (CA30, and CA30-TEOS-APTES-IBF(3%)) present a higher hydraulic permeability for the monophasic hybrid membrane.

Table 5.7 summarizes the $Lp^{25^{\circ}C}$, in $Kg \cdot h^{-1} \cdot m^{-2} \cdot bar^{-1}$ and $mL \cdot min^{-1} \cdot cm^{-2} \cdot mmHg^{-1}$ of all the membranes analyzed in the AK setup as well as in CELFA P-28.

As mentioned previously, Low Flux (LF) membrane dialyzers feature ultrafiltration rates lower than 15 $mL \cdot mmHg^{-1} \cdot h^{-1}$ and elimination of small toxins with MW of up to 5 kDa. Due to this limitation, High Flux (HF) membrane dialyzers have ultrafiltration rates higher than 15 $mL \cdot mmHg^{-1} \cdot h^{-1}$ and pore structures that allow for the passage of so-called middle molecules with MWs up to 20 kDa. Typical hemodialyzers have an effective permeation area between 0.8 and 2.5 m^2 [11, 78]. For this purpose, it was calculated the ultrafiltration flux, J, for an average effective permeation area of 1.5 m^2 in order to classify each membrane as suitable for high flux or low flux dialyzer. These results are present in Table 5.7 and it can be seen that all the membranes are suitable for a high flux dialyzer except the CA22-APT-

IBF(15%) that only achieved an ultrafiltration of 1.98 $mL \cdot mmHg^{-1} \cdot h^{-1}$ and thus, is suitable for a low flux membrane dialyzer.

Membrane	Experimental Setup	Lp ($kg/h/m^2/bar$)	Lp ($mL/min/cm^2/mmHg$)	J ($mL/h//mmHg$) for 1.5 m^2
CA22	AK	20.4	$4.5 \cdot 10^{-5}$	40.5
CA22	CELFA P-28	24.0	$5.3 \cdot 10^{-5}$	47.7
CA22-APT	CELFA P-28	8.7	$2.1 \cdot 10^{-5}$	18.9
CA22-APT-IBF(15%)	CELFA P-28	1.0	$2.2 \cdot 10^{-6}$	2.0
CA30	AK	68.6	$1.5 \cdot 10^{-4}$	135.0
CA30	CELFA P-28	50.7	$1.1 \cdot 10^{-4}$	99.0
CA30-TEOS-APT-IBF(3%)	AK	97.6	$2.2 \cdot 10^{-4}$	198.0
CA33	AK	54.6	$1.2 \cdot 10^{-4}$	108.0
CA35	AK	64.5	$1.4 \cdot 10^{-4}$	126.0
CA35	CELFA P-28	73.9	$1.6 \cdot 10^{-4}$	144.0

Table 5.7: Effective permeation area in m^2, hydraulic permeability at $25^\circ C$, $Lp^{25^\circ C}$, in $kg/h/m^2/bar$ and $mL/min/cm^2/mmHg$ of all the membranes analyzed in the AK setup as well as in CELFA P-28.

An ultrafiltration or permeate flowrate of 1 mL/min is regarded as sufficient for ensuring efficient excess fluid removal from CKD patients [13]. The effective area required to achieve this ultrafiltration flow rate was calculated for each characterised membrane and is present in Table 5.8. The membrane with the highest hydraulic permeability (CA30-TEOS-APT-IBF), as expected, will require a smaller effective area to achieve the ultrafiltration flow rate of 1 mL/min. Since typical hemodialyzers have an effective permeation area between 0.8 and 2.5 m^2, only the CA22-APT, and CA22-APT-IBF will require a larger effective area to efficiently remove excess fluid from patients.

Membrane	Effective Area (m^2)
CA22	1.89 - 2.22
CA22-APT	4.76
CA22-APT-IBF(15%)	45.45
CA30	0.67- 0.91
CA30-TEOS-APT-IBF(3%)	0.45
CA33	0.83
CA35	0.62 - 0.71

Table 5.8: Effective permeation area in m^2 for all the membranes analyzed in the AK setup as well as in CELFA P-28.

5.3.2 Molecular Weight Cut-Off (MWCO)

The MWCO of the CA22, CA30, CA30-TEOS-ATP-IBF(3%), and CA35 was determined from the apparent rejection coefficients to PEGs of increasing molecular weights (PEG 1000, 3000, 6000, 10 000, 20 000, and 35 000 Da) and dextran T40 (MW 40 kDa). The value of MWCO is obtained by two different methods: 1) intersection of the rejection coefficient curve, as a function of the PEGs molecular weight, with the 90% rejection line, 2) intersection of the linearized rejection curve of $log(\frac{f}{1-f})$, as a function of the solutes molecular weight, with the 90% rejection line ($log(\frac{f}{1-f})$ = 0.95).

Figure 5.11 plots the determination of the MWCO of all the enumerated membranes where the rejection factor curve is represented with the points representing the PEGs tested in each membrane; there are two horizontal lines that correspond to the rejection of 90%, as well as the $log(\frac{f}{1-f})$ = 0.95; and the linear straight line with the respective lineralized values. The expected theoretical behaviour of the rejection factor profile for each membrane is characterised by a crescent linear curve until approximately 90% rejection is achieved, and then a plateau phase is reached. Thus, based on the graphic representation of each analysed membrane, it can be concluded that: 1) the rejection factor curve of the CA22 and CA30 membranes is consistent with theoretical behaviour; 2) the CA35 membrane exhibit a different behaviour pattern, another PEG analysis should have been performed to better evaluate the rejection curve's behaviour and the first point of the curve should be repeated; 3) the rejection curve for the CA30-TEOS-ATP-IBF(3%) membrane appears to have the expected behaviour; however, another PEG higher than 35 000 Da should also have been performed to confirm the results.

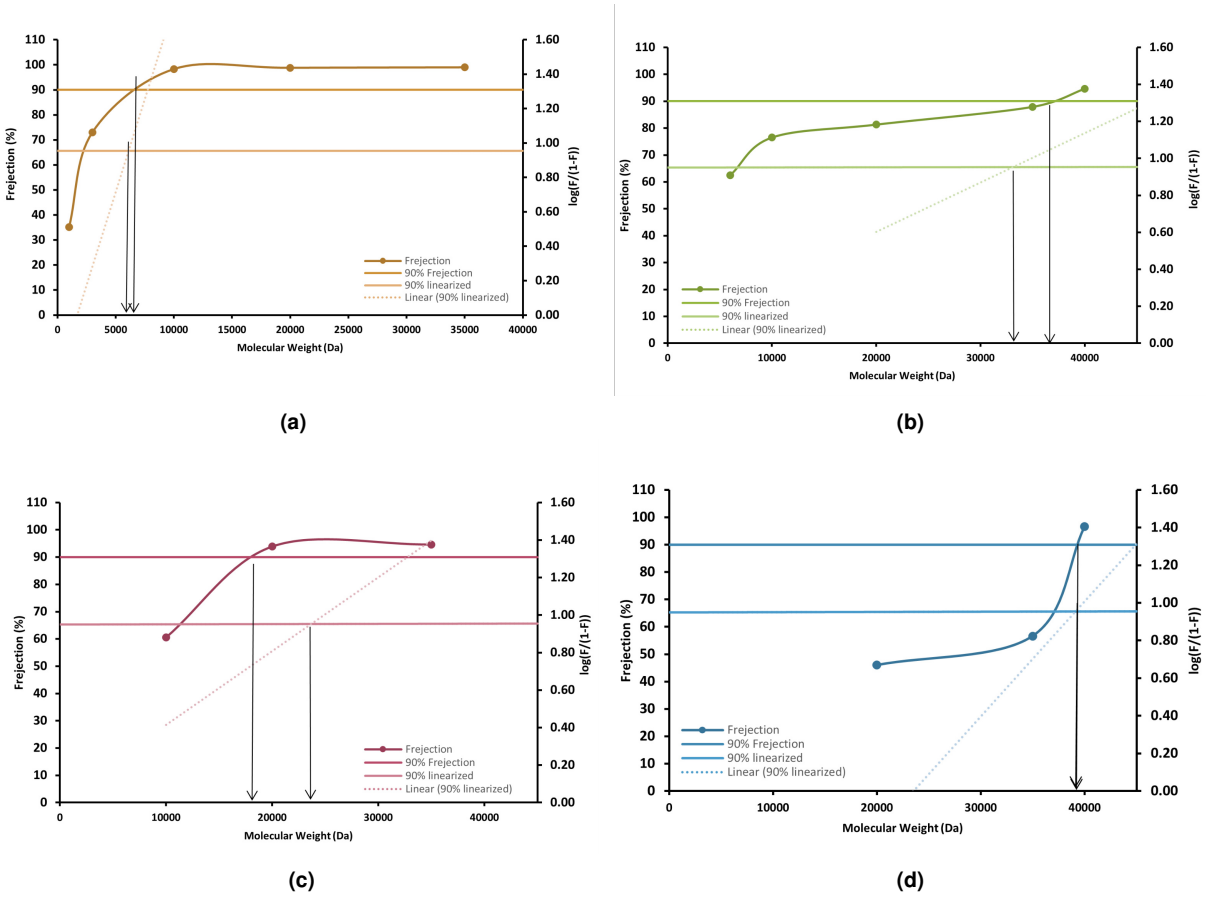

Figure 5.11: Rejection factor profile for (a) CA22, (b) CA30, (c) CA30-TEOS-APT-IBF(3%), and (d) CA35 membranes to PEG increasing molecular weight. The horizontal dashed lines indicate a rejection of 90% and log(f/(1-f))=0.954.

Table 5.9 depicts the determined values of MWCOs for the CA22, CA30, CA30-TEOS-APT-IBF(3%)

membranes where the MWCO range presented for each membrane corresponds to the intersection point of the plotted rejection coefficient curve ($MWCO_1$) and subsequent linearization ($MWCO_2$) with the respective horizontal rejection line represented in Figure 5.11.

Membrane	MWCO range (kDa)
CA22	6.6 - 7.7
CA30	32.9 - 36.6
CA30-TEOS-APT-IBF(3%)	18.9 - 23.2
CA35	39.2 - 39.8

Table 5.9: MWCO range, in Da, of the CA22, CA30, CA30-TEOS-APT-IBF(3%), and CA35 membranes.

Because formamide is responsible for the formation of pores in the membrane, the membrane with a lower formamide percentage is expected to have a lower MWCO. Therefore, results show that, as expected, the MWCO of the pure cellulose acetate membranes increases with the increase of formamide concentration in the casting solution. Hence, the MWCO increased from 6.6-7.7 kDa for the CA22 membrane to 39.2-39.8 kDa for the CA35 membrane and the CA30 membrane exhibits an intermediate MWCO value of 32.9 – 36.6 kDa. *Janeca et al.* [47] reported a MWCO of the CA30 membrane between 17.6 and 18.6 kDa which is slightly below the value obtained for the CA30 membrane in this study. The results do not follow the same order as was seen for the Lp. To elaborate, the membrane with higher $Lp^{25^\circ C}$ in CELFA P-28 (CA35) also display higher values of MWCO. However, from the $Lp^{25^\circ C}$ results of the AK setup, it can be observed that the membrane with the highest hydraulic permeability (CA30-TEOS-APT-IBF(3%)) does not exhibit the highest MWCO. Comparing the MWCO of CA30, and CA30-TEOS-APT-IBF(3%) it can be observed that the introduction of the TEOS-APT-IBF precursor into the polymer matrix decreased the MWCO from 32.9 – 36.6 kDa to 18.9 – 23.3 kDa. *Janeca et al.* [47] also reported another membrane with 30% of formamide which incorporated APTES as a silica precursor and for this membrane the MWCO assumed a value between 22.2 and 26.7 kDa which is also very similar to the one obtained for the CA30-TEOS-APT-IBF-(3%) membrane.

It is important to reinforce that membranes are from different batches and it is normal that there exists some variations in the membrane structure and thus in the MWCO. The evaporation time of the solvent and the conditions of the casting solution can also influence the membrane structure.

Since all membranes reject solutes with MWs greater than 40 kDa, it is predicted that vital blood components such as albumin and other proteins, which have MWs larger than 60 kDa, will be successfully retained by the membranes. In addition, because they can cross the membrane, molecules belonging to two different classes of uremic toxins - small water-soluble compounds and middle molecules - are expected to be able to cross the membranes and ultimately be removed from the blood.

5.3.3 Permeation to uremic toxins

5.3.3.A Protein-Bound Uremic Toxins (PBUTs)

The permeation to PBUTs was evaluated in the AK setup with the CA30-TEOS-APT-IBF(3%), and CA30 membranes. For this purpose, it was spiked 40 mg/L of indoxyl sulphate (IS) into 200 mL of plasma. The total, free, and bound forms are calculated as explained before in the Section 4.7.3.B. Since it is known that approximately 90-98% of IS circulate in the blood bound to HSA, while only 2-10% of these PBUTs circulate in their free form or unbound to HSA, it is critical to quantify both the free and bound forms.

Starting by the experiment performed with CA30-TEOS-APT-IBF(3%) membrane, after incubating the plasma with IS, a IS free percentage of 2.03 ± 0.04 and 2.02 ± 0.11 % was obtained at the beginning (T = 0 min) and at the end (T = 390 min) of the experiment, respectively. These result are consistent with previous studies in which 98% of the total concentration of IS binds to HSA [14]. Table 5.10 shows the total IS concentration (mg/L) and IS mass (µg) quantified in the feed solution, in their free, total and bound form, obtained at the beginning (t = 0 min) and at the end of the experiment (t = 390 min). According to the results, the total concentration of IS at the end of the experiment (52.3 mg/L) was higher than the real concentration used (40.0 mg/L), being an incoherent result. In addition, the total form of IS decreased from 4838.7 to 4807.6 µg during the experiment, suggesting that 31.1 µg of IS were permeated by the membrane. On the other hand, the IS free form decreased only 1.4 µg throughout the experiment.

Elapsed test time	[IS] total (mg/L)	IS free form (%)	IS total mass (μg)	IS free mass (μg)	IS bound mass (μg)
T = 0 min	38.7	2.03 ± 0.04	4838.7	98.4	4740.3
T = 390 min	52.3	2.02 ± 0.11	4807.6	97.0	4710.6

Table 5.10: [IS] (mg/L), IS free form (%), IS mass (μg) in the feed solution (free total, and bound form) obtained at the beginning (t=0 min) and at the end of the experiment (t = 390 min) for the CA30-TEOS-APT-IBF(3%) membrane.

Table 5.11 contains the data obtained regarding the IS removal thought the CA30-TEOS-APT-IBF(3%) membrane. Figure 5.12 plots the IS concentration (mg/L) collected in the permeate reservoir at different times of the experiment (5.12a) as well as their cumulative mass (µg) collected thought the entire experiment (5.12b). Throughout the observations of these results it can be concluded that: 1) IS was reported in the permeate, and its removal is constant throughout the test - except for the first half hour, the permeate concentration was always around 1 mg/L; 2) At the end of the assay, 31.1 µg of IS were removed from the feed solution; 3) When compared to the IS concentration in the feed solution (40 mg/L), the concentration of IS permeated was very low (1 mg/L); 4) The free form of IS (98.4 µg) in the feed solution was not totally permeated by the CA30-TEOS-APT-IBF(3%) membrane.

Aside from that, the IS quantification in the feed solution (Table 5.10) suggests that 31.1 µg has been removed during the experiment. In addition, the IS quantification in the permeate samples (Table 5.11)

reveals that the CA30-TEOS-APT-IBF(3%) membrane effectively permeated 31.1 µg and thus, demonstrating that both quantification's, in feed and permeate solutions, are consistent. Furthermore, because the free portion of IS decreased only 1.40 µg in the feed solution while 31.1 µg of IS was quantified in the permeate, this finding may indicate that IS from the bound part may dissociate from the HSA during the experiment and become free in the solution and thus, able to be permeated. Nonetheless, there is the possibility of HSA-IS dissociation during the experiment, and these results must be confirmed.

Time (min)	[IS] mg/L	IS mass (µg)
0	0	0
30	0.07	0.20
90	1.03	6.16
150	0.99	5.60
210	1.00	5.19
270	0.99	4.80
330	0.96	4.30
390	1.13	4.81

Table 5.11: Data of IS permeation through the CA30-TEOS-APT-IBF(3%) membrane.

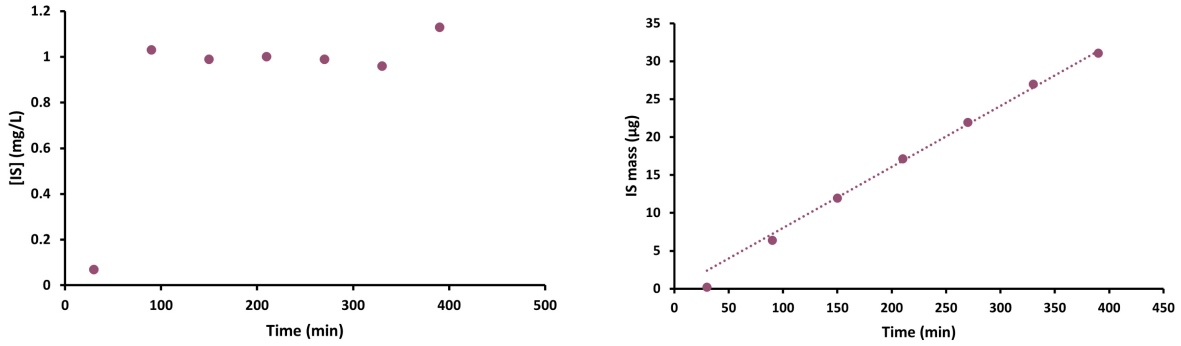

(a) [IS] (mg/L) collected in the permeate over time (min).

(b) Cumulative IS removal (µg) over time (min).

Figure 5.12: IS permeation through the CA30-TEOS-APT-IBF(3%) membrane.

The results obtained for the CA30 membrane will be discussed in the same sense than the results obtained for CA30-TEOS-APT-IBF(3%) membrane. After incubating the plasma with IS, an IS free percentage of 1.76 $\pm$ 0.02 and 1.67 $\pm$ 0.12 % was obtained at the beginning and at the end of the experiment, respectively. These result are consistent with the results obtained for the CA30-TEOS-APT-IBF(3%) membrane. Table 5.12 contains the details regarding the IS permeation through the CA30 membrane. According to the data, the total concentration of IS in the feed solution is higher (49.6 mg/L) than the real concentration used (40 mg/L). Furthermore, the total portion of IS decreased from 4838.7 to 4814.3 µg, inferring that 24.4 µg of IS was permeated during the assay while free IS only decreased 4.6 µg. These results might suggest that the IS form bounded to HSA maybe become dissociated during the experiment and thus, able to be permeated by the membrane. Otherwise, the bound form of the IS

is not enable to pass through this membrane.

Elapsed test time	[IS] total (mg/L)	IS free form (%)	IS total mass (μg)	IS free mass (μg)	IS bound mass (μg)
T = 0 min	38.7	1.76 ± 0.02	4838.7	85.0	4753.7
T = 270 min	49.6	1.67 ± 0.12	4814.3	80.4	4733.9

Table 5.12: [IS] (mg/L), IS free form (%), IS mass (μg) in the feed solution (free total, and bound form) obtained at the beginning (t=0 min) and at the end of the experiment (t = 270 min) for the CA30 membrane.

Table 5.13 contains the data obtained regarding the IS permeation thought the CA30 membrane. Figure 5.13 plots the IS concentration (mg/L) collected in the permeate reservoir at different times of experiment (5.13a) as well as their cumulative mass (µg) collected thought the entire assay (5.13b). According to the data, IS was reported in the permeate samples, and its removal was constant throughout the experiment assuming a concentration very close to 1 mg/L; during the experiment, 24.4 µg of IS was removed from the feed solution; the initial free portion of IS present in the feed solution (85.0 µg) was not completely removed.

Similarly to the previous results for the CA30-TEOS-APT-IBF(3%) membrane, the quantification of IS in the permeate and feed samples are concordant (24.4 µg).

Time (min)	[IS] mg/L	IS mass (µg)
0	0	0
30	0.70	1.80
90	0.86	5.70
150	0.97	5.80
210	0.87	5.20
270	0.87	5.90

Table 5.13: Data of IS permeation through the CA30 membrane.

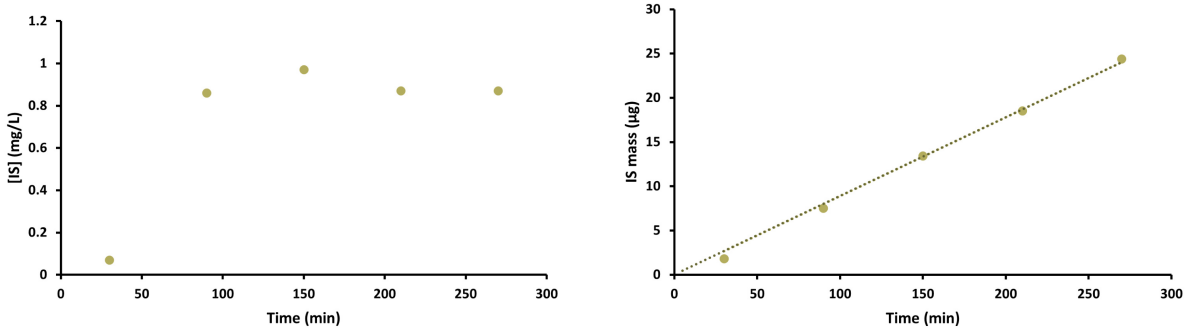

(a) [IS] (mg/L) collected in the permeate over time (min).

(b) cumulative IS removal (µg) over time (min).

Figure 5.13: IS permeation through the CA30 membrane.

Figure 5.14 shows the comparison of the cumulative IS removal (µg) over time (min) for the CA30, and CA30-TEOS-APT-IBF(3%) membranes. Comparing the results, it is possible to evaluate that, for the

same time of experiment (270 min), the CA30 permeated more IS (24.4 µg) than the CA30-TEOS-APT-IBF(3%) membrane (21.9 µg). However, the Lp of the CA30-TEOS-APT-IBF(3%) membrane is higher (97.6 $Kg \cdot h^{-1} \cdot m^{-2} \cdot bar^{-1}$) than the CA30 membrane (68.6 $Kg \cdot h^{-1} \cdot m^{-2} \cdot bar^{-1}$) and as a result, higher permeation rates were predicted for this membrane.

A higher effective area of permeation is necessary to permeate all of the free IS present in the feed solution. Thought the results obtained, cannot be determine whether the IS permeated by the CA30-TEOS-APTES-IBF(3%) membrane corresponds to the free or bound portion. The effect of the binding competitor IBF can be detected by higher permeation rates or by a significantly increase in the free form of IS in the feed solution. Moreover, the HSA-IS association/dissociation rates during the experiment must be further investigated.

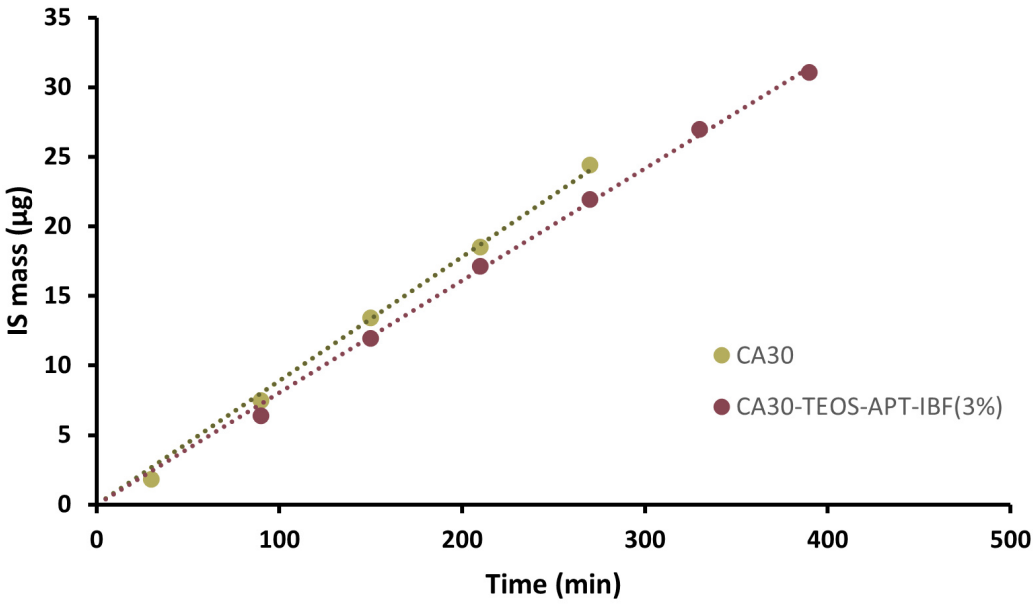

Figure 5.14: Cumulative IS removal (µg) over time (min) for the CA30 and CA30-TEOS-APT-IBF(3%) membranes.

5.3.4 Long-term HSA filtration

Figure 5.15 represents the concentration profiles of HSA as well as the pressure profiles (TMP and ΔP) during long term HSA filtration experiments performed in the AK setup. Figures 5.15a, 5.15b and 5.15c show the results obtained for the CA30, CA30-TEOS-APT-IBF(3%), and CA35 membranes, respectively. Analysis of these results give information regarding the rejection of HSA and give evidence of any membrane fouling that may have occurred.

The results showed that for the CA30, CA30-TEOS-APT-IBF(3%), and CA35 membranes, the highest HSA concentration detected in the permeate samples was 5.6, 4.6, and 2.3 mg/L, respectively. Taking

into account that the initial concentration of HSA ranging between 40 000 to 50 000 mg/L, the rejection factor to albumin for each membrane was 100%.

The ΔP remained roughly constant throughout the entire experiment for the CA30, and CA35 membranes. The TMP varied between 190 to 196 mmHg and 207 to 211 over 270 minutes for the CA30 and CA35 membranes, respectively.

However, for the CA30-TEOS-APT-IBF(3%) membrane, it can be observed that there is some variations in the TMP as well as ΔP over time: the TMP increased from 250 mmHg to 290 mmHg during the assay; the ΔP also assumed some variations over time, oscillating between 30 to 45 mmHg. As a result, these pressure differences may indicate some deposition and accumulation of unwanted components at the membrane's surface. Since these results were not obtained for the pure cellulose acetate membranes, CA30 and CA35, it can be an indicator that albumin linked to IBF present at the surface of the membrane, resulting in their deposition increasing the pressure, consequently. Nevertheless, fluid removal over time, which leads to an increase in protein concentration and, as a result, an increase in plasma viscosity, can also justify these observations.

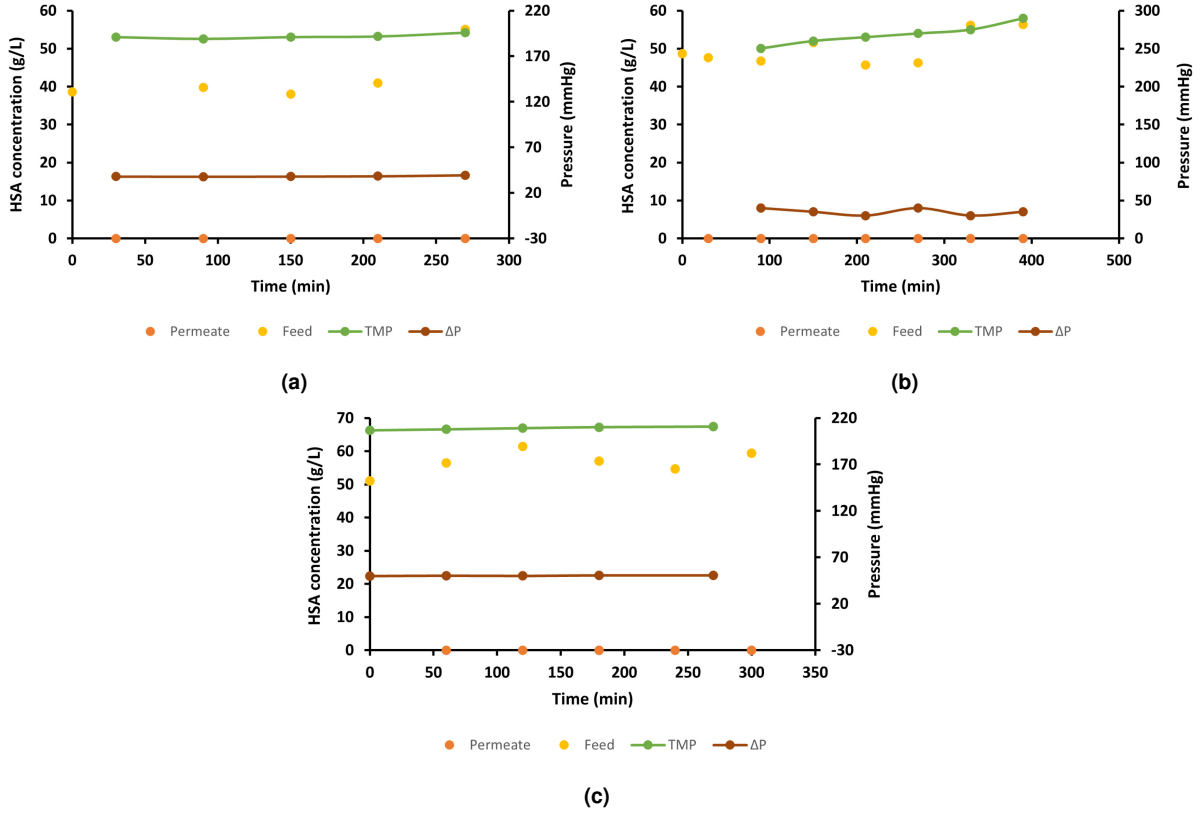

Figure 5.15: HSA concentration and pressure profiles (g/L) for (a) CA30, (b) CA30-TEOS-APT-IBF(3%), and (c) CA35 membranes, regarding feed (yellow) and permeate (orange) samples along the time (min).

Figure 5.16 depicts the ultrafiltration flow rate over time measured during the plasma experiment

tested in the AK setup with the CA30-TEOS-APT-IBF(3%) membrane. These results are concordant with the previous hypothesis since the ultrafiltration rate decreases significantly after 200 minutes of experiment. As a result, this could be another indicator of fouling events.

As mentioned previously, for all the membranes analyzed, CA30, CA30-TEOS-APT-IBF(3%), and CA35, it was obtained a rejection coefficient of 100%. These findings are consistent with the predictions due to the MW of HSA, and the MWCO of each membrane which is below 40 kDa for all of them. Moreover, CA30, CA30-TEOS-APT-IBF(3%), and CA35 membranes show promising results in terms of inhibiting albumin leakage, which is highly undesirable in a clinical scenario, during HD sessions.

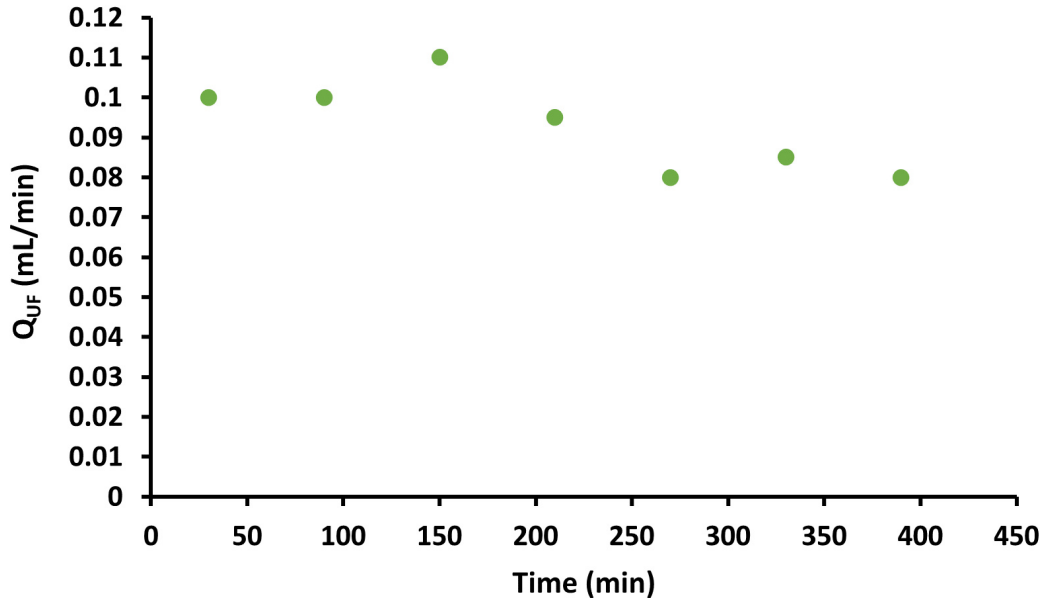

Figure 5.16: Ultrafiltration flow rate (mL/min) over time (min) of CA30-TEOS-APT-IBF(3%).

6

Conclusion and Future Work

The integral asymmetric, hybrid monophasic cellulose acetate/silica were characterized and incorporated with novel compounds to enhance Protein-Bound Uremic Toxins (PBUT)s removal.

PBUTs are regarded as the main bottleneck to the efficient removal of all uremic toxins and are associated with a variety of Chronic Kidney Disease (CKD) complications. The infusion of HSA binding competitors into the bloodstreams of End Stage Renal Disease (ESRD) patients opened a new research pathway for the removal of PBUTs. However, the side effects of long-term administration of large amounts of pharmaceutical drugs into ESRD patients' bloodstreams highlight the need for another alternative.

The development of novel HD membranes with the incorporation of HSA binding competitors is another interesting approach to improve PBUTs removal without the administration of drugs into the blood circulation.

This work proved the synthesis of integral asymmetric, hybrid monophasic cellulose acetate/silica with the incorporation of IBF as a binding competitor. The novel CA30-TEOS-APT-IBF(3%) membrane showed a hydraulic permeability similar than pure cellulose acetate membranes and successfully permeated IS and rejected 100% of HSA.

Future studies could address the reproduction of permeation experiments with indoxyl sulphate (IS); carry out experiments in the AK setup with blood to evaluate the shear rate and shear stress at the walls; evaluate the permeation of competitive binding membranes to Small Water-Soluble Compounds (SWSC); use a larger effective area of membrane; perform a leaching assay to evaluate the binding of IBF to the membrane; and use a higher content of the compound IBF-APTES to better evaluate their effect in the membrane performance.

Bibliography

[1] N. I. of Diabetes, Digestive, and K. Diseases. Hemodialysis. (October, 2022). [Online]. Available: https://www.niddk.nih.gov/health-information/kidney-disease/kidney-failure/hemodialysis

[2] *Synthetic Membranes: Science, Engineering and Applications*, 1986.

[3] F. S. C. Rodrigues, "Design of new membrane housings for a Portable Artificial Kidney Chemical Engineering," 2021.

[4] M. Sousa, "Clarificação e estabilização proteica de vinhos por Ultrafiltração," MSc Dissertation, Instituto Superior Técnico, Lisboa, 2017.

[5] F. Duranton, G. Cohen, R. De Smet, M. Rodriguez, J. Jankowski, R. Vanholder, and A. Argiles, "Normal and pathologic concentrations of uremic toxins," *Journal of the American Society of Nephrology*, vol. 23, no. 7, pp. 1258–1270, 2012, DOI: https://doi.org/10.1681/ASN.2011121175.

[6] R. Vanholder, R. De Smet, G. Glorieux, A. Argilés, U. Baurmeister, P. Brunet, W. Clark, G. Cohen, P. P. De Deyn, R. Deppisch, B. Descamps-Latscha, T. Henle, A. Jörres, H. D. Lemke, Z. A. Massy, J. Passlick-Deetjen, M. Rodriguez, B. Stegmayr, P. Stenvinkel, C. Tetta, C. Wanner, and W. Zidek, "Review on uremic toxins: Classification, concentration, and interindividual variability," *Kidney International*, vol. 63, no. 5, pp. 1934–1943, 2003, DOI: https://doi.org/10.1046/j.1523-1755.2003.00924.x.

[7] X. Tao, S. Thijssen, N. Levin, P. Kotanko, and G. Handelman, "Enhanced Indoxyl Sulfate Dialyzer Clearance with the Use of Binding Competitors," *Blood Purification*, vol. 39, no. 4, pp. 323–330, 2015, DOI: https://doi.org/10.1159/000381008.

[8] M. Faria and M. N. de Pinho, "Challenges of reducing protein-bound uremic toxin levels in chronic kidney disease and end stage renal disease," *Translational Research*, vol. 229, pp. 115–134, 2021, DOI: https://doi.org/10.1016/j.trsl.2020.09.001.

[9] C. Ronco and W. R. Clark, "Haemodialysis membranes," *Nature Reviews Nephrology*, vol. 14, no. 6, pp. 394–410, 2018, DOI: http://dx.doi.org/10.1038/s41581-018-0002-x.

[10] E. Sánchez-Álvarez, M. Rodríguez-García, F. Locatelli, C. Zoccali, A. Martín-Malo, J. Floege, M. Ketteler, G. London, J. L. Górriz, B. Rutkowski *et al.*, "Survival with low-and high-flux dialysis," *Clinical kidney journal*, vol. 14, no. 8, pp. 1915–1923, 2021, DOI: https://doi.org/10.1093/ckj/sfaa233.

[11] A. S. C.C. Magee, J.K. Tucker, *Core Concepts in Dialysis and Continuous Therapies*. Springer US, 2016.

[12] *Synthetic Membranes: Science, Engineering and Applications*, 1986.

[13] M. Lopes, "Towards nanostructured membranes for the artificial kidney," MSc Dissertation, Instituto Superior Técnico, Lisboa, 2021.

[14] Y. Itoh, A. Ezawa, K. Kikuchi, Y. Tsuruta, and T. Niwa, "Protein-bound uremic toxins in hemodialysis patients measured by liquid chromatography/tandem mass spectrometry and their effects on endothelial ROS production," *Analytical and Bioanalytical Chemistry*, vol. 403, no. 7, pp. 1841–1850, 2012.

[15] R. Vanholder, N. Hoefliger, R. De Smet, and S. Ringoir, "Extraction of protein bound ligands from azotemic sera: Comparison of 12 deproteinization methods," *Kidney International*, vol. 41, no. 6, pp. 1707–1712, 1992.

[16] N. Jourde-Chiche, L. Dou, C. Cerini, F. Dignat-George, R. Vanholder, and P. Brunet, "Protein-bound toxins - Update 2009," *Seminars in Dialysis*, vol. 22, no. 4, pp. 334–339, 2009, DOI: https://doi.org/10.1111/j.1525-139X.2009.00576.x.

[17] L. Sultatos, "Drug reservoirs," *xPharm: The Comprehensive Pharmacology Reference*, pp. 1–2, 2007.

[18] V. Maheshwari, X. Tao, S. Thijssen, and P. Kotanko, "Removal of protein-bound uremic toxins using binding competitors in hemodialysis: A narrative review," *Toxins*, vol. 13, no. 9, 2021, DOI: https://doi.org/10.3390/toxins13090622.

[19] T. Peters Jr, *All about albumin: biochemistry, genetics, and medical applications*. Academic press, 1995.

[20] T. Sakai, K. Yamasaki, T. Sako, U. Kragh-Hansen, A. Suenaga, and M. Otagiri, "Interaction mechanism between indoxyl sulfate, a typical uremic toxin bound to site ii, and ligands bound to site i of human serum albumin," *Pharmaceutical Research*, vol. 18, no. 4, pp. 520–524, 2001.

[21] T. Sakai, A. Takadate, and M. Otagiri, "Characterization of binding site of uremic toxins on human serum albumin," *Biological Pharmaceutical Bulletin*, vol. 18, no. 12, pp. 1755–1761, 1995, DOI: https://doi.org/10.1248/bpb.18.1755.

[22] T. Itoh, Y. Saura, Y. Tsuda, and H. Yamada, “Stereoselectivity and enantiomer-enantiomer interactions in the binding of ibuprofen to human serum albumin,” *Chirality*, vol. 9, no. 7, pp. 643–649, 1997, DOI: https://doi.org/10.1002/(SICI)1520-636X(1997)9:7⟨643::AID-CHIR1⟩3.0.CO;2-8.

[23] M. H. Rahman, T. Maruyama, T. Okada, T. Imai, and M. Otagiri, “Study of interaction of carprofen and its enantiomers with human serum albumin-II. Stereoselective site-to-site displacement of carprofen by ibuprofen,” *Biochemical Pharmacology*, vol. 46, no. 10, pp. 1733–1740, 1993, DOI: https://doi.org/10.1016/0006-2952(93)90577-J.

[24] S. Evoli, D. Mobley, R. Guzzi, and B. Rizzuti, “Multiple binding modes of ibuprofen in human serum albumin identified by absolute binding free energy calculations,” 2016.

[25] M. Abe, I. Masakane, A. Wada, S. Nakai, K. Nitta, and H. Nakamoto, “Dialyzer Classification and Mortality in Hemodialysis Patients: A 3-Year Nationwide Cohort Study,” *Frontiers in Medicine*, vol. 8, no. August, pp. 1–14, 2021.

[26] K. Oshvandi, R. Kavyannejad, S. R. Borzuo, and M. Gholyaf, “High-Flux and Low-Flux Membranes: Efficacy in Hemodialysis,” *Nursing and Midwifery Studies*, vol. 3, no. 3, 2014.

[27] C. Zweigart, A. Boschetti-de Fierro, M. Hulko, L. G. Nilsson, W. Beck, M. Storr, and B. Krause, “Medium cut-off membranes - closer to the natural kidney removal function,” *International Journal of Artificial Organs*, vol. 40, no. 7, pp. 328–334, 2017, DOI: https://doi.org/10.5301/ijao.5000603.

[28] G. Lesaffer, R. De Smet, N. Lameire, A. Dhondt, P. Duym, and R. Vanholder, “Intradialytic removal of protein-bound uraemic toxins: Role of solute characteristics and of dialyser membrane,” *Nephrology Dialysis Transplantation*, vol. 15, no. 1, pp. 50–57, 2000, DOI: https://doi.org/10.1093/ndt/15.1.50.

[29] R. De Smet, A. Dhondt, S. Eloot, F. Galli, M. A. Waterloos, and R. Vanholder, “Effect of the super-flux cellulose triacetate dialyser membrane on the removal of non-protein-bound and protein-bound uraemic solutes,” *Nephrology Dialysis Transplantation*, vol. 22, no. 7, pp. 2006–2012, 2007, DOI: https://doi.org/10.1093/ndt/gfm065.

[30] D. H. Krieter, A. Hackl, A. Rodriguez, L. Chenine, H. L. Moragues, H. D. Lemke, C. Wanner, and B. Canaud, “Protein-bound uraemic toxin removal in haemodialysis and post-dilution haemodiafiltration,” *Nephrology Dialysis Transplantation*, vol. 25, no. 1, pp. 212–218, 2010, DOI: https://doi.org/10.1093/ndt/gfp437.

[31] M. S. Tijink, M. Wester, J. Sun, A. Saris, L. A. Bolhuis-Versteeg, S. Saiful, J. A. Joles, Z. Borneman, M. Wessling, and D. F. Stamatialis, “A novel approach for blood purification: Mixed-matrix membranes combining diffusion and adsorption in one step,” *Acta Biomaterialia*, vol. 8, no. 6, pp. 2279–2287, 2012, DOI: http://dx.doi.org/10.1016/j.actbio.2012.03.008.

[32] G. La Greca, A. Brendolan, P. M. Ghezzi, R. De Smet, C. Tetta, R. Gervasio, and C. Ronco, "The concept of sorbent in hemodialysis," *International Journal of Artificial Organs*, vol. 21, no. 6, pp. 303–308, 1998, DOI: https://doi.org/10.1177/039139889802100604.

[33] M. S. Tijink, M. Wester, G. Glorieux, K. G. Gerritsen, J. Sun, P. C. Swart, Z. Borneman, M. Wessling, R. Vanholder, J. A. Joles, and D. Stamatialis, "Mixed matrix hollow fiber membranes for removal of protein-bound toxins from human plasma," *Biomaterials*, vol. 34, no. 32, pp. 7819–7828, 2013, DOI: https://doi.org/10.1016/j.biomaterials.2013.07.008.

[34] D. L. Kim and D. Stamatialis, "High flux mixed matrix membrane with low albumin leakage for blood plasma detoxification," *Journal of Membrane Science*, vol. 609, no. February, p. 118187, 2020, DOI: https://doi.org/10.1016/j.memsci.2020.118187.

[35] L. Lu and J. T. Yeow, "An adsorption study of indoxyl sulfate by zeolites and polyethersulfone–zeolite composite membranes," *Materials and Design*, vol. 120, pp. 328–335, 2017, DOI: http://dx.doi.org/10.1016/j.matdes.2017.01.094.

[36] S. Zeng, Y. Hou, Y. Zhou, X. Zhou, S. Ye, M. Wang, and L. Ren, "Adsorptive removal of uremic toxins using Zr-based MOFs for potential hemodialysis membranes," *Journal of Materials Science*, vol. 57, no. 4, pp. 2909–2923, 2022, DOI: https://doi.org/10.1007/s10853-021-06783-4.

[37] X. Tao, S. Thijssen, P. Kotanko, C. H. Ho, M. Henrie, E. Stroup, and G. Handelman, "Improved dialytic removal of protein-bound uraemic toxins with use of albumin binding competitors: An in vitro human whole blood study," *Scientific Reports*, vol. 6, no. December 2015, pp. 2–10, 2016.

[38] D. Padula, L. D. I. Bari, F. Santoro, H. Gerlach, and A. Rizzo, "Analysis of the Electronic Circular Dichroism Spectrum of $(-)-$ [9](2, 5)Pyridinophane," *Chirality*, vol. 1004, no. May, pp. 994–1004, 2012, DOI: https://doi.org/10.1002/chir.22087.

[39] J. Li, Y. Wang, X. Xu, W. Cao, Z. Shen, N. Wang, J. Leng, N. Zou, E. Shang, Z. Zhu, J. Guo, and J. Duan, "Improved dialysis removal of protein-bound uremic toxins by salvianolic acids," *Phytomedicine*, vol. 57, no. July 2018, pp. 166–173, 2019, DOI: https://doi.org/10.1016/j.phymed.2018.12.018.

[40] M. Madero, K. B. Cano, I. Campos, X. Tao, V. Maheshwari, J. Brown, B. Cornejo, G. Handelman, S. Thijssen, and P. Kotanko, "Removal of protein-bound uremic toxins during hemodialysis using a binding competitor," *Clinical Journal of the American Society of Nephrology*, vol. 14, no. 3, pp. 394–402, 2019, DOI: https://doi.org/10.2215/CJN.05240418.

[41] B. S. Lalia, V. Kochkodan, R. Hashaikeh, and N. Hilal, “A review on membrane fabrication: Structure, properties and performance relationship,” *Desalination*, vol. 326, pp. 77–95, 2013, DOI: https://doi.org/10.1016/j.desal.2013.06.016.

[42] R. A. Zoppi and M. C. Gonçalves, “Hybrids of cellulose acetate and sol-gel silica: Morphology, thermomechanical properties, water permeability, and biodegradation evaluation,” *Journal of Applied Polymer Science*, vol. 84, no. 12, pp. 2196–2205, 2002, DOI: https://doi.org/10.1002/app.10427.

[43] A. Ahmad, S. Waheed, S. M. Khan, S. e Gul, M. Shafiq, M. Farooq, K. Sanaullah, and T. Jamil, “Effect of silica on the properties of cellulose acetate/polyethylene glycol membranes for reverse osmosis,” *Desalination*, vol. 355, pp. 1–10, 2015, DOI: https://doi.org/10.1016/j.desal.2014.10.004.

[44] F. T. Minhas, S. Farrukh, A. Hussain, and M. Mujahid, “Comparison of silica and novel functionalized silica-based cellulose acetate hybrid membranes in gas permeation study,” *Journal of Polymer Research*, vol. 22, no. 4, pp. 1–13, 2015.

[45] P. Wojciechowska, Z. Foltynowicz, and M. Nowicki, “Synthesis and characterization of modified cellulose acetate propionate nanocomposites via sol-gel process,” *Journal of Spectroscopy*, vol. 1, no. 1, 2013, DOI: https://doi.org/10.1155/2013/616159.

[46] G. Mendes, M. Faria, A. Carvalho, M. C. Gonçalves, and M. N. de Pinho, “Structure of water in hybrid cellulose acetate-silica ultrafiltration membranes and permeation properties,” *Carbohydrate Polymers*, vol. 189, pp. 342–351, 2018, DOI: http://dx.doi.org/10.1016/j.carbpol.2018.02.030.

[47] A. Janeca, F. S. Rodrigues, M. C. Gonçalves, and M. Faria, “Novel cellulose acetate-based monophasic hybrid membranes for improved blood purification devices: Characterization under dynamic conditions,” *Membranes*, vol. 11, no. 11, 2021, DOI: https://doi.org/10.3390/membranes11110825.

[48] J. E. Flythe, S. E. Kimmel, and S. M. Brunelli, “Rapid fluid removal during dialysis is associated with cardiovascular morbidity and mortality,” *Kidney International*, vol. 79, no. 2, pp. 250–257, 2011, DOI: http://dx.doi.org/10.1038/ki.2010.383.

[49] B. Kunst and S. Sourirajan, “An approach to the development of cellulose acetate ultrafiltration membranes,” *Journal of Applied Polymer Science*, vol. 18, no. 11, pp. 3423–3434, 1974, DOI: https://doi.org/10.1002/app.1974.070181121.

[50] A. S. Figueiredo, A. R. Garcia, M. Minhalma, L. Ilharco, and M. N. De Pinho, “The ultrafiltration performance of cellulose acetate asymmetric membranes: A new perspective on the correlation with the infrared spectra,” *Journal of Membrane Science and Research*, vol. 6, no. 1, pp. 70–80, 2020.

[51] R. E. Kesting and A. Menefee, “The role of formamide in the preparation of cellulose acetate membranes by the phase inversion process,” *Kolloid-Zeitschrift Zeitschrift für Polymere*, vol. 230, no. 2, pp. 341–346, 1969.

[52] R. E. Kesting, “Phase Inversion Membranes.” *ACS Symposium Series*, no. 1967, pp. 131–164, 1985.

[53] H. Strathmann and K. Kock, “The formation mechanism of phase inversion membranes,” *Desalination*, vol. 21, no. 3, pp. 241–255, 1977, DOI: https://doi.org/10.1016/S0011-9164(00)88244-2.

[54] S. Loeb, S., Sourirajan, “Saline Water Conversion”II,” *Sea Water Demineralization by Means of an Osmotic Membrane*, pp. 117–132, 1963.

[55] C.J. Brinker; G. W. Scherer, “Sol-Gel Science The physics and chemistry of sol-gel processing - Brinker 1990.pdf,” p. 462, 1990.

[56] M. C. Andrade, J. C. Pereira, N. de Almeida, P. Marques, M. Faria, and M. C. Gonçalves, “Improving hydraulic permeability, mechanical properties, and chemical functionality of cellulose acetate-based membranes by co-polymerization with tetraethyl orthosilicate and 3-(aminopropyl)triethoxysilane,” *Carbohydrate Polymers*, vol. 261, no. November 2020, 2021, DOI: https://doi.org/10.1016/j.carbpol.2021.117813.

[57] E. Staude *et al.*, “Characterization of ultrafiltration membranes by drying,” *Journal of membrane science*, vol. 28, no. 2, pp. 209–223, 1986, DOI: https://doi.org/10.1016/S0376-7388(00)82211-5.

[58] Z. Jawad, A. Ahmad, S. Low, T. Chew, and S. Zein, “Influence of solvent exchange time on mixed matrix membrane separation performance for co2/n2 and a kinetic sorption study,” *Journal of Membrane Science*, vol. 476, pp. 590–601, 2015, DOI: https://doi.org/10.1016/j.memsci.2014.11.008.

[59] K. Khulbe, C. Feng, and T. Matsuura, *Synthetic Polymeric Membranes: Characterization by Atomic Force Microscopy*, 01 2008.

[60] M. Mulder and J. Mulder, *Basic principles of membrane technology*. Springer science & business media, 1996.

[61] A. Lui, F. Talbot, A. Fouda, T. Matsuura, and S. Sourirajan, “Studies on the solvent exchange technique for making dry cellulose acetate membranes for the separation of gaseous mixtures,” *Journal of applied polymer science*, vol. 36, no. 8, pp. 1809–1820, 1988, DOI: https://doi.org/10.1002/app.1988.070360808.

[62] V. S. Vaidhyanathan, *Transport phenomena*, 1980, vol. 36, no. 11.

[63] S. S. Lee, K. H. Ahn, S. J. Lee, K. Sun, P. T. Goedhart, and M. R. Hardeman, "Shear induced damage of red blood cells monitored by the decrease of their deformability," *Korea-Australia Rheology Journal*, vol. 16, no. 3, pp. 141–146, 2004.

[64] Q. Lu, B. V. Hofferbert, G. Koo, and R. A. Malinauskas, "In vitro shear stress-induced platelet activation: Sensitivity of human and bovine blood," *Artificial Organs*, vol. 37, no. 10, pp. 894–903, 2013, DOI: https://doi.org/10.1111/aor.12099.

[65] N. J. Ofsthun, S. Karoor, and M. Suzuki, *Hemodialysis Membranes*, 2008.

[66] Definition of Molecular weight cut-off. (January, 2022). [Online]. Available: https://synderfiltration.com/learning-center/articles/membranes/molecular-weight-cut-off/

[67] Z. Filutowicz, K. Łukaszewski, and K. Pieszyński, "Remarks on spectra-photometric monitoring of urea in dialysate," *Journal of Medical Informatics and Technologies*, vol. 8, 2004.

[68] O. E. ter Beek, M. K. van Gelder, C. Lokhorst, D. H. Hazenbrink, B. H. Lentferink, K. G. Gerritsen, and D. Stamatialis, "In vitro study of dual layer mixed matrix hollow fiber membranes for outside-in filtration of human blood plasma," *Acta Biomaterialia*, vol. 123, pp. 244–253, 2021, DOI: https://doi.org/10.1016/j.actbio.2020.12.063.

[69] L. Yang, M. Biswas, and P. Chen, "Study of binding between protein a and immunoglobulin g using a surface tension probe," *Biophysical Journal*, vol. 84, no. 1, pp. 509–522, 2003, DOI: https://doi.org/10.1016/S0006-3495(03)74870-X.

[70] M. M. Bradford, "A rapid and sensitive method for the quantitation of microgram quantities of protein utilizing the principle of protein-dye binding." *Analytical biochemistry*, vol. 72, pp. 248–54, 1976, DOI: https://doi.org/10.1016/0003-2697(76)90527-3.

[71] T. Zor and Z. Selinger, "Linearization of the bradford protein assay increases its sensitivity: Theoretical and experimental studies," *Analytical Biochemistry*, vol. 236, no. 2, pp. 302–308, 1996, DOI: https://doi.org/10.1006/abio.1996.0171.

[72] M. Faria, C. Moreira, T. Eusébio, P. Brogueira, and M. N. de Pinho, "Hybrid flat sheet cellulose acetate/silicon dioxide ultrafiltration membranes for uremic blood purification," *Cellulose*, vol. 27, no. 7, pp. 3847–3869, 2020.

[73] M. Lopes, "Synthesis and Characterization of Novel Monophasic Hybrid Membranes of Cellulose Acetate by Co-polymerization with Tetraethly Orthosilicate and 3-(Aminopropyl)triethoxysilane," MSc Dissertation, Instituto Superior Técnico, Lisboa, 2021.

[74] M. R. Pereira and J. Yarwood, “ATR-FTIR spectroscopic studies of the structure and permeability of sulfonated poly(ether sulfone) membranes Part 2. - Water diffusion processes,” *Journal of the Chemical Society - Faraday Transactions*, vol. 92, no. 15, pp. 2737–2743, 1996.

[75] R. Al-Oweini and H. El-Rassy, “Synthesis and characterization by FTIR spectroscopy of silica aerogels prepared using several $Si(OR)_4$ and $R"Si(OR')_3$ precursors,” *Journal of Molecular Structure*, no. 1-3, pp. 140–145, 2009, DOI: http://dx.doi.org/10.1016/j.molstruc.2008.08.025.

[76] P. A. Holme, U. Ørvim, M. J. Hamers, N. O. Solum, F. R. Brosstad, R. M. Barstad, and K. S. Sakariassen, “Shear-induced platelet activation and platelet microparticle formation at blood flow conditions as in arteries with a severe stenosis,” *Arteriosclerosis, Thrombosis, and Vascular Biology*, vol. 17, no. 4, pp. 646–653, 1997, DOI: https://doi.org/10.1161/01.ATV.17.4.646.

[77] D. Božič, S. Sitar, I. Junkar, R. Štukelj, M. Pajnič, E. Žagar, V. Kralj-Iglič, and K. Kogej, “Viscosity of plasma as a key factor in assessment of extracellular vesicles by light scattering,” *Cells*, vol. 8, no. 9, 2019.

[78] F. M. Care. Understanding dialyzer types. (October, 2022). [Online]. Available: https://fmcna.com/insights/articles/Understanding-Dialyzer-Types/

A

Appendix: Calibration Curves

A.1 Artificial Kidney setup pump

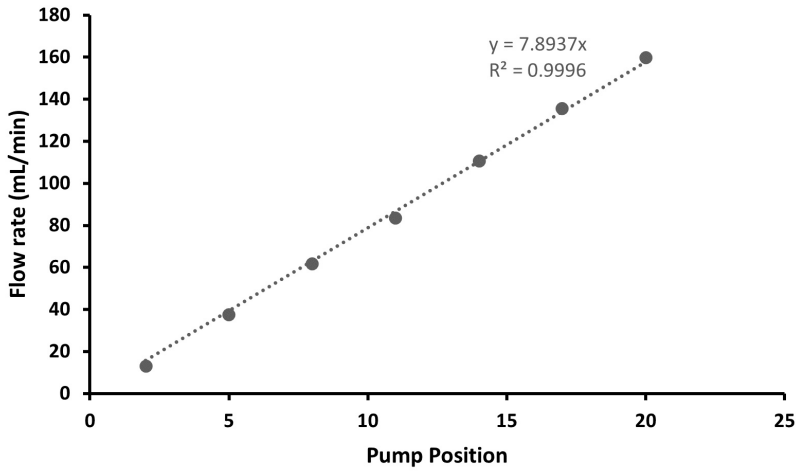

Figure A.1: Artifical kidney Calibration Curve.

A.2 CELFA P-28

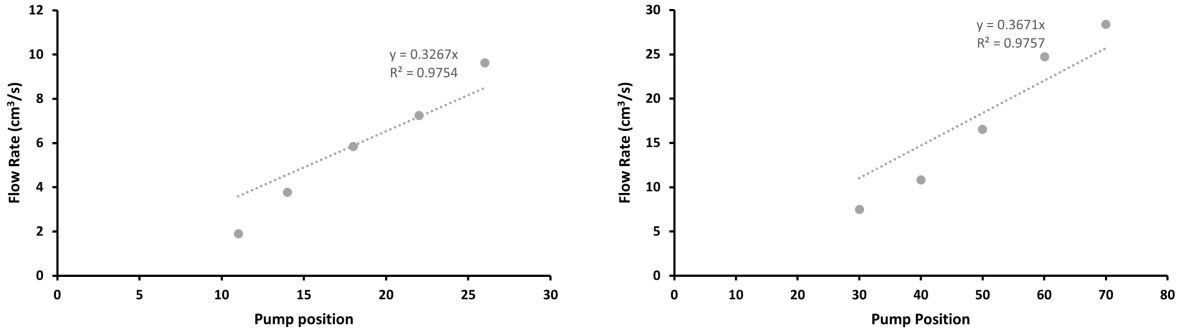

(a) 0.5 bar **(b)** 2 bar

Figure A.2: CELFA P-28 Calibration Curve.

A.3 Total Organic Carbon

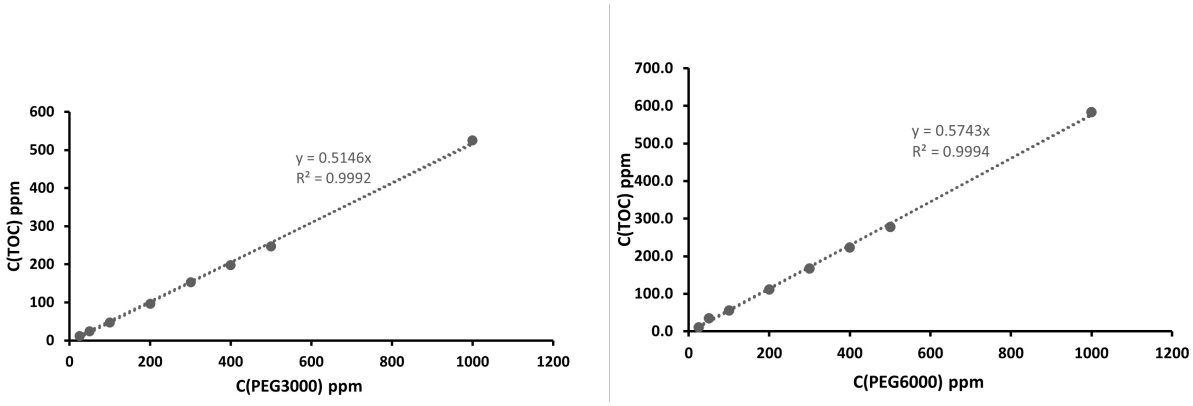

(a) PEG 3000 **(b)** PEG 6000

Figure A.3: Total organic carbon concentration (ppm), as a function of known concentrations (ppm) of PEG aqueous solutions. The equations are the result of a linear fit to the data, with the respective coefficient of correlation (R^2).

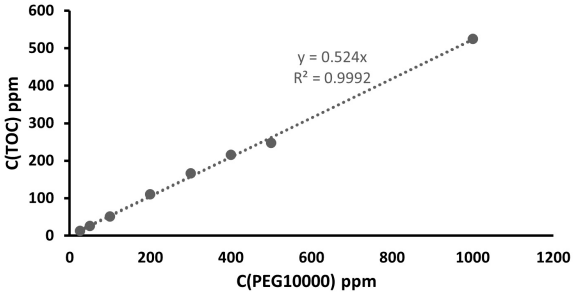

(a) PEG 10 000

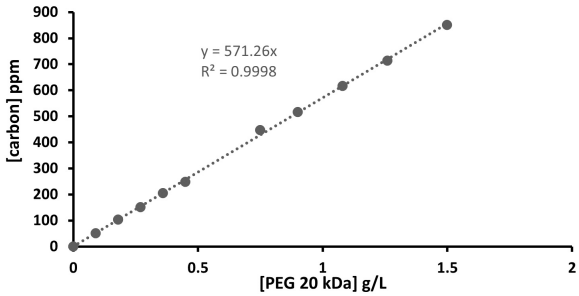

(b) PEG 20 000

Figure A.4: Total organic carbon concentration (ppm), as a function of known concentrations (ppm) of PEG aqueous solutions. The equations are the result of a linear fit to the data, with the respective coefficient of correlation (R^2).

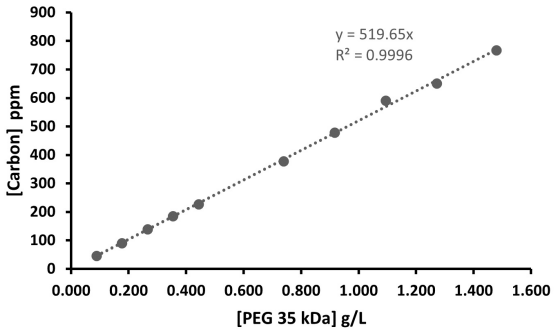

(a) PEG 35 000

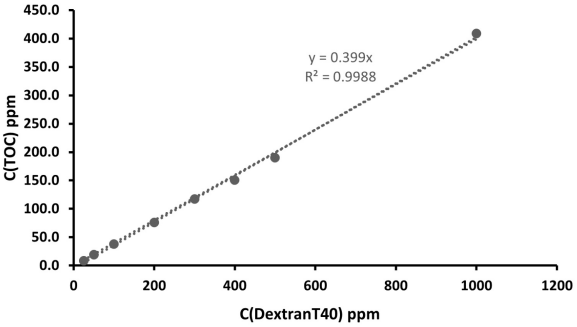

(b) DEXTRAN T40

Figure A.5: Total organic carbon concentration (ppm), as a function of known concentrations (ppm) of PEG aqueous solutions. The equations are the result of a linear fit to the data, with the respective coefficient of correlation (R^2).

A.4 Fluorescence Spectroscopy

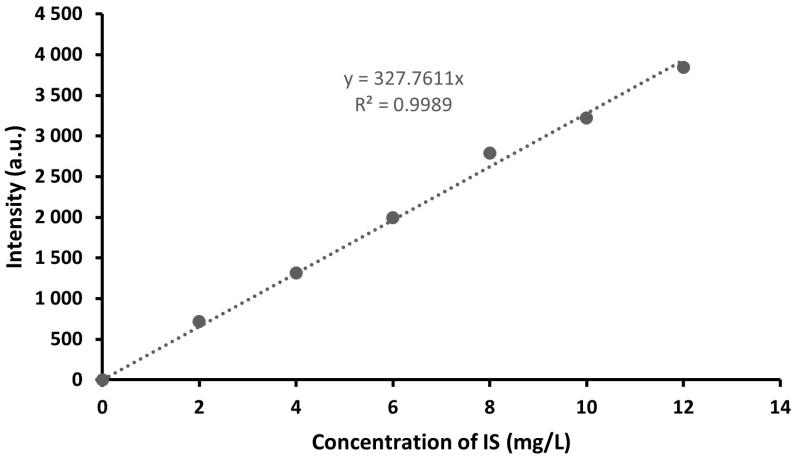

Figure A.6: Intensity as a function of the IS concentration in PBS solution.

A.5 UV-VIS Spectroscopy

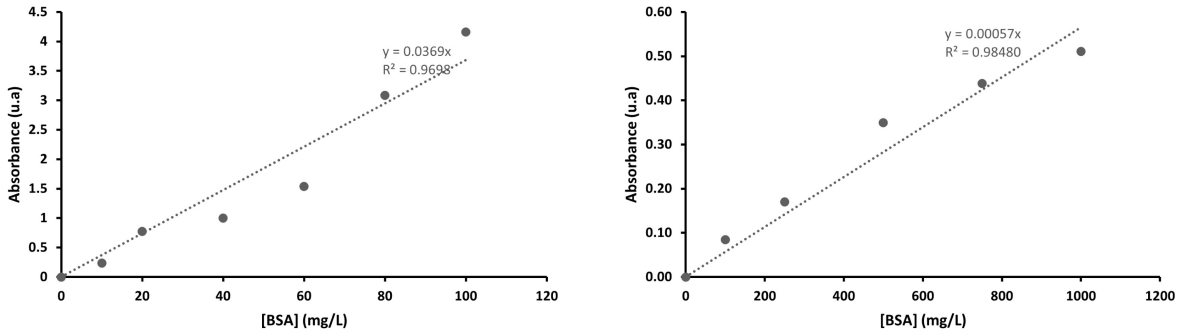

(a) Low Concentrations

(b) High Concentrations

Figure A.7: Absorbance as a function of the BSA concentration.

B

Appendix: Hydraulic permeability

TMP (mmHg)	J ($mL/min/cm^2$)
125.14	0.018
136.96	0.021
162.82	0.024
184.78	0.027
229.96	0.036

Table B.1: Ultrafiltration flux, J , in $mL/min/cm^2$, and transmembrane pressure (TMP), in mmHg, for the CA30 membrane measured in the AK setup.

TMP (mmHg)	J ($mL/min/cm^2$)
134.9	0.028
150.32	0.031
171.33	0.037
185.72	0.041
208.17	0.047

Table B.2: Ultrafiltration flux, J , in $mL/min/cm^2$, and transmembrane pressure (TMP), in mmHg, for the CA30-TEOS-APT-IBF(3%) membrane measured in the AK setup.

TMP (mmHg)	J ($mL/min/cm^2$)
103.26	0.014
125.19	0.018
151.95	0.022
178.12	0.026
196.16	0.028

Table B.3: Ultrafiltration flux, J , in $mL/min/cm^2$, and transmembrane pressure (TMP), in mmHg, for the CA35 membrane measured in the AK setup.

TMP (mmHg)	J ($mL/min/cm^2$)
107.45	0.012
135.72	0.015
171.08	0.021
213.46	0.026
245.82	0.030

Table B.4: Ultrafiltration flux, J , in $mL/min/cm^2$, and transmembrane pressure (TMP), in mmHg, for the CA33 membrane measured in the AK setup.

TMP (bar)	J ($Kg/h/m^2$)
0.5	3.2
1	18.6
1.5	35.0
2	46.5
2.5	65.8

Table B.5: Ultrafiltration flux, J , in ($Kg/h/m^2$), and transmembrane pressure (TMP), in bar, for the CA22 membrane measured in the CELFA P-28.

TMP (bar)	J ($Kg/h/m^2$)
0.5	3.2
1	18.6
1.5	35.0
2	46.5
2.5	65.8

Table B.6: Ultrafiltration flux, J , in ($Kg/h/m^2$), and transmembrane pressure (TMP), in bar, for the CA22-APT membrane measured in the CELFA P-28.

TMP (bar)	J ($Kg/h/m^2$)
2	0.85
2.5	2.08
3	2.83
3.5	3.83
4	4.79

Table B.7: Ultrafiltration flux, J , in ($Kg/h/m^2$), and transmembrane pressure (TMP), in bar, for the CA22-APT-IBF(15%) membrane measured in the CELFA P-28.